TÉCNICO LISBOA

Modelling the Natural Gas Sweetening and Dehydration prior to Liquefaction

Mariana Ribeiro Marques

Thesis to obtain the Master of Science Degree in

Chemical Engineering

Supervisors: Prof. Dr. Henrique Aníbal Santos de Matos
Dr. Klaas Martÿn Nauta

Examination Committee

Chairperson: Prof. Dr. Sebastião Manuel Tavares Silva Alves
Supervisor: Prof. Dr. Henrique Aníbal Santos de Matos
Member of the Committee: Prof. Dr. Vítor Manuel Geraldes Fernandes

November 2014

This page was intentionally left blank.

A person who never made a mistake never tried anything new.

Albert Einstein

This page was intentionally left blank.

Acknowledgments

In the first place, I would like to express my gratitude to Professor Henrique Matos, Professor Carla Pinheiro and especially to Professor Costas Pantelides for the amazing opportunity to work at Process Systems Enterprise Ltd and learn about gPROMS®.

I would also like to thank everyone at PSE that was available to help me with any sort of problem: a huge word of appreciation goes to my PSE's supervisor Maarten Nauta, for his experience and vast knowledge and for helping me, with patience, whenever he could. Also, a special thanks goes to Thomas Laffite for all the support with gSAFT®, to Mário Calado for all the great ideas, and to Charles Brand who supported me when Maarten was not available.

Also, a word of appreciation goes to everyone at PSE for making me feel very welcome and as a part of the "PSE family", especially to the friendly Portuguese "community" at PSE, particularly to Leonor Rosa who could always put a smile on my face when I was feeling down.

To my fellow interns from Porto: Rubina Franco and Catarina Marques, it has been the most wonderful experience to get to know you, work side by side with you and share gPROMS® "experiences". I am really lucky to be friends with such amazing people.

To Artur Andrade and Renato Wong, my housemates: there are not enough words to express my gratitude. Thank you so much for all the fun moments, the support and for making me feel less homesick.

A word of appreciation also goes to my friends at Instituto Superior Técnico, for accompanying me in this turbulent 5 years journey: without them, I would not be who I am today. A special thanks goes to Ana Sofia Borrego, who, no matter what, always believed in me since the beginning.

Huge thanks to my beloved family, especially my parents and my brother, who educated me in the best possible way, supported me no matter what, and loved me unconditionally.

Last, but not least, I want to thank Francisco Borralho for his never ending support, belief in me, and enormous patience, not only in this past 7 months but also in the last 4 years. Without you, things would not be the same.

This page was intentionally left blank.

Abstract

The present work comprises the modelling of natural gas (NG) purification prior to liquefaction, more precisely its sweetening and dehydration.

Since NG exists in underground reservoirs it contains several impurities that must be removed in order to meet liquefied natural gas (LNG) specifications, since they can cause corrosion, plugging and others. In this way, the sweetening of NG using diethanol amine (DEA) was simulated in gPROMS®, as well as its dehydration using in the first place a glycol solvent (absorption) and then molecular sieves (adsorption).

The first two processes are very similar and both use absorption columns with equilibrium stages to promote intimate contact between the solvent and the impurities. Then, both solvents are regenerated in distillation columns with trays. Regarding the dehydration of NG via adsorption, zeolite 5A was used, and some custom models were developed. In this case, the adsorption of water was simulated using an isothermal adsorption bed.

In the sweetening of NG, a sweet gas was obtained with CO_2 concentration of $1.3x10^{-4}$ mol. % and H_2S concentration of 5.2 mol. %, using DEA with a concentration of 35 wt. %, and at the expense of 7.3 GJ/ton acid gases absorbed.

In the simulation of NG dehydration with triethylene glycol (TEG), a dried gas was obtained with 41 ppmv of water, at the expense of 5.4 GJ/ton water absorbed and using a solvent with 99 wt. % concentration.

Finally, in the simulation of NG dehydration with zeolite a breakthrough time equal to 1336 minutes was obtained.

Keywords

gPROMS, LNG, sweetening, dehydration, absorption, adsorption

This page was intentionally left blank.

Resumo

O presente trabalho compreende a modelação da purificação do gás natural (NG) antes de liquefacção, mais precisamente *sweetening* e desidratação.

Uma vez que o NG existe em reservatórios subterrâneos, contém várias impurezas que devem ser removidas para ir ao encontro das especificações do gás natural liquefeito (LNG), visto que podem causar corrosão, entupimentos e outros. Desta forma, simulou-se o *sweetening* de NG com dietanol amina (DEA) em gPROMS®, assim como a sua desidratação usando, em primeiro lugar, glicol (absorção) seguido de peneiros moleculares (adsorção).

Os primeiros dois processos são semelhantes e ambos usam colunas de absorção com andares de equilíbrio para promover contacto íntimo entre solvente e impurezas. De seguida, os solventes são regenerados em colunas de destilação com pratos. No que toca à desidratação de NG via adsorção, usou-se zeólito 5A e alguns modelos foram desenvolvidos. Neste caso, simulou-se a adsorção de água num leito de adsorção isotérmico.

No *sweetening* de NG, obteve-se um gás doce com concentração de CO_2 de $1.3x10^{-4}$ % (mol) e de H_2S de 5.2 % (mol), usando DEA com uma concentração de 35 % (massa) e à custa de 7.3 GJ/ton gases ácidos absorvidos.

Na simulação da desidratação de NG com trietileno glicol (TEG), um gás seco foi obtido com 41 ppmv de água, à custa de 5.4 GJ/ton água absorvida e usando um solvente com concentração de 99 % (massa).

Finalmente, na simulação da desidratação de NG com zeólito obteve-se um tempo de *breakthrough* igual a 1336 minutos.

Palavras-Chave

gPROMS, LNG, *sweetening*, desidratação, absorção, adsorção

This page was intentionally left blank.

Contents

This page was intentionally left blank.

List of Figures

This page was intentionally left blank.

List of Tables

This page was intentionally left blank.

Nomenclature

Symbol	Description	Unit
a	1st Virial coefficient	m^6
a_c	1st Virial coefficient at critical temperature	m^6
A	Helmholtz energy	J
	Adsorption bed area	m^2
A_{ij}	Auxiliary adsorption equilibrium parameter	mol.K/kg or mol/kg
b	2nd Virial coefficient	m^3
b_c	2nd Virial coefficient at critical temperature	m^3
b_o	Pre-exponential factor	kPa^{-1}
C_p	Heat capacity at constant pressure	kJ/K
d	Diameter	m
D_0	Diffusional pre-exponential factor	m^2/s
D_{1j}	Diffusivity coefficient	m^2/s
D_{ax}	Axial dispersion coefficient	m^2/s
D_c	Crystalline diffusivity	m^2/s
D_m	Molecular diffusivity	m^2/s
E	Adsorption energy	J/mol
	Diffusional activation energy	J/mol
f	Fugacity	-
F	Mass flowrate	kg/s
G	Gibbs energy	J
h	Mass specific enthalpy	kJ/kg
H	Enthalpy	J/mol
k_0	Temperature independent constant for BIP	-
k_1	1st order temperature dependent constant for BIP	K^{-1}
k_2	2nd order temperature dependent constant for BIP	K^{-2}
k	Binary interaction parameter	-
	LDF coefficient	s^{-1}
	Heat transfer coefficient	$W/(m^2.K)$
L	Auxiliary parameter in the TST $a(T)$ equation	-
M	Auxiliary parameter in the TST $a(T)$ equation	-
MW	Molecular weight	kg/mol
N	Auxiliary parameter in the TST $a(T)$ equation	-
n	Number of moles	mol
p	Partial pressure	kPa
P	Total pressure	bar
q_c	Mass adsorbed into the micropore volume	mol/kg
q_c^*	Equilibrium concentration in the adsorbed phase	mol/kg
q_s	Specific saturation capacity	mol/kg
R	Ideal gas constant	J/(mol.K)
R_c	Adsorbent crystal radius	m
T	Absolute temperature	K
t	Time	s
u	Interstitial gas velocity	m/s
U	Internal energy density	kJ/m^3

(continuation of previous table)

V	Total volume	m^3
x	Mass fraction	kg/kg
Y	Molar fraction in the adsorbed phase	mol/mol
z	Axial direction	m
Z_c	Compressibility factor	-

Greek letters

Symbol	Description	Unit
Δ	Variation	-
β	Affinity parameter	kPa^{-1}
γ	Auxiliary parameter for axial dispersion coefficient	-
ε	Porosity	m^3/m^3
κ	Auxiliary parameter for a_c	-
ρ	Density	kg/m^3
ω	Acentric factor	-
τ	Excess energy binary interaction parameter	-
α	NRTL binary interaction parameter	-
λ	Thermal conductivity	kW/mK
υ	Dynamic viscosity	Pa.s

Subscripts

Symbol	Description
$\emptyset$	Pure component property at working temperature and 1 bar
b	Adsorbent bed property
c	Critical property
f	Fluid property
i	Component property
ij	Interaction property between components i and j
in	Inlet property
j	Adsorption site property
p	Adsorbent particle property
r	Reduced property
ref	Property at reference state
t, bw	From bed to wall
tot	Total
vdw	van der Waals property
w	Wall property
z	Effective bed property

Superscripts

Symbol	Description
$*$	Reduced property
ads	Adsorption property
E	Excess property
l	Liquid phase property
v	Vapour phase property

This page was intentionally left blank.

List of Abbreviations

Abbreviation	Description
bcm	Billions cubic meters
BIP	Binary interaction parameter
DEA	Diethanol amine
DEG	Diethylene glycol
DGA	Diglycol amine
DIPA	Diisopropanol amine
EG	Monoethylene glycol
gML	gPROMS® model library
GPE	General process engineering
KPI	Key performance indicator
LDF	Linear driving force
LNG	Liquefied natural gas
MDEA	Methyldiethanol amine
MEA	Monoethanol amine
MTZ	Mass transfer zone
NG	Natural gas
NGL	Natural gas liquids
PR	Peng-Robinson
PSE	Process Systems Enterprise Ltd
RKS	Redlich-Kwong-Soave
SAFT	Statistical associating fluid theory
SAFT-VR SW	SAFT-Variable range square well
TEG	Triethylene glycol
TREG	Tetraethylene glycol
VLE	Vapour-liquid equilibrium

This page was intentionally left blank.

1. Introduction

Natural gas (NG) is used primarily as a fuel and as a raw material in manufacturing. It is used in home furnaces, water heaters, and cooking stoves. As an industrial fuel it is used in brick, cement and ceramic-tile kilns, in glass making, for generating steam in water boilers, and as a clean heat source for sterilization and processing of foods. As a raw material in petrochemical manufacturing, NG is used to produce hydrogen, sulphur, carbon black, and ammonia, and as a secondary feedstock for manufacturing other chemicals, such as nitric acid and urea. Ethylene, an important petrochemical, is also produced from NG [1].

NG offers important environmental benefits when compared to other fossil fuels, being considered as an environmentally friendly clean fuel. Thus, NG has superior environmental qualities over coal or crude oil since its emissions of sulphur dioxide are negligible and the levels of nitrous oxide and carbon dioxide emissions are lower in up to 60%. This helps to reduce problems of acid rain, ozone layer, or greenhouse gases. NG is also a very safe source of energy when transported, stored, and used [1]. Therefore, the shift toward NG will carry tremendous benefits for consumers and the environment since it is affordable, efficient, and available [2].

The reserves of conventional NG have grown by 36% over the past two decades and its production by 61%. Between 2010 and 2013, the proved NG reserves have grown by 3% and production by 15% [3].

Table 1: NG reserves and production in the top 5 countries [3]

Country	Reserves (bcm)		Production (bcm)	
	1993	**2011**	**1993**	**2011**
Russian Federation	48 160	47 750	604	670
Iran	20 659	33 790	27	150
Qatar	7 079	25 200	14	117
Turkmenistan	2 860	25 213	57	75
Saudi Arabia	5 260	8 028	36	99
Rest of World	57 317	69 761	1 438	2 407
Global Totals	141 335	209 742	2 176	3 518

In 2012, for the first time in many years, the growth in NG demand surpassed that of coal [3]. By 2025, NG is expected to have overtaken coal as the second most consumed fuel, after oil [2]. Despite the current economic difficulties, the global gas market is expected to reach 4 700 bcm by 2030. This growth is supported by an increase in gas production potential and expansion of international trade based on a growing number of liquefied natural gas (LNG) facilities and high pressure pipelines. At the same time, the share of NG in primary energy supply is expected to rise from 22% in 2010 to 25% in 2030. The most significant growth for gas is likely to be in power generation (expected to account for 40% of the total gas market in 2030), while the highest regional growth is expected to take place in Asia, driven by the continuous expansion of the Chinese gas market [3].

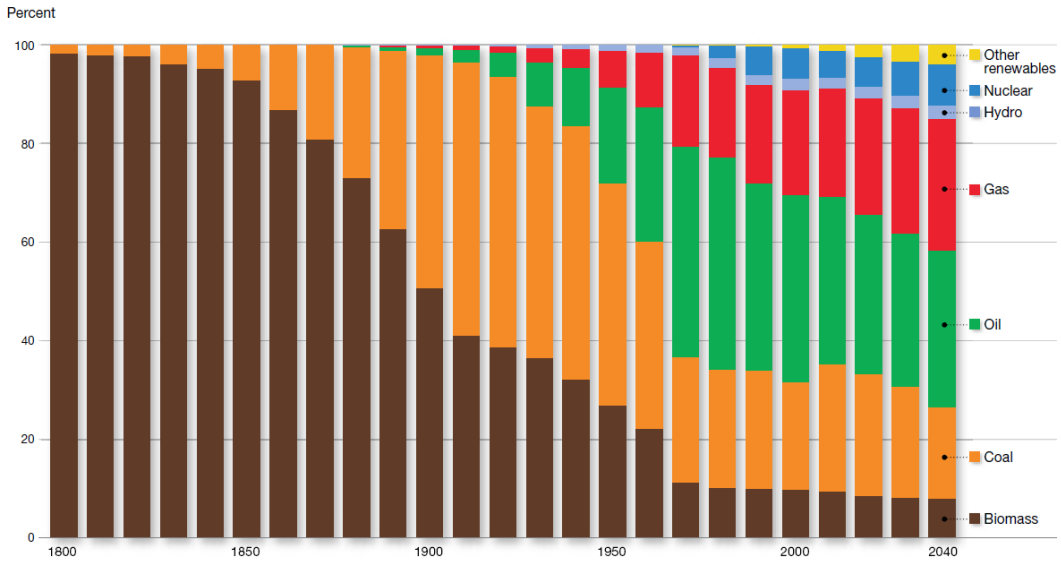

Figure 1: Distribution of the primary energy sources [2]

The International Energy Agency estimates there is about 793 000 bcm of remaining NG resources around the world, which is believed to meet current demand levels for more than 200 years [2].

1.1. Motivation

The growing demand of the world for NG implies improving the existing processes for production, treatment, energy harvesting, and pollution control. When NG is transported by ship, liquefaction is an important step in the supply chain, due to a 1/600 volume reduction. Since NG exists in deep underground reservoirs, it may contain several impurities, which are undesirable compounds that can cause several technical problems, such as corrosion, environment pollution, plugging, and others. So, they need to be removed from NG to meet the LNG specifications.

This work has been developed in Process Systems Enterprise Ltd (PSE), a worldwide company that is a leading supplier of advanced process modelling technology and related model-based engineering, and innovation services to the process industries. This project was integrated in the General Processes department, using models that existed in the General Process Engineering (GPE) library. The main motivation for this project is to extend PSE's library to include processes required for the purification of NG, more precisely for its dehydration and sweetening, steps that are essential prior to its liquefaction.

1.2. Original Contributions

The main contributions of this thesis were: the development of a flowsheet for acid gases removal from NG in gPROMS® ProcessBuilder using gSAFT® as the physical properties package the development of a complete flowsheet in gPROMS® ModelBuilder for the dehydration of NG using triethylene glycol (TEG); the assembling of a dynamic adsorption bed for the dehydration of NG in gPROMS® ProcessBuilder with custom models for zeolite 5A.

1.3. Dissertation Outline

This thesis is arranged as follows: in Chapter 2, a literature review is presented regarding mainly NG processing, its importance, and the different technologies available. Also, different flowsheets for some steps in gas processing are shown and explained. Chapter 3 describes the software used for modelling/simulation, as well as the physical properties packages available. In Chapter 4, a description of the models used in the flowsheets implementation is done, as well as a summary of their purpose and specifications required. Chapter 5 regards the flowsheets implementation description, the modelling work performed, and the results obtained. Finally, Chapter 6 presents the conclusions of the present thesis, as well as some future work.

This page was intentionally left blank.

2. Literature Review

A literature review was made to be acquainted with what was already done and developed about the purification of natural gas (NG). In this way, the present chapter presents a detailed explanation about all different technologies used in NG processing plants, which are available in any books regarding gas processing and purification. The sweetening and dehydration of NG are explained with more detail than the others step in the NG purification. The complete flowsheets for sweetening and dehydration with glycol solvent replicated in this project are well represented in Kidnay et al. [1] and Mokhatab et al. [4], and also in some articles/dissertations that provide typical industrial operating conditions (reported by Abdulrahman et al. [5], and Ghati [6]). Regarding the dehydration of NG with molecular sieves, information about adsorption equilibria of water vapour and detailed modelling of the adsorption process is available in some articles, as well as some operating conditions (reported by Gholami et al. [7]).

2.1. Natural Gas Origin and Composition [1], [8]

NG exists in nature under pressure in rock reservoirs in the Earth's crust, either in conjunction with and dissolved in heavier hydrocarbons and water, or by itself. NG has been formed by the degradation of organic matter accumulated in the past millions of years.

The principal constituent of NG is methane. Others include paraffinic hydrocarbons such as ethane, propane, and butanes. Most of NGs contain nitrogen, as well as carbon dioxide and hydrogen sulphide. Table 2 outlines the typical composition of NG being treated.

Table 2: Typical composition of NG [1]

Component	Formula	Volume (%)
Methane	CH_4	>85
Ethane	C_2H_6	3-8
Propane	C_3H_8	1-2
Butane	C_4H_{10}	<1
Pentane	C_5H_{12}	<1
Carbon dioxide	CO_2	1-2
Hydrogen sulphide	H_2S	<1
Nitrogen	N_2	1-5
Helium	He	<0.5

Water is almost always present but is typically not shown in the analysis. Unless the gas has been dehydrated before the gas processing plant, the common practice is to assume the entering gas is saturated with water at the plant inlet conditions.

The composition of NG varies depending on the field, formation, or reservoir from which it is extracted. It is considered a "dry gas" when it is composed of almost pure methane, after most of the other associated hydrocarbons and impurities are removed. Otherwise, it is referred to as "wet gas".

2.2. Shipping [1], [8]

Due to its storage difficulties, gas needs to be transported immediately to its destination after production. Therefore, there are several options for transporting NG from oil and gas fields to the market. These include pipelines, liquefied natural gas (LNG), compressed NG[1], gas to solids[2], gas to power[3], and gas to liquids[4].

Pipelines are a very convenient method of transport but are not flexible. If the pipeline has to be shut down, the production and receiving facilities often also have to be shut down because gas cannot be readily stored.

LNG technology has been proven to be effective since the mid-1970s. LNG is the liquid form of NG, i.e., gas cooled to approximately -162 ^{o}C with a 1/600 volume reduction. The costs of building a LNG plant have lowered since the mid-1980s due to improved thermodynamic efficiencies, making LNG a major gas export method around the world.

Since the production of LNG requires low temperatures, the allowable impurity concentrations in the gas to be liquefied are much tighter than that of a pipeline gas, as shown in Table 3.

Table 3: Composition specifications for LNG plant and pipeline gas [1]

Impurity	Feed to LNG plant	Pipeline gas
H_2O	<0.1 ppmv	150 ppmv
H_2S	<4 ppmv	5.7-22.9 mg/Sm^3
CO_2	<50 ppmv	3-4 mol %
Total sulphur	<20 ppmv	115-459 mg/Sm^3
N_2	<1 mol %	3 mol %
Hg	<0.01 μg/Nm^3	-
C_4H_{10}	<2 mol %	-
C_5^+	<0.1 mol %	-
Aromatics	<2 ppmv	-

2.3. Gas Processing

The three basic reasons for processing raw NG are the following: purification (i.e., removal of materials that inhibit the use of the gas as a fuel), separation (i.e., splitting out of components that have greater value as petrochemical feedstocks, stand-alone fuels, or industrial gases), and liquefaction (i.e., increase of the energy density of the gas for storage or transportation, as stated before) [1].

In summary, the objective of gas processing is to separate condensate, non-condensables, acid gases, and water from a gas-producing well to meet NG sales specifications [8]. A typical process operation for NG processing is shown in Figure 2.

[1] Gas transported at high pressures.
[2] Gas transported as a solid (gas hydrate).
[3] Gas transported as fuel for electricity generation.
[4] Gas converted to a liquid, such as syncrude methanol and ammonia.

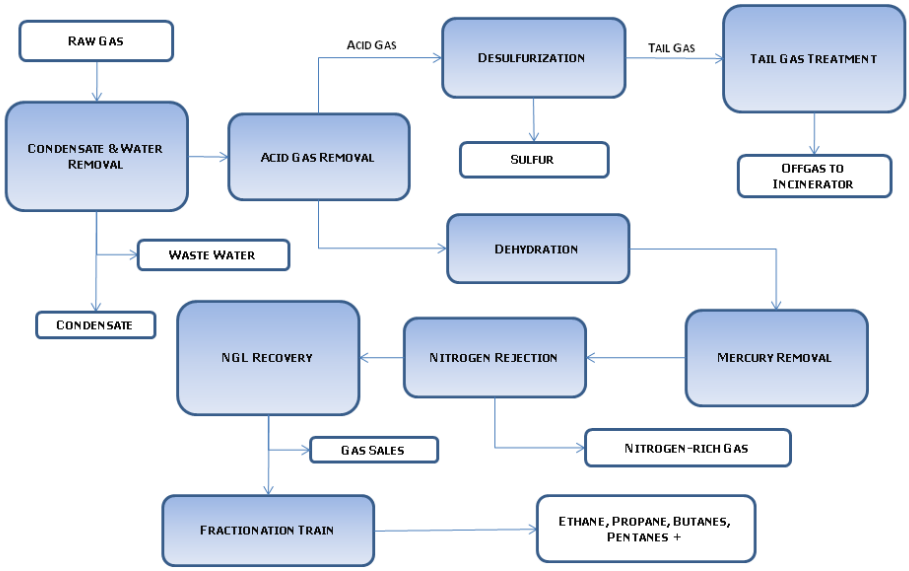

Figure 2: Typical process flow diagram for NG processing plants [9]

Some of the operations shown may not be present in every gas plant. However, most NG processing plants require equipment for the removal of impurities, water, and excess hydrocarbon liquid. Also, the modules may not be arranged in the sequence shown above, although this is a typical one [8].

Unless the gas is completely free of any liquids, the NG must go into an inlet receiving facility, i.e., condensate and water removal once the gas enters the plant, where the initial gas-liquid separation is made. In this module, condensed water, hydrocarbon liquids, and solids are removed. After that, water and solids are processed for disposal, whereas the hydrocarbon liquids go on to liquid processing. This initial separation takes place in a slug catcher, i.e., a gas-liquid separator sized to hold the biggest slug a plant can experience [1].

The next step in NG processing is sweetening, or acid gas removal. NG often contains CO_2, H_2S, and other sulphur-containing species that require partial or complete removal since they can form acids in the presence of water. Therefore, these compounds are known as “acid gases”. So, both CO_2 and H_2S are undesirable compounds, as they cause corrosion and pose a major safety risk [8]. There are several available processes to remove them, depending on various factors, being the most common ones solvent absorption (chemical, physical or hybrid), solid adsorption, and membrane separation. After their removal, the acid gases can be used in different manners. CO_2 can be used as an injection fluid in enhanced oil recovery projects, or it can be vented if it satisfies the environmental regulations. On the other hand, H_2S can suffer incineration and venting, react with scavengers (such as iron sponge), be converted to elemental sulphur, or disposed by injection into a suitable underground formation [1].

Since the gas leaving the sweetening unit is usually water saturated, almost all plants have a dehydration step. Also, most gas streams contain too much water to enter the cryogenic section of the plant [1]. Dehydration is therefore necessary to meet specifications, reduce corrosion, and to prevent hydrate formation. Gas hydrate formation is a major concern for engineers in NG industries, as it causes

choking/plugging of pipelines [8]. In order to perform the required dehydration, the most common processes are absorption and adsorption.

The next step in the gas processing plant is usually mercury removal. Mercury must be removed from gas streams since it corrodes aluminium heat exchangers used in cryogenic processes, as it amalgamates with the aluminium to weaken the material. Also, mercury is toxic to humans as well as a poison to many catalysts. Mercury can be removed using chemisorption, a sulphur-impregnated carbon adsorbent or silver on molecular sieves [1].

The nitrogen rejection step is a less common one in the gas processing industry and it is typically a cryogenic process, although membrane and absorbent technology can also be used [1]. Nitrogen needs to be removed due to its impact in NG combustion properties and because its presence increase the size and cost of LNG plants and NG processing facilities [10].

Most NGs are processed to remove heavier hydrocarbon liquids from the gas stream. These heavier hydrocarbon liquids, referred to as "natural gas liquids" (NGL), include ethane, propane, butane, and natural gasoline (condensate). In the NGL recovery several processes are available such as mechanical refrigeration, self-refrigeration, cryogenic refrigeration, and lean oil absorption [8].

2.3.1. Sweetening

In the presence of water H_2S forms a weak, corrosive acid (sulphuric acid), and besides that is highly toxic. When H_2S concentrations are above the ppmv level, other sulphur species can be present, such as carbon disulphide (CS_2), mercaptans (RSH), sulphides (RSR), and elemental sulphur [1].

On the other hand, besides forming carbonic acid in the presence of water, CO_2 is non-flammable and therefore it is undesirable in a fuel in large quantities [1].

The selectivity of the sweetening process represents the preference with which it removes one acid gas component over the other. Therefore, there are some possible scenarios for NG sweetening: CO_2 removal from a gas that contains no H_2S; H_2S removal from a gas that contains no CO_2; simultaneous removal of both acid gases; selective removal of H_2S from a gas that contains both acid gases components [8].

Because NG has a wide range of composition, processes for the removal of acid gases are subject to choice based on the desired end product. Thus, several factors must be considered [1], [8]:

- Types and concentrations of contaminants and hydrocarbons in the gas;
- The degree of contaminant removal desired;
- The selectivity of acid gas removal required;
- The temperature, pressure, volume, and composition of the gas to be processed (high partial pressures of the acid gases in the feed favour physical solvents);
- The CO_2-H_2S ratio in the gas;
- The capital and operating costs for the process;
- The desirability of sulphur recovery.

In this manner, no single process is distinctly superior in all the circumstances and many processes are currently used, as one can see in Figure 3.

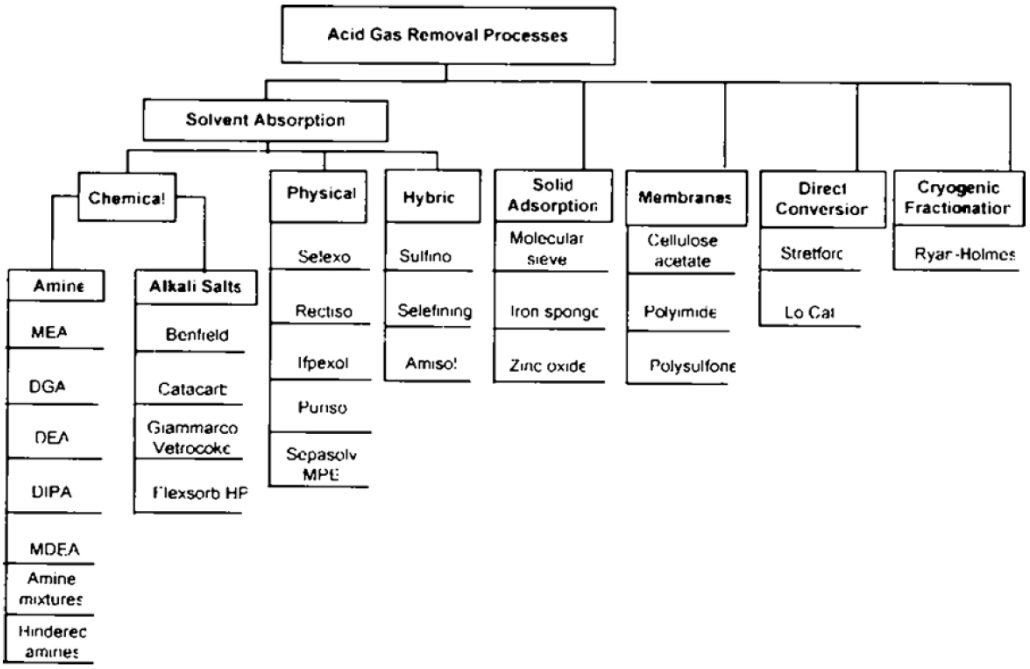

Figure 3: Available sweetening processes [1]

There are available some guidelines for the selection of solvent-based processes for acid gases removal of NG streams, taking into account the partial pressure of the acid gases in the feed. An example is shown in Figure 4 for the simultaneous removal of H_2S and CO_2. Note that “hybrid” denotes mixed-solvent systems that contain both an amine and a physical solvent [1].

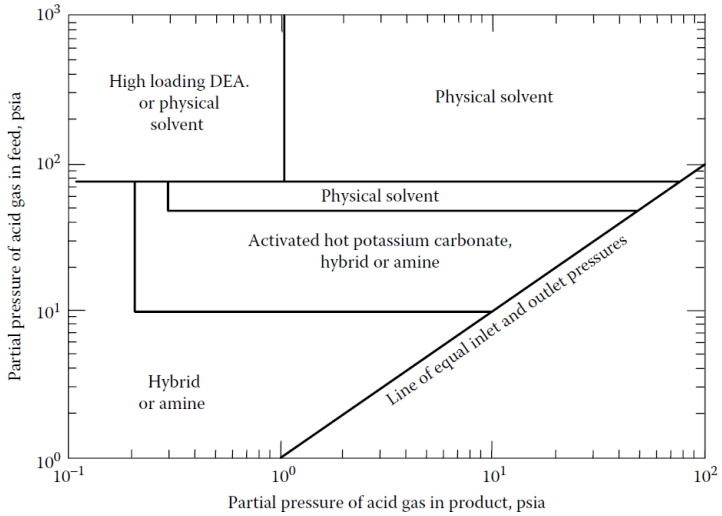

Figure 4: Process selection chart for simultaneous removal of H_2S and CO_2 [1]

Table 4 shows a detailed summary of the more widely used gas treating processes, including the degree of purification achievable, the selectivity for H_2S removal, and the removal of sulphur compounds.

Table 4: CO_2 and H_2S removal processes for sweetening [1]

Process	Capable of meeting H_2S specification	Removal of COS, CS_2, and mercaptans	Selective H_2S removal	Minimum CO_2 level obtainable	Solution subject to degradation? (Degradating species)
Monoethanol amine (MEA)	Yes	Partial	No	100 ppmv at low to moderate pressures	Yes (COS, CO_2, CS_2, SO_2, SO_3, and mercaptans)
Diethanol amine (DEA)	Yes	Partial	No	50 ppmv	Some (COS, CO_2, CS_2, HCN, and mercaptans)
Methyldiethanol amine (MDEA)	Yes	Slight	Some	Bulk removal only	No
Diglycol amine (DGA)	Yes	Partial	No	100 ppmv at moderate to high pressures	Yes (COS, CO_2, and CS_2)
Diisopropanol amine (DIPA)	Yes	COS only	Yes	Not applicable	Resistant to degradation by COS
Sulfinol®	Yes	Partial	Yes (Sulfinol-M)	50 ppmv	Some (CO_2 and CS_2)
Selexol®	Yes	Slight	Some	Can be slipped or absorbed	No
Rectisol®	Yes	Yes	No	1 ppmv	Not reported
Molecular sieves	Yes	Yes (excluding CS_2)	Some	Can meet cryogenic spec when CO_2 feed content < 2%	Not applicable
Membranes	No	Slight	No	Feed concentration dependent	Not applicable

In Table 5, a comparison is made between physical and chemical solvents.

Table 5: Comparison of chemical and physical solvents [1]

Chemical Solvents	
Advantages	**Disadvantages**
Relatively insensitive to H_2S and CO_2 partial pressure	High energy requirements for regeneration of solvent
Can reduce H_2S and CO_2 to ppm levels	Generally not selective between CO_2 and H_2S
-	Amines are in a water solution and the treated gas leaves saturated with water
Physical Solvents	
Advantages	**Disadvantages**
Low energy requirements for regeneration	May be difficult to meet H_2S specifications
Can be selective between H_2S and CO_2	Very sensitive to acid gases partial pressure

2.3.1.1. Chemical Solvent Absorption

There are several available processes for the removal of acid gases from NG using chemical absorption, as seen before in Figure 3. However, the most common one is with amines (or alkanolamines) and this process is explained with detail in the following sub-chapter.

2.3.1.1.1. Amines Process

Alkanolamines, or amines, are compounds formed from ammonia (NH_3) by replacing one or more of the hydrogen atoms with a hydrocarbon group with OH groups attached to it. Replacement of single hydrogen produces a primary amine (the most reactive), replacement of two hydrogen atoms produces a secondary amine, and replacement of all the hydrogen atoms produces a tertiary amine. The amines are used in water solutions in concentrations from 10 to 65 wt.% amines [1].

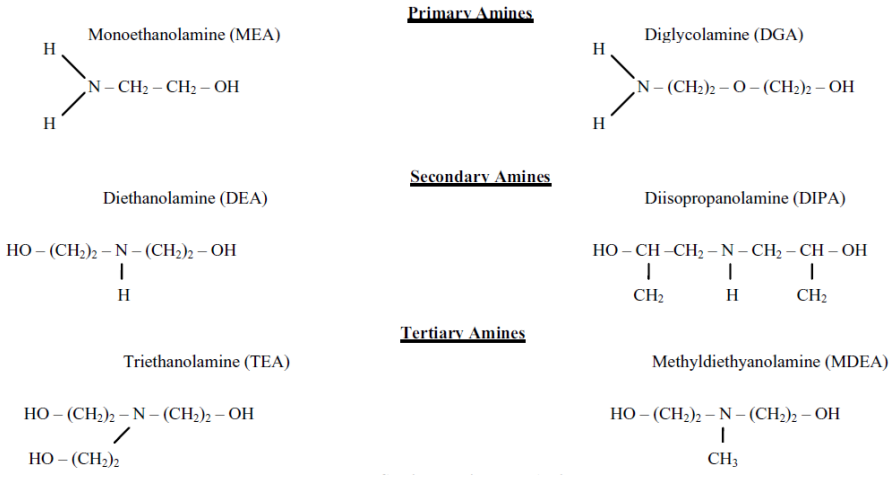

Figure 5: Molecular structures of commonly used alkanolamines [1]

Amines remove acid gases in two steps: first the gas dissolves in the liquid (physical absorption) and then the dissolved gas reacts with the amine. While the absorption from the gas phase is ruled by the partial pressure of the acid gases in the feed, the reactions in the liquid phase are governed by the reactivity of the dissolved species [1].

Amines are bases and they have the ability to form salts with the weak acid formed by the acid gases in an aqueous solution. The acid gases react to form a soluble acid-base complex and this reaction is highly exothermic [1].

H_2S reacts rapidly with amines regardless of the structure via a direct proton-transfer reaction, as shown below, to form the amine hydrosulphide [1]:

$$R_1R_2R_3N + H_2S \leftrightarrow R_1R_2R_3NH^+HS^- \quad (1)$$

Note that the previous reaction is shown for a tertiary amine but it also applies for the other amines.

For CO_2 the reaction is more complex, because it can occur via two different mechanisms. When dissolved in water CO_2 hydrolyses to form carbonic acid (H_2CO_3), which then slowly dissociates to bicarbonate (HCO_3^-). The bicarbonate then reacts in an acid-base reaction with the amine [1].

$$CO_2 + H_2O \leftrightarrow H_2CO_3 \quad (2)$$

$$H_2CO_3 \leftrightarrow H^+ + HCO_3^- \quad (3)$$

$$H^+ + R_1R_2R_3N \leftrightarrow R_1R_2R_3NH^+ \quad (4)$$

$$CO_2 + H_2O + R_1R_2R_3N \leftrightarrow R_1R_2R_3NH^+HCO_3^- \ (overall\ reaction) \quad (5)$$

This reaction is not as rapid as that of H_2S, since the dissociation of H_2CO_3 is relatively slow.

The other reaction mechanism requires the presence of reactive hydrogen in the molecular structure of the amine, as shown below, and is faster than the previous one. CO_2 reacts with the amine molecule to form the carbamate intermediate ($R_1R_2N^+HCOO^-$), which reacts with a second amine molecule to form the amine salt [1].

$$CO_2 + R_1R_2NH \leftrightarrow R_1R_2N^+HCOO^- \quad (6)$$

$$R_1R_2N^+HCOO^- + R_1R_2NH \leftrightarrow R_1R_2NCOO^- + R_1R_2NH_2^+ \quad (7)$$

$$CO_2 + 2R_1R_2NH \leftrightarrow R_1R_2NH_2^+R_1R_2NCOO^- \ (overall\ reaction) \quad (8)$$

This reaction is called the carbamate formation reaction and only occurs with primary or secondary amines, since tertiary amines do not have reactive hydrogens.

For primary and secondary amines, little difference exists between the H_2S and CO_2 reaction rates due to the availability of the carbamate formation for CO_2 absorption. Thus, primary and secondary amines are capable of complete removal of H_2S and CO_2. However, since tertiary amines have no reactive hydrogen available, they cannot form the carbamate. Therefore, they must react with CO_2 via the first and slower mechanism and MDEA (and other formulated MDEA products) yield significant selectivity towards H_2S: all of the H_2S is removed while some of the CO_2 goes through with the gas [1].

For all the reversible reactions above, high pressures and low temperatures drive the reactions to the right, while high temperatures and low pressures favour the reverse reaction [1].

A typical flowsheet for the removal of acid gases from NG using MEA is shown in Figure 6. Note that the operating conditions shown are representative and not definitive.

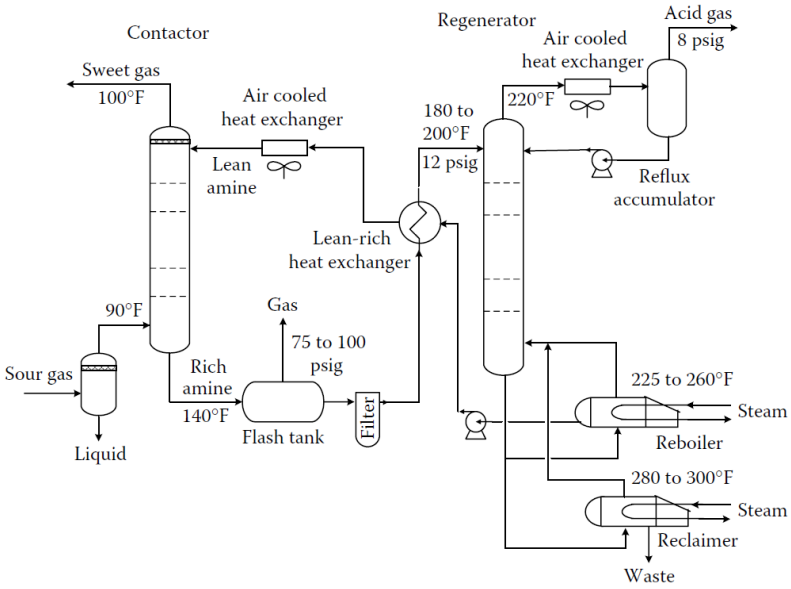

Figure 6: Process flow diagram for NG sweetening using MEA [1]

The sour gas usually enters the plant through an inlet separator to remove free liquids and/or solids that may be present [8]. The sour gas enters the bottom of the contactor and flows upward, counter current to the lean amine that enters the top of the absorber. The contactor is either filled with trays or

packing to achieve an intimate contact between the gas and the amine solution. The contactor operates above ambient temperature because of the combined exothermic heat of absorption and reaction [1]. A common practice is to operate with lean solvent's temperatures 5 to 8 ^{o}C higher than the NG's feed temperature to avoid foaming due to hydrocarbon condensation [11].

The sweet gas leaves the top of the absorber and passes through an outlet separator (not represented in Figure 6) to remove any amine lost and is usually directed to a dehydration unit [8]. The rich amine solution leaves the bottom of the tower and enters a flash tank, where the pressure is reduced to flash dissolved hydrocarbons present.

The rich amine is then heated and enters the regeneration column. The reboiler of the column generates vapour at the bottom that flows upward through trays or packing, contacting the rich amine and stripping the acid gases from the liquid that flows down. A stream of lean amine is removed from the stripper, cooled, and re-entered at the top of the contactor to cool and condense the vapour stream. The vapour, mostly acid gases and water vapour, exits at the top of the column. The lean amine leaving at the bottom of the regenerator is pumped and cooled before entering the absorber [1].

Particulates formed in the plant and being transported pose several issues. So, a filtration scheme of mechanical and activated carbon filters is necessary [8].

Amines can react with contaminants such as O_2 to form organic acids. These acids then react with the amine to form heat stable salts, which, as their name implies, are heat stable and must be removed since they accumulate in the amine solution. For MEA and DGA processes, heat stable salts are removed through a reclaimer that uses semi-continuous distillation. The reclaimer is filled with lean amine and a strong base (such as sodium carbonate) is added to neutralize the salts. A stream of 1-3% of the circulating amine is added to the reclaimer while the mixture is heated. Water and amine vapour are removed at the top and the contaminants stay in the liquid bottoms. DEA does not form a significant amount of non-regenerable degradation products and so it requires a more complex reclaiming through vacuum distillation or ion exchange [1].

2.3.1.2. Physical Solvent Absorption

In chemical absorption processes, acid gases are removed via physical absorption followed by chemical reaction. In processes such as Selexol® or Rectisol®, the sweetening of NG depends entirely on physical absorption.

2.3.1.2.1. Selexol® Process [1], [4]

The solvent used in this process is a mixture of homologues of the dimethyl ether of polyethylene glycol, shown to be chemically stable, non-toxic, and biodegradable.

$$CH_3—O—CH_2—(CH_2—O—CH_2)_N—CH_2—O—CH_3$$

Figure 7: General formula of Selexol® [1]

Since Selexol® has several applications, there is no common process flow diagram available, but an example is shown in Figure 8:

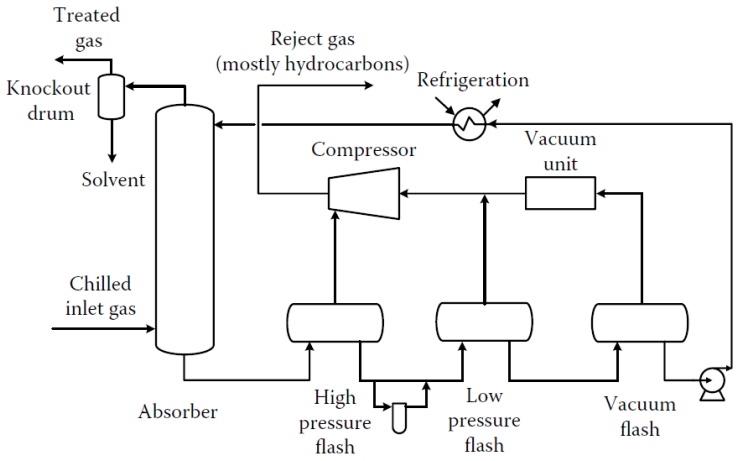

Figure 8: Flowsheet for a Selexol® gas treating plant [1]

The lean solvent is cooled with propane refrigerant before entering the absorber, where it absorbs CO_2 and some ethane and heavier hydrocarbons. The rich solvent is then regenerated by reducing the pressure in three flash drums from around 41.6 bar to 0.21 bar. The lean solvent is then recompressed and sent to the propane chiller. The sweet gas leaves at the top of the absorber and through a knockout drum and filter separator to remove entrained solvent and condensed hydrocarbons.

2.3.1.2.2. Rectisol® Process [4]

This process uses methanol as solvent and operates at much lower temperatures than other physical processes, with operating temperatures as low as -73 ^oC. This process can achieve very low concentrations, in the range of ppm, but due to the low temperatures and the need for low level refrigerants it has high plant costs.

2.3.1.3. Hybrid Solvent Absorption

In order to take advantage of the strengths of both chemical and physical solvents, some hybrid processes are available for NG sweetening, combining physical solvents with amines. Sulfinol® is one of the more commonly used hybrid processes and is explained with further detail in the following sub-chapter.

2.3.1.3.1. Sulfinol® Process [1], [4]

This process uses a physical solvent (sulfolane), a chemical solvent, such as DIPA or MDEA, and water. The solvent with DIPA is referred to as Sulfinol-D, while the one with MDEA is called Sulfinol-M.

The physical solvent removes the bulk of the acid gases while the chemical solvent purifies the gas to the final specification, all in a single step. A typical flow diagram of a Sulfinol® unit is shown in Figure 9, which is similar to that of a typical amine sweetening plant.

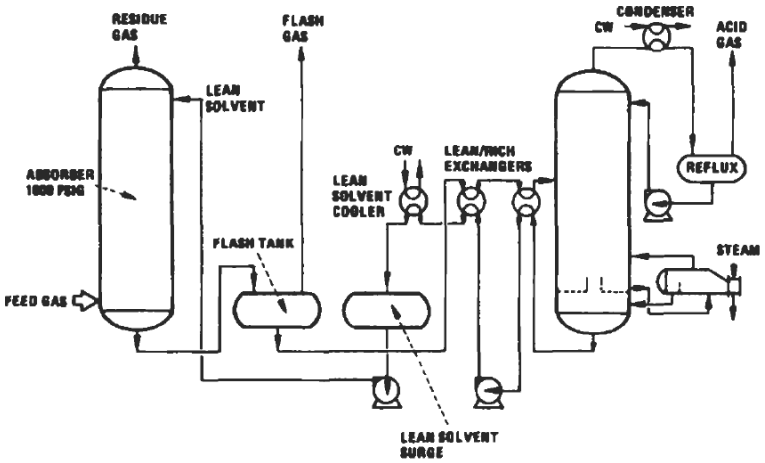

Figure 9: Flow diagram of Sulfinol® process [4]

2.3.1.4. Physical Adsorption [1]

Physical adsorption on synthetic zeolites can be effective in the removal of acid gases from NG, as well as for the removal of water. A typical flow diagram for removal of H_2S from NG is represented in Figure 10. Since the regeneration gas contains high quantities of H_2S, as well as water, as it leaves the adsorbent bed, it must be treated.

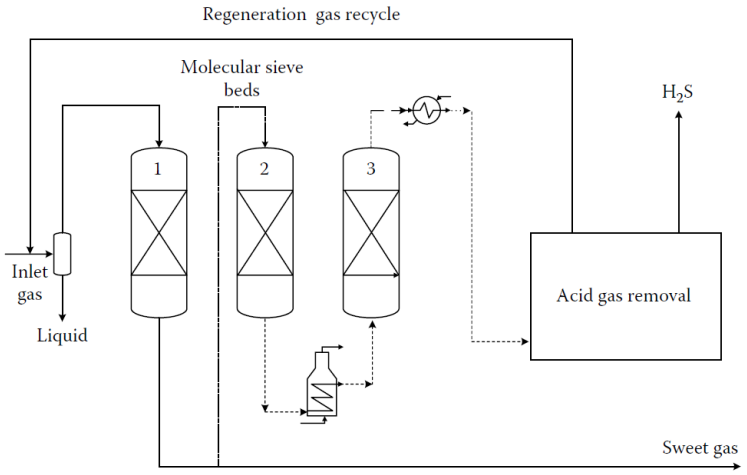

Figure 10: Process flow diagram of NG desulfurization plant [1]

2.3.1.5. Membranes [1]

Membranes are fundamentally used for bulk CO_2 removal and many different types have been developed or are under development for industrial separations. However, the industry standard is cellulose acetate: membranes of the solution-diffusion type, in which a thin layer of cellulose acetate is on top of a thicker layer of a porous support material. Permeable compounds dissolve into the membrane, diffuse into it, and then travel through the support material.

Commercial membrane configurations are either hollow fiber elements or flat sheets wrapped into spirally wound elements.

2.3.1.6. Industrial Application

In the present thesis, a flowsheet for the sweetening of NG is simulated using DEA as solvent. This chapter presents a simplified overview of some industrial applications of this solvent.

The SNPA-DEA process was developed by Societe Nationale des Petroles d'Aquitaine (SNPA, today Total) to treat a sour gas discovered in Lacq (southern France) in the 1950s. This process is used for high pressure and high acid gas content streams. The original process has been improved and PROSERNAT, who works in cooperation with Total and IFP Energies Nouvelles, proposed the use of high DEA solution concentrations up to 40 wt. %. In this way, AdvAmine™ processes have been developed for more than 50 years for all types of NG sweetening applications, including the HiLoadDEA process, which uses DEA as a solvent, for complete acid gases removal [12], [13]. This process is used in several plants, whose data is presented in Table 6.

Table 6: Data for some HiLoadDea units for NG sweetening [14]

Feed gas pressure (bar)	Feed gas H_2S (vol. %)	Feed gas CO_2 (vol. %)	Start-up year
65	4.2	6.0	1984
66	8.5	9.5	1980
66	21.5	14.7	1987
70	15.8	9.8	1957
70	34.6	6.1	1972

Although in Table 6 the locations of the plants are not specified, it is known that from 1969 the SNPA-DEA process predominated for recovery of sulphur from NG in Alberta, Canada [4].

There is also a gas plant operated by BP, located in South Lousiana and opened in 1970, which uses DEA as solvent, with a concentration of 30 wt. %. This plant has a NG feed with a concentration in CO_2 of 8.08 mol. % and in H_2S of 40 ppm and it was designed to remove 95% of acid gases from 120 MMSCFD raw NG [15].

However, the use of mixed amines, such as MDEA and DEA, is an increasing concept that can increase the amine solution concentration without increasing corrosion problems. An example of a conversion to mixed amines is Union Pacific Resources' Bryan gas plant, in Texas, which used DEA as a solvent. This plant was designed to process 35 MMSCFD of gas containing 2.91 % of CO_2 and 0.06 gr/100 ft_3 of H_2S by using a DEA solution of 35 wt. %. Since the plant was built in 1980, the CO_2 concentration in the inlet gas increased until the amine unit could not handle this increased concentration and the gas product specification was not met. The solution was adding MDEA to the existing DEA solution, increasing the CO_2 absorption without a significant increase in corrosion [16].

Also, see Appendix A-1.1 for projects regarding NG sweetening units using different solvents.

2.3.2. Dehydration

Typically, dehydration is important in three areas [1]:

- Gas gathering: water must be removed to reduce pipeline corrosion and prevent line blockage caused by hydrate formation;
- Product dehydration: both gas and liquid products have specifications on water content. Sales gas that leaves a plant is usually dry if cryogenic hydrocarbon liquid recovery is used. Liquid and gas streams may be water saturated after amine treatment or coming from underground storage. Most product specifications, except for propane, require that no free water be present.
- Hydrocarbon recovery: most plants use cryogenic processes to recover the C_2^+ fraction from inlet gas. If acid gases are removed by use of amine processes, the exit gas leaves water saturated. To prevent hydrate formation in the cryogenic section of hydrocarbon recovery, the water concentration should be 0.1 ppmv or less.

There are a number of processes available to perform the dehydration of NG. However, absorption and adsorption are the most common ones and therefore will be presented and explained with detail. Some less conventional methods include desiccant processes (use of a consumable salt desiccant, such as $CaCl_2$), membrane processes (attractive to meet pipeline specifications), refrigeration process with methanol, Twister® technology (offshore applications), and vortex tube technology (used to remove water from gas stored underground) [1].

2.3.2.1. Physical Absorption [1], [8]

Water levels in NG can be reduced to the 10 ppmv range with a physical absorption method in which the gas is contacted with a liquid that preferentially absorbs the water vapour. In order to do so, the solvent used should have the following properties:

- High affinity for water and a low one for hydrocarbons;
- Low volatility at the absorption temperature in order to reduce vaporization losses;
- Low viscosity for ease of pumping and to allow a good contact between the gas and liquid phases;
- Good thermal stability to prevent decomposition during regeneration;
- Low potential for corrosion.

Glycols (monoethylene glycol (EG), diethylene glycol (DEG), triethylene glycol (TEG), tetraethylene glycol (TREG), and propylene glycol) are the most commonly used absorbents in NG dehydration. Some of the more important properties of these glycols are shown in Table 7.

Table 7: Physical properties of commonly used glycols [1]

Property	EG	DEG	TEG	TREG
Formula	$C_2H_6O_2$	$C_4H_{10}O_3$	$C_6H_{14}O_4$	$C_8H_{18}O_5$
Molar mass (kg/kmol)	62.07	106.12	150.17	194.23
Normal boiling point (°C)	197.1	245.3	288	329.7 (decomposes)
Vapour pressure at 20 °C (kPa)	0.0075	0.0003	<0.001	<0.001

(continuation of previous table)				
Specific gravity at 20 ^{o}C	1.1153	1.1182	1.1255	1.1247
Viscosity at 20 ^{o}C (cP)	25	35.7	49	58.3
Critical pressure (bar)	82	46.05	33.1	25.9
Critical temperature (^{o}C)	446.85	406.85	440	522
Onset of initial decomposition (^{o}C)	240	240	240	240
Autoignition temperature (^{o}C)	427	364	349	358
Flammable limits in air, lower (vol%)	-	2	0.9	-
Flammable limits in air, upper (vol%)	-	12.3	9.2	-

TEG is the most common liquid desiccant used in NG dehydration, due to the following reasons:

- TEG is regenerated more easily to a concentration of 98-99 wt. % in an atmospheric stripper due to its higher boiling point and decomposition temperature, minimizing vaporisation losses;
- TEG has an initial theoretical decomposition temperature of 206.7 ^{o}C, whereas that of DEG is only 164.4 ^{o}C;
- Capital and operating costs are lower. Although TREG has a lower vapour pressure and tolerates higher regeneration temperatures, the additional cost outweighs the marginal increased benefits.

Figure 11 shows a typical and simplified flowsheet for a glycol absorption unit, which is similar to the flowsheet for a NG sweetening plant (see Figure 6).

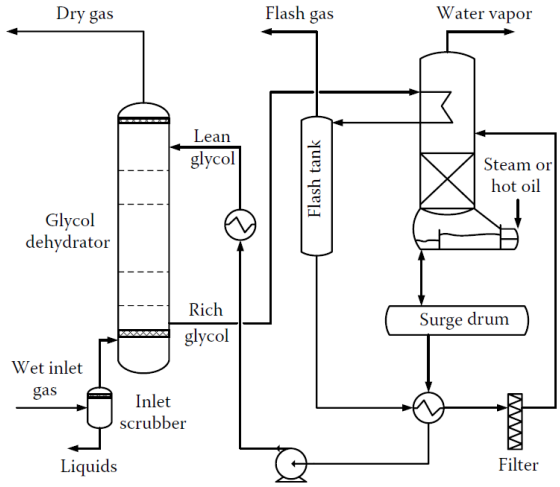

Figure 11: Schematic of a typical glycol dehydrator unit [1]

The wet gas passes through an inlet scrubber to remove solids and free liquids and then enters the bottom of the glycol contactor. Gas flows upward in the contactor, while the lean glycol solution (with little or no water) flows down over the trays or packing. The glycol solution absorbs water and leaves the column through the bottom, while dry gas exists at the top. If solvent is lost at the top of the column, a separator should be used to recover the solvent.

The rich glycol flows through a heat exchanger at the top of the still where it is heated and provides the coolant for the still's condenser. The heated solution then goes to a flash tank, where dissolved gases, mainly hydrocarbons, are removed.

The rich glycol from the flash tank is further heated with the still bottoms and then is fed to the still. Before entering the still, the rich glycol solution is filtered to prevent impurities such as solids and heavy hydrocarbons from plugging the regenerator and fouling the reboiler. The still produces water at the top and a lean glycol at the bottom, which goes to a surge tank before being returned to the contactor in order to assure constant flow of solvent to the absorber.

2.3.2.1.1. Enhanced Stripping Processes [4]

The operation of atmospheric pressure distillation units for glycol regeneration is limited by the maximum temperature tolerated without excessive decomposition of the solvent. Therefore, concentration of TEG from 98.5 to 99 wt. % is possible in a simple atmospheric pressure still, as the one shown in Figure 11. The use of an enhanced stripping process, such as the one in Figure 12, is necessary when higher concentrations of glycol are needed to meet strict dehydration requirements.

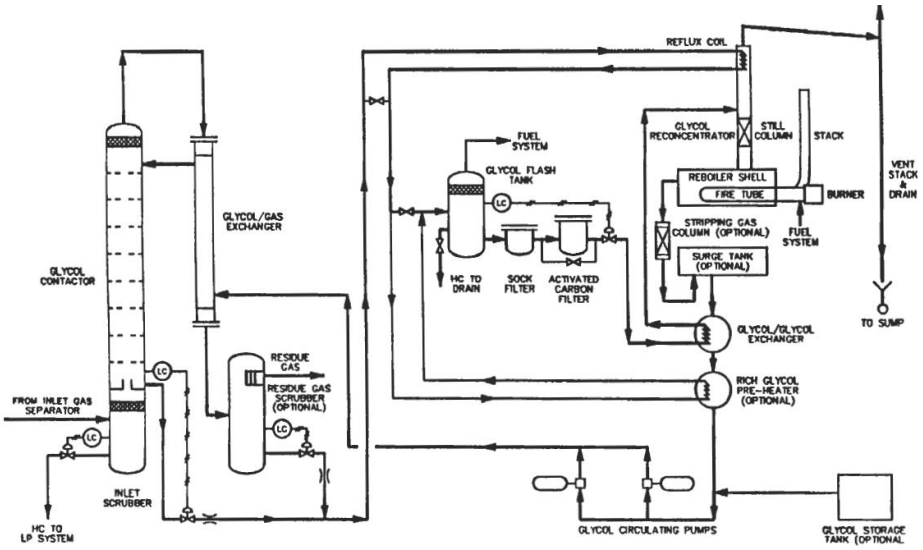

Figure 12: Flow diagram of a typical glycol enhanced stripping dehydration process [4]

The flowsheet in Figure 12 shows an optional stripping gas column between the reboiler and the surge tank, which operates on the hot lean glycol flowing from the reboiler to the surge tank. When this column is used, a small stream of dry NG is fed into the bottom of the stripping gas column to reduce the partial pressure of water vapour in the gas phase. The gas finally leaves the primary stripping column with the vented water vapour. It is possible to achieve glycol concentrations as high as 99.9 wt. % with this process.

Enhanced stripping can also be achieved by operating the reconcentrator under vacuum, as shown in Figure 13.

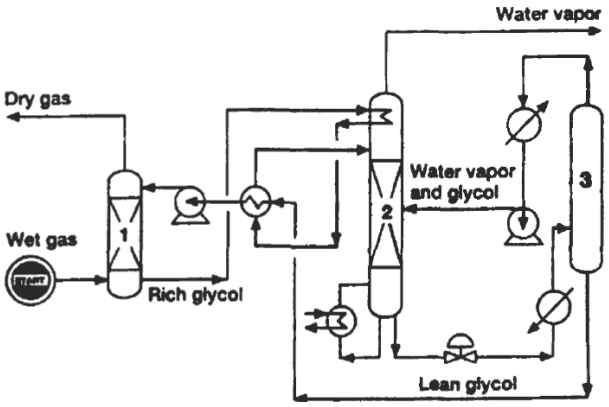

Figure 13: Flow diagram of glycol dehydration plant with vacuum dehydration [4]

The rich glycol is first concentrated by atmospheric pressure stripping in a conventional reconcentrator **(2)**. The partially regenerated glycol is flashed to subatmospheric pressure, reheated, and fed into a vacuum drum **(3)**. Vapours from the vacuum drum are partially condensed and pumped into the conventional regenerator. Glycol from the vacuum drum, at a concentration as high as 99.9 wt. %, is cooled and recycled back to the absorber **(1)**.

2.3.2.2. Physical Adsorption

Physical adsorption processes are also used for dehydrating NG streams. This process involves the transfer and consequent equilibrium distribution of one or more solutes between a fluid phase and particles, and the selectivity of a sorbent towards multiple solutes makes possible to separate solutes from a bulk fluid phase or from each other. Molecules are attracted to the sorbent surface due to two types of forces: dispersion-repulsion forces (van der Waals forces) and electrostatic forces, which are a result of a molecule or surface group having a permanent electric dipole, quadrupole moment, or net electric change [17].

Physical adsorption is an equilibrium process. Thus, for a given partial pressure (vapour-phase concentration) and temperature, an equilibrium concentration exists on the adsorbent surface that is the maximum concentration of the adsorbate on the surface. In addition to this, the polarity of the adsorbate influences its concentration on the adsorbent surface: polar molecules, such as water, will be more strongly adsorbed than weakly polar or non-polar components. Therefore, methane is displaced by the weakly polar acid gases, which are displayed by the strongly polar water [1].

Two steps are involved in adsorption processes: first, the component contacts the surface of the particles; after this, the adsorbate has to travel through the pathways inside the adsorbent. Because this process has two steps and since the second step is relatively slow, solid adsorbents take longer to achieve equilibrium with the gas phase than absorption processes [1].

Since the adsorption process is not instantaneous, formation of a mass transfer zone (MTZ) occurs in the bed. Therefore, there are three distinguishable zones in an adsorbent bed, as represented in Figure 14: equilibrium zone, MTZ, and active zone [1].

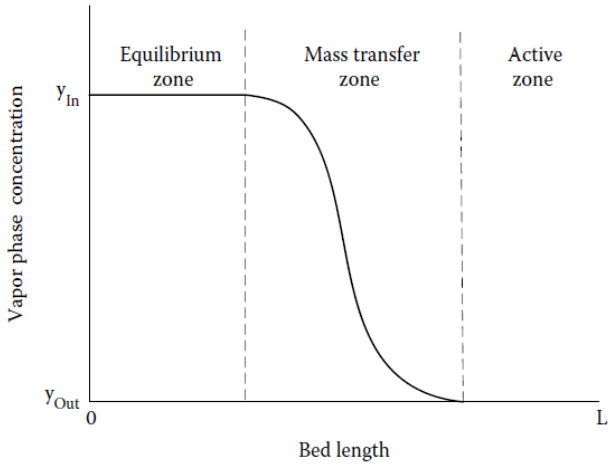

Figure 14: Adsorbate vapour-phase concentration profile in the different zones of an adsorption bed [1]

Analysing Figure 14 it is possible to see that, at any instant in the adsorption step, the adsorbent particles upstream and downstream the MTZ do not participate in the mass transfer process. Upstream the MTZ (equilibrium zone) the adsorbent is in equilibrium with the feed and no further adsorption takes place (the adsorbent is saturated). Downstream the MTZ (active zone), no adsorption has yet occurred since the adsorbent is not in contact with any adsorbate molecules [1], [18].

As the fluid is passed through the bed, transfer of adsorbate molecules initially takes place at the bed entrance, until the adsorbent in this region becomes saturated with the adsorbate molecules. Once this happens, the zone in which the mass transfer takes place moves progressively through the bed towards the exit, which is represented in Figure 15. When breakthrough takes place the adsorbent must be regenerated [18].

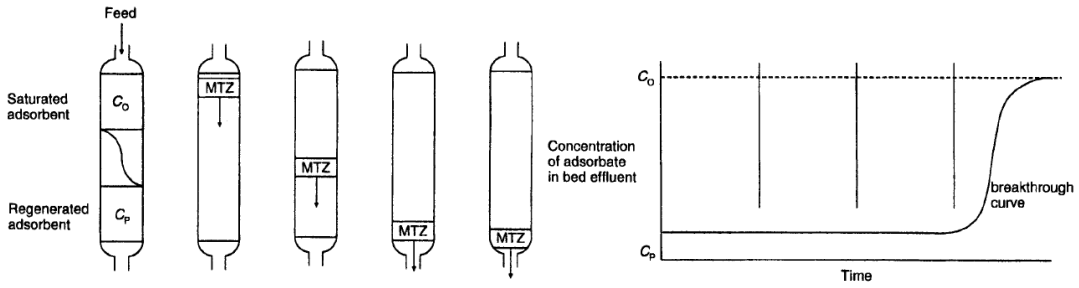

Figure 15: Concentration profile, mass transfer movement and breakthrough curve in adsorption bed [18]

The adsorption process holds several advantages over the absorption one [4]:

- Provides extremely low dew points;
- Is insensitive to moderate changes in gas temperature, flowrate, pressure, etc.;
- The operation and design is simple;
- Is free from problems of corrosion, foaming, etc..

However, there are also some disadvantages associated, such as [4]:

- High initial costs;
- Higher pressure drops;
- Adsorbent susceptible to poison or breakup;
- High heat requirements;

- Use of fixed bed process that requires two or more beds for continuous operation;
- Limited capacity and infeasibility for removing large amounts of water.

Nonetheless, for LNG production, which has a tight water specification, adsorption processes are much more effective than absorption ones since water is much more strongly removed than any other components in the NG stream [4].

There are several solid desiccants commercially available. Therefore, the selection of a proper desiccant is a complex problem. The following properties are desirable for desiccants used in NG dehydration [8]:

- High adsorption capacity at equilibrium, which lowers the required adsorbent volume, allowing the use of smaller vessels with reduced costs;
- High selectivity, which minimizes the undesirable removal of valuable components, while reducing operating costs;
- Easy regeneration, minimizing overall energy requirements and operating expenses;
- Low pressure drop;
- Good mechanical properties in order to lower maintenance requirements;
- Inexpensive, noncorrosive, nontoxic, chemically inert, high bulk density and no significant volume change upon adsorption and desorption.

The most common commercial desiccants used in this application are silica gel, molecular sieves, and activated alumina. Some of their properties are summarized in Table 8.

Table 8: Properties of commercial solid desiccants for dehydration of NG [1]

Property	Silica Gel	Activated Alumina	Molecular Sieve 4A
Shape	Spherical	Spherical	Pellets and beads
Bulk density (kg/m^3)	785	769	640-720
Particle size	5-2 mm	3 mm, 5 mm, 6 mm diameter	1.6 mm, 3.2 mm, 6 mm diameter cylinders
Packed bed (% voids)	35	35	35
Specific heat (kJ/(kg.K))	1.05	1.00	1.00
Surface area (m^2/g)	650-750	325-360	600-800
Pore volume (cm^3/g)	0.36	0.5	0.28
Regeneration temperature (^{o}C)	190	160-220	200-315
Average pore diameter (Å)	22	-	3, 4, 5, 10
Minimum dew point temperature of effluent (^{o}C)	-60	-75	-100
Average minimum moisture content of effluent gas (ppmv)	5-10	10-20	0.1

Silica gel (manufactured from sulphuric acid and sodium silicate, $SiO_2.nH_2O$) is widely used for gas and liquid dehydration and hydrocarbon recovery from NG [8] and is useful where high capacity is required at low temperature and moderate vapour pressures [19]. Activated alumina is a manufactured or natural occurring form of aluminium oxide that is activated by heating [8]. The capacity of activated alumina is higher than silica gel at high temperatures and it was therefore used for drying warm air or

gas streams. However, it has been replaced by molecular sieves, since they exhibit a higher capacity and lower equilibrium vapour pressure [19].

Molecular sieves are crystalline alkali metal alumina silicates with a three-dimensional interconnecting network of silica and alumina tetrahedral. Molecular sieves are the most versatile desiccants because they can be manufactured for a specific pore size. They are [8]:

- Capable of dehydration to less than 0.1 ppm water content;
- The best choice for dehydration prior to cryogenic processes;
- Excellent for H_2S and CO_2 removal, dehydration, high temperature dehydration, heavy hydrocarbons liquids removal, and highly selective removal;
- More expensive, but offer greater dehydration;
- Require higher temperatures for regeneration, having higher operating costs.

Figure 16 shows a diagram of a two-bed adsorber system. One bed (adsorber #1 in Figure 16) dries the gas while the other (adsorber #2 in Figure 16) goes through a regeneration cycle. The wet gas feed goes through an inlet separator to remove entrained liquids before it enters the top of the active bed. The gas flows down the bed to avoid fluidisation. The dried gas then goes through a dust filter to catch fines before the gas exits the unit. This filter is extremely important, especially if the gas goes on to a cryogenic section with plate-fin heat exchangers, since dust can accumulate and reduce heat transfer and increase pressure drop [1].

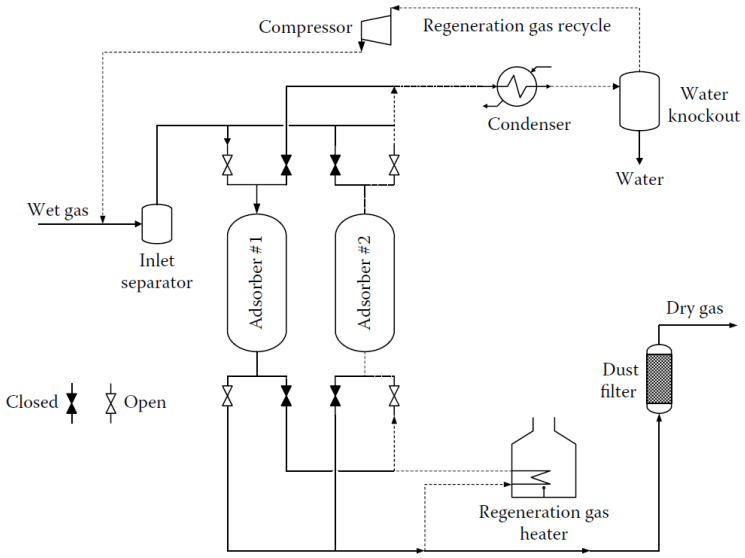

Figure 16: Schematic of a two-bed adsorption unit [1]

In Figure 16, there is a slip stream of dry gas returning to the bed that is being regenerated. This regeneration involves heating the bed, removing the water, and cooling. The regeneration gas is heated to both heat the bed and remove adsorbed water. The regeneration gas enters at the bottom of the bed, counter current to flow during adsorption, to make sure that the lower part of the bed is the driest and that any contaminants trapped in the upper section stay out of the lower one. The hot and wet regeneration gas then goes through a cooler and inlet separator to remove the water before being recompressed and mixed with the incoming wet feed gas. To complete the regeneration cycle, unheated regenerated gas passes through the bed to cool it before it is placed in drying service [1].

There are different ways to regenerate the bed other than increase the bed temperature, such as reduce the total pressure, reduce the partial pressure with a stripping gas, or displace the adsorbent [4].

2.3.2.3. Industrial Application

The dehydration of NG is one of the most important steps in NG processing. Therefore, it is widely used in the industry, as it can be seen in Appendix A-1.2.

3. Materials and Methods

In the present thesis, flowsheets were assembled for the simulation of the natural gas (NG) sweetening and its dehydration. For their development, gPROMS®, a process simulator software provided by Process Systems Enterprise Ltd. (PSE), was used. So, gPROMS® ModelBuilder and gPROMS® ProcessBuilder were used to build, validate and execute, and deploy steady-state and dynamic process models [20], and its functioning, as well as the physical properties packages used for their estimation, are presented in the present chapter.

3.1. gPROMS® as Model Builder [21], [22]

A model developed in gPROMS® is defined as a set of quantities and mathematical equations that, when coupled with a set of specifications, describe the behaviour of a system. Thus, a model includes a set of equations, variables, and parameters. The value of the parameters is defined on the SET section of the model, whereas variables can either be calculated from equations or assigned on the ASSIGN section of the model. Each variable belongs to a variable type and has upper and lower bounds, and a default value. In the TOPOLOGY section of the model, the connections between objects are defined. These connections can be either written by code or by dragging and dropping objects from the Project Tree and connecting them. Therefore, it is possible to build models in gPROMS® graphically in the TOPOLOGY tab of the model.

A component model is a set of equations (LANGUAGE tab) that describes the physical and chemical behaviour of a unit. These models are usually taken from an existing library, such as the GPE libraries. In this manner, a flowsheet is a composite model, i.e., a model that contains other entities as sub-models, built up from component models that represent a process made up of connected unit operations. The required specifications are made using specification dialogs for each component model, which correspond to setting parameters and assigning variables. An illustrating specification dialog box is shown for a heat exchanger (HE_5) in Figure 17, where a temperature of 30 ºC was attributed.

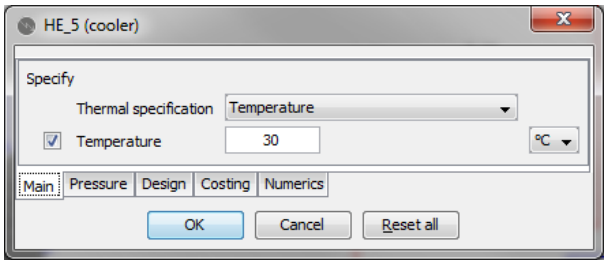

Figure 17: Specification dialog of the cooler model

3.2. Physical Properties Package

Most process models in gPROMS® make use of physical properties such as density, enthalpy, and fugacity, which are usually function of temperature, pressure, and composition [23]. Thus, the choice of the right model for the prediction of these properties is a key factor.

In this way, Multiflash™, with the Peng-Robinson (PR) equation of state (Appendix A-2), was used for the physical properties estimation of the dehydration of NG with glycol and molecular sieves, whereas gSAFT® was used in the sweetening flowsheet using amines. In the following sub-chapters, a detailed explanation of each one is presented.

3.2.1. Multiflash™ [24], [25]

Multiflash™ is an advanced software package that allows complex equilibrium calculations. The crucial thermodynamic property calculation performed in this package is the determination of phase equilibrium. This is based on the fundamental relationship that at equilibrium the fugacity of a component is equal in all phases. For a single vapour-liquid system:

$$f_i^v = f_i^l \tag{9}$$

where f_i^v is the fugacity of component i in the vapour phase and f_i^l is the fugacity of component i in the liquid phase. The models used in Multiflash™ to represent the fugacities fall into two categories: equation of state methods and activity coefficient methods. With an equation of state method, all thermal properties can be derived from an equation of state. On the other hand, an activity coefficient method derives the vapour phase properties from an equation of state, whereas the liquid properties are determined from the summation of the pure component properties to which a mixing term or an excess term has been added.

Equations of state can be used over wide ranges of temperature and pressure, including the sub-critical and supercritical regions. They are used for ideal and slightly non-ideal systems such as the oil and gas industry, where modelling of hydrocarbons systems is common.

The simple cubic equations of state PR and Redlich-Kwong-Soave (RKS) are widely used in gas processing, refinery, and petrochemical applications. They require limited pure component data, are robust and efficient, and usually give broadly similar results. However, there is some evidence that RKS gives better fugacities and PR better volumes (densities). The PR equation is accurate for calculating enthalpy, entropy departures, vapour-liquid equilibrium (VLE), liquid densities, and vapour density in NG processing operations.

3.2.1.1. Binary Interaction Parameters

Equations of state describe systems more accurately when binary interaction parameters (BIPs) have been derived from the regression of experimental VLE data. BIPs are adjustable factors used to obtain adequate predictions for mixtures. The closer the binary system is to ideality, the smaller the size of the BIP, which will be zero for ideal systems [25].

BIPs were therefore estimated from experimental VLE data for the dehydration of NG with glycol for a more accurate prediction, since most of the BIPs present in Multiflash™ were equal to zero, which does not correspond to the reality. In this way, several VLE data obtained in the literature was used for the following binary systems:

Table 9: Binary systems considered for BIP estimation and respective references

Binary system	Literature reference	Binary system	Literature reference
CH_4-C_2H_6	[26]	n-C_4H_{10}-CO_2	[26]
CH_4-C_3H_8		i-C_5H_{12}-CO_2	
CH_4-n-C_4H_{10}		i-C_5H_{12}-H_2S	
CH_4-n-C_6H_{14}		n-C_5H_{12}-n-C_6H_{14}	
CH_4-N_2		n-C_5H_{12}-CO_2	
CH_4-CO_2		n-C_5H_{12}-H_2S	
CH_4-H_2S		n-C_6H_{14}-N_2	
C_2H_6-C_3H_8		n-C_6H_{14}-CO_2	
C_2H_6-i-C_4H_{10}		n-C_6H_{14}-H_2S	
C_2H_6-n-C_4H_{10}		H_2O-H_2S	
C_2H_6-n-C_5H_{12}		N_2-CO_2	
C_2H_6-n-C_6H_{14}		CH_4-H_2O	[27]
C_2H_6-N_2		CH_4-TEG	[28]
C_2H_6-CO_2		C_2H_6-TEG	
C_3H_8-n-C_5H_{12}		C_3H_8-TEG	
C_3H_8-H_2O		CO_2-TEG	
C_3H_8-CO_2		H_2S-TEG	
i-C_4H_{10}-CO_2		C_3H_8-i-C_4H_{10}	[29]
i-C_4H_{10}-H_2S		C_3H_8-n-C_4H_{10}	
n-C_4H_{10}-H_2O		H_2O-TEG	[30], [31], [32]
n-C_4H_{10}-N_2		-	-

For isothermal P-x data the pressure for the bubble point of the mixture was calculated, while for isothermal P-y data the pressure for the dew point was determined. Then, the residue between the experimental and predicted Multiflash™ data was minimized by varying the BIP for the binary system. This was made using PR equation of state and connecting Multiflash™ to Microsoft Excel®.

An example is shown in Figure 18 for the H_2O-TEG system using a 303.15 K experimental isotherm and comparing it to Multiflash™'s predictions with the default BIP (-0.24) and the optimized one (-0.60).

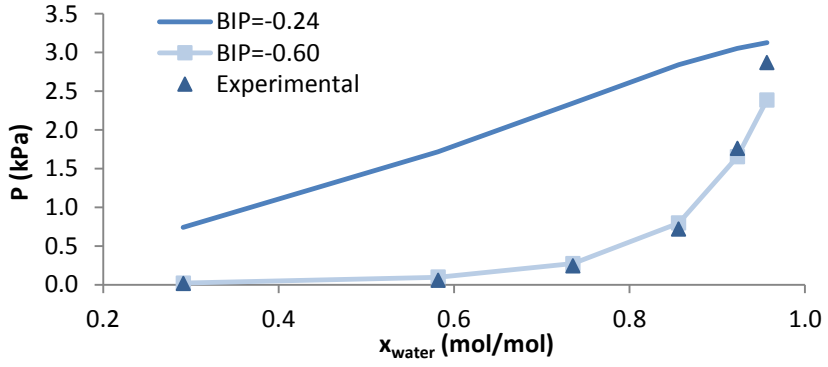

Figure 18: 303.15 K isotherm P-x for the binary system H_2O-TEG

There is a notable deviation between the experimental data and the pressure profile using Multiflash™'s default BIP. By minimizing the residue between these two profiles, one can see that both profiles are now more similar, resulting in a value of -0.60 for the optimized BIP.

BIPs can have a constant, linear, or quadratic dependence of the temperature depending on how strong this dependence is, according to the following equation:

$$k_{ij} = k_0 + k_1 T + k_2 T^2 \quad (10)$$

So, the relation between optimized BIPs and temperature for each binary system was adjusted to either a constant, linear, or quadratic relation. Then, the different k constants (Appendix A-3) were introduced on Multiflash™.

3.2.2. gSAFT®

The Statistical Associating Fluid Theory (SAFT) is an advanced molecular thermodynamic method that is able to predict thermodynamic properties of mixtures. SAFT has significant advantages over the traditional equations of state such as PR, which is better suited to near-spherical molecules. The main advantage of SAFT is that it is predicted by a representation of the molecule that includes its shape, size, and specific interactions with other molecules within the mixture, which means that SAFT accounts for non-spherical molecules, attraction and repulsion between molecules, and strong directional interactions. Therefore, SAFT is capable of predicting properties beyond the range of conditions covered by experimental data. Since SAFT's approach accounts for electrostatic, polar, and other association forces, this method is a great tool for modelling the behaviour of systems with polar solvents, hydrogen bonded fluids, and polymers, considered complex materials [20].

gSAFT® Physical Properties Package, a PSE's product platform, is an efficient implementation of SAFT-Variable Range Square Well (SAFT-VR SW) and SAFT-γ Mie equations of state [22].

SAFT-VR SW considers molecules as a whole or as associating chains of a small number of segments, whereas SAFT-γ Mie deals with molecules constructed from well-defined functional groups such as $–CH_2$ and $–CH_3$ [20].

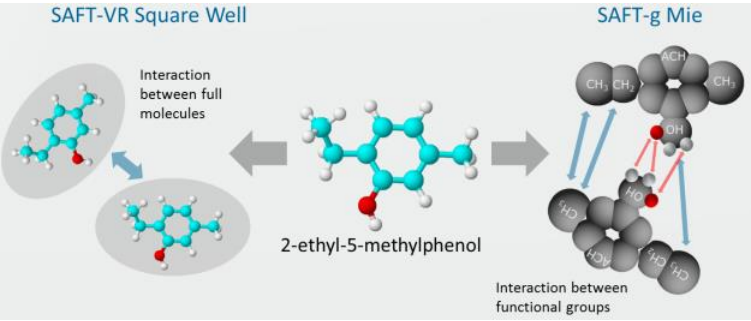

Figure 19: Difference between the two SAFT methods using 2-ethyl-5-methylphenol as an example [20]

SAFT-VR SW is used in the simulation of the sweetening flowsheet. This equation of state is an extension of the original SAFT methodology, which deals with systems with variable polarities. As stated before, molecules are considered as associating chains of spherical segments with variable attractive interactions. Outside the areas of parameter fit, SAFT-VR SW predictions may be less accurate than the ones using SAFT-γ Mie due to a smaller number of parameters. However, predictions by SAFT-VR SW are computationally faster [20].

For further information on SAFT-VR SW equation of state refer to Gil-Villegas et al. [33] and Galindo et al. [34].

4. Components Model Description [24]

This chapter presents an overview of the models used in the flowsheets' implementation, summarizing their purpose and the main specifications needed for each one. All the models shown already existed in the General Process Engineering (GPE) model library of gPROMS®. This library is a collection of commonly used process equipment and is designed to allow quick construction of process flowsheets models that are suitable in steady state and dynamic simulations.

In all the models present in this chapter, the blue ports represent material ports, whereas red ports represent energy connections. On the other hand, the green ports can be connected to auxiliary models such as the adj_spec model, which is presented in Chapter 4.5.1.

4.1. Basic Models

4.1.1. Source_material

The source_material model defines a material stream entering the process and it is used to represent the streams entering the gas processing flowsheets. The physical property package to be used must be specified, as well as the temperature (or vapour fraction), and pressure. The molar/mass fractions of the components and the overall flowrate, or the component flowrates, also need to be specified.

Figure 20: Topology representation of the source_material model

4.1.2. Source_material_reversible

This model is similar to the one presented before except for the adding of an option that allows the monitoring of the total amount of material entering and leaving the source during a dynamic simulation.

Figure 21: Topology representation of the source_material_reversible model

4.1.3. Sink_material

The sink_material model, opposite to the source one, is used to define a material stream leaving the flowsheet. Since there are no flow reversal situations nothing needs to be specified for this model.

Figure 22: Topology representation of the sink_material model

4.1.4. Sink_material_reversible

Since this model allows flow reversal situations, one can specify the pressure at the system boundary for the purposes of pressure-driven flow (dynamic simulation). Also, the composition and temperature of the stream that would enter the system when flow reversal takes place need to be assigned.

Figure 23: Topology representation of the sink_material_reversible model

4.1.5. Mixer

This model represents a mixer where a value for the pressure may be specified. The mixers used in the flowsheets assume the outlet pressure as the minimum of the inlet pressures.

Figure 24: Topology representation of the mixer model

4.1.6. Stream_analyzer

This model, when connected to a stream, gives detailed information about the stream conditions such as temperature, pressure, components flowrates, components mass fractions, vapour fraction, and others.

Figure 25: Topology representation of the stream_analyzer model

4.2. Separation Models

4.2.1. Separator

The separator model, used as an inlet scrubber, a flash tank, and a vacuum drum, separates a stream in a vapour phase (at the top) and a liquid one (at the bottom). One can specify the heat duty, temperature, vapour fraction, or others.

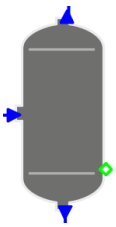

Figure 26: Topology representation of the separator model

For all the separators used in the simulations, the only specification that was made was that the separators worked adiabatically.

4.2.2. Column_section

The column_section model represents an absorber with equilibrium stages for the separation of impurities from a natural gas (NG) stream through physical/chemical absorption. The absorber has two inlets and two outlets, and works in counter current flow. In this model, the number of stages needs to be assigned, as well as the pressure of the column and, optionally, the pressure drop.

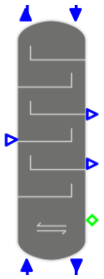

Figure 27: Topology representation of the column_section model

4.2.3. Distillation_column

The regenerators in the flowsheets are represented by a distillation_column model with equilibrium stages. The number of stages and the feed(s) stage(s) are assigned, in addition to the pressure and, optionally, the pressure drop, the reboiler and condenser type, and the boilup and reflux ratios.

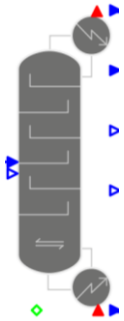

Figure 28: Topology representation of the distillation_column model

4.2.4. Adsorption_bed_alternative_multilayer

This model is used to represent the adsorption bed in the water adsorption scheme. The model describes an axially distributed adsorption bed in terms of mass and energy transport through the bed, as well as the mass and energy transport between the gas phase and the adsorbent. The direction of the mass flow can change depending on the pressures specified in the sinks and sources models connected to this model. One needs to specify the bed and adsorbent properties, information regarding mass and heat transfer, data for the adsorption isotherm and an initial gas composition in the bed.

Figure 29: Topology representation of the adsorption_bed_alternative_multilayer model

The mass and energy balances of this model, which already existed in the GPE adsorption library, are presented in Appendix A-7.1

4.3. Heat Transfer Models

4.3.1. Heater

This model represents a heat exchanger that provides heat to a fluid stream (blue ports in Figure 30). Some thermal specifications are available, such as outlet temperature, heat duty, and others. Also, one can specify the pressure drop along the heater. The heat duty of the heat exchanger may be specified as from an external energy connection that would be connected to the red port shown in Figure 30.

Figure 30: Topology representation of the heater model

4.3.2. Cooler

This model represents a heat exchanger that cools a fluid stream. It is similar to the heater model, with the same specifications required.

Figure 31: Topology representation of the cooler model

4.3.3. Heat_exchanger

This model calculates the heat exchanged between a hot and a cold stream, and it represents the lean-rich solvent heat exchangers. The specifications are similar to the ones concerning the heater and cooler models, but in this particular model one can choose to specify variables regarding either the hot stream or the cold stream, or both.

Figure 32: Topology representation of the heat_exchanger model

4.4. Flow Transportation Models

4.4.1. JT_valve

This model represents a Joule-Thomson valve where the pressure, flow coefficient, or temperature may be specified.

Figure 33: Topology representation of the JT_valve model

4.4.2. JT_valve_reversible

The JT_valve_reversible model is similar to previous model if the design option is deactivated. However, one can choose other options in the *Design* tab, presented in Figure 34: *Performance* or *Design*.

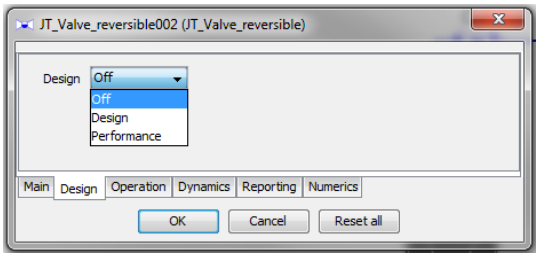

Figure 34: JT_valve_reversible dialog box (*Design* tab)

If the *Design* option is chosen, the leakage fraction and the outlet pressure need to be assigned. On the other hand, if the *Performance* option is activated, the pressure does not need assignment, only the leakage fraction, the valve coefficient, and the recovery factor (when vapour phase is chosen).

Also, in the *Operation* tab shown in Figure 35 the user may fix the stem position (*Specified here*), choose to determine the stem position by connecting the valve to a scheduling model (control of the valve according to the operation schedule defined) by activating the *From connection* option, or choose *Perfect Control (no dynamics)* where the stem position is perfectly controlled to maintain the outlet specification.

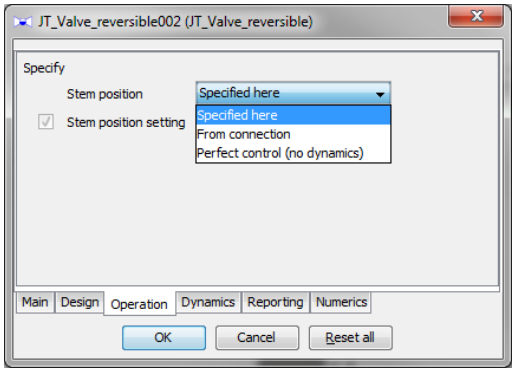

Figure 35: JT_valve_reversible dialog box (*Operation* tab)

4.4.3. Pump

This model describes a pump for liquid transportation and increase in pressure. It is possible to specify the outlet pressure, pressure difference, or pressure ratio.

Figure 36: Topology representation of the pump model

4.5. Other Models

4.5.1. Adj_spec

The adj_spec model allows the user to assign a variable with a target value that must be met by changing a second variable. All this is made by connecting the different models to the adj_spec model through the green ports in Figure 37.

Figure 37: Topology representation of the adj_spec model

4.5.2. Recycle_breaker

The recycle_breaker model is used to facilitate the initialization of units with closed loops and recycles, solving numerical issues.

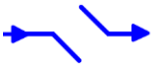

Figure 38: Topology representation of the recycle_breaker model

5. Modelling of Natural Gas Purification

In this chapter, the implementation of different flowsheets is presented with detail. Firstly, is presented the flowsheet for the sweetening of natural gas (NG), i.e., the removal of CO_2 and H_2S using amines. Then, it will be shown the flowsheet for NG's dehydration with glycol. At the end, a sub-chapter relating to the dehydration of NG with molecular sieves is also presented.

5.1. Sweetening with Amines

In the present work, a simulation was made for the sweetening of NG using a diethanol amine (DEA) solution in gPROMS® ProcessBuilder. The flowsheet replicated is based on data from Abdulrahman et al. [5] and its assembling is presented in the next sub-chapter, as well as the operating conditions specified in the different models. Next, the simulation results obtained are shown, as well as some sensitivity analyses performed.

5.1.1. Flowsheet Assembling [5], [35]

The flowsheet assembled in gPROMS® for the sweetening of NG is presented in Figure 39.

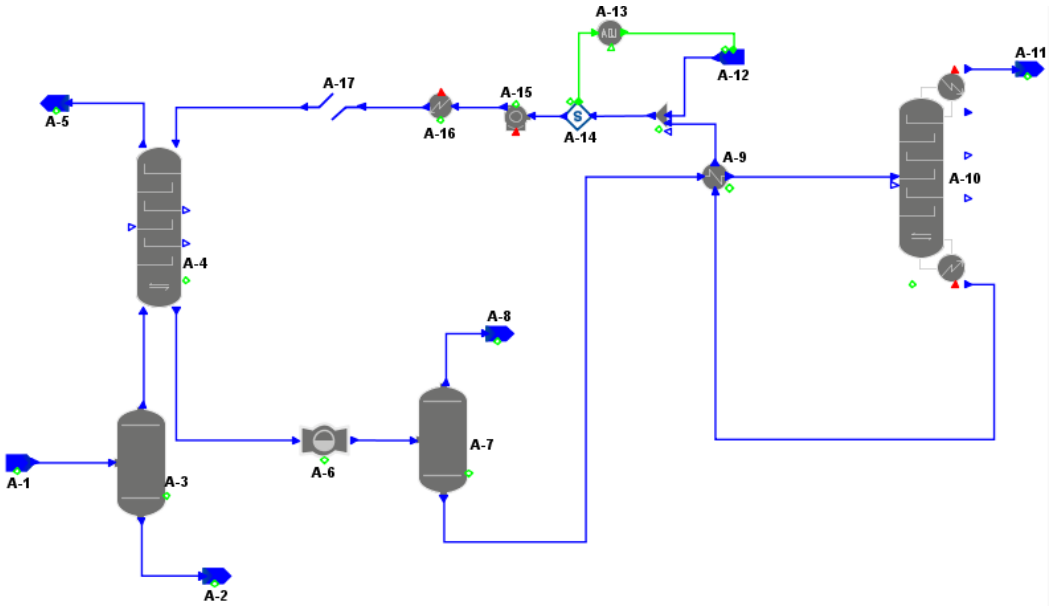

Figure 39: NG sweetening assembled flowsheet

The NG feed (**A-1**) entering the sweetening unit (Figure 39) is at 38 ºC and 35.5 bar, and at a flowrate of 120 $stdm^3/h$, with the following composition:

Table 10: Composition of NG feed [5]

Component	Molar composition (%)
H_2S	5.37
CO_2	4.47
N_2	0.11
H_2O	0.13

(continuation of previous table)	
CH_4	63.27
C_2H_6	13.88
C_3H_8	6.02
i-C_4H_{10}	1.36
n-C_4H_{10}	2.44
i-C_5H_{12}	1.03
n-C_5H_{12}	0.73
C_6H_{14}	1.19

The gas goes through a knock out drum (**A-3**) in order to remove free liquids (**A-2**) carried with the gas. The gas is then sent to the bottom of the absorption column (**A-4**), which is also fed with a solvent solution (**A-17**). The solvent is a DEA solution (35 wt. %), which enters at the top of the column at a volumetric rate of 400 m^3/h and at 40 ^oC and 35.5 bar. The absorber has 20 equilibrium stages and the pressure is specified (35.5 bar).

The rich amine is directed to a valve (**A-6**) in order to reduce the pressure to 620 kPa and then to be flashed in a flash tank (**A-7**), where at the top the hydrocarbons (as well as some CO_2 and H_2S) are recovered. The rich amine solution leaving the flash tank is heated to 95 ^oC (the lean amine after regeneration is the hot stream) with a pressure drop in the heat exchanger **A-9** of 70 kPa.

The rich solvent needs to be regenerated before being recycled back to the absorber and this is done with a distillation column (**A-10**) with a kettle reboiler and a partial condenser. The specifications made for the regenerator are presented in Table 11. Note that the value of the boilup ratio was defined in order to obtain the desired DEA concentration in the regenerated solvent stream.

Table 11: Operating conditions specified for the regenerator [5], [35]

Number of stages	23
Feed stage	4
Condenser set	Full reflux[5]
Average column pressure (bar)	1.9
Boilup ratio (mol/mol)	0.12
Reflux ratio (mol/mol)	1.5

The regenerated amine is cooled in the amine-amine heat exchanger (**A-9**) and a water make-up (**A-12**, at 25 ^oC) is added to the solvent solution in order to obtain a flowrate of 400 m^3/h entering the absorber. This flowrate adjustment is done with the help of an adj_spec model (**A-13**), which achieves the desired solvent's flowrate by adjusting the flowrate of make-up.

Table 12: Specification of the adj_spec (**A-13**) model

Variable	Specification	Unit
Target variable	Mass flowrate	-
Target value	111.7	kg/s
Adjust signal variables	Mass flowrate	-
Adjusted variable initial guess	1	kg/s

[5] Top product liquid flowrate set to 0 kg/h.

Finally, the lean solvent is pumped (**A-16**, outlet pressure: 35.5 bar) and cooled again (**A-15**, to 40 ^{o}C) before being recycled to the absorber.

5.1.2. Simulation Results

gPROMS® simulation results are presented in this sub-chapter regarding the units featured in Figure 39.

5.1.2.1. Separation Models

The results for the inlet scrubber (**A-3**) are presented in Table 13. This unit removes any free liquids at the bottom from the NG feed stream and a vapour stream is obtained at the top, which will enter the absorber column (**A-4**).

Table 13: Inlet and outlets of inlet scrubber (**A-3**)

	NG feed (A-1)	**Vapour outlet**	**Liquid outlet (A-2)**
Temperature (^{o}C)	35	35	35
Pressure (bar)	35.5	35.5	35.5
Mass flowrate (kg/s)	37.7	34.2	3.5
Mass composition (%)			
H_2S	7.2	7.4	5.1
CO_2	7.8	8.3	2.9
N_2	0.1	0.1	0
H_2O	0.1	0.1	0.1
CH_4	40.1	43.8	3.1
C_2H_6	16.5	17.5	6.0
C_3H_8	10.5	10.6	9.6
i-C_4H_{10}	3.1	2.7	7.2
n-C_4H_{10}	5.6	4.9	12.9
i-C_5H_{12}	2.9	1.8	13.7
n-C_5H_{12}	2.1	1.3	9.7
C_6H_{14}	4.0	1.4	29.9

Mainly hydrocarbons are removed in the knock-out drum.

Next, the results for the absorption column are given in Table 14.

Table 14: Absorber (**A-4**) inlets and outlets results

	Lean solvent	**Acid gas**	**Rich solvent**	**Sweet gas (A-5)**
Temperature (^{o}C)	40	35	53.2	40.1
Pressure (bar)	35.5	35.5	35.5	35.5
Mass flowrate (kg/s)	111.7	34.2	114.6	31.3
Mass composition (%)				
H_2S	0	7.4	0.1	7.8
CO_2	0.2	8.3	2.6	$2.6x10^{-6}$
N_2	0	0.1	0	0.1
H_2O	64.6	0.1	62.9	0.2
CH_4	0	43.8	0	47.9

(continuation of previous table)				
C_2H_6	0	17.5	0	19.2
C_3H_8	0	10.6	0	11.6
i-C_4H_{10}	0	2.7	0	3.0
n-C_4H_{10}	0	4.9	0	5.3
i-C_5H_{12}	0	1.8	0	2.0
n-C_5H_{12}	0	1.3	0	1.4
C_6H_{14}	0	1.4	0	1.6
DEA	35.3	0	34.4	0

As it can be seen in Table 14 the sweet gas still has a high concentration of H_2S. In order to better understand these results, Table 15 shows the sweetening efficiencies in the absorber, whereas Table 16 presents the concentrations of acid gases in the sweet gas for both simulations.

Table 15: Removal efficiencies of acid gases in the absorber

CO_2 removal (%)	99.997
H_2S removal (%)	4.8

Table 16: Comparison between results for sweet stream

	Abdulrahman et al. [5]	**gPROMS®**
CO_2 in sweet gas (mol. %)	$3.74x10^{-2}$	$1.34x10^{-4}$
H_2S in sweet gas (mol. %)	$3.42x10^{-4}$	5.24

Looking first at Table 15, the removal efficiencies in the absorber are quite different and unexpected. Also, the sweet gas composition regarding the acid gases, presented in Table 16, is very different for both simulations. As explained in Chapter 2.3.1.1.1, the removal of both acid gases should be approximately the same, or at least happen at the same extent, due to the availability of the carbamate formation for CO_2 absorption, since DEA is a secondary amine. However, the removal efficiency for H_2S is quite low. This is due to the fact that gSAFT® is not yet validated with data for H_2S, regarding its removal with amines. However, it is well validated for CO_2 removal, and a significantly higher removal is obtained (almost 100%).

The CO_2 content in the sweet gas is about 1.3 ppmv, far less than the 50 ppmv required for liquefaction (see Table 3). On the other hand, the minimum CO_2 concentration attainable with DEA is 50 ppmv (see Table 4), so such a low concentration of CO_2 in the sweet gas was not expected. It is important to notice that a higher removal rate (even higher than what is considered usual) of CO_2 could be expected, because the absorption in the amine is competitive: since H_2S is not being absorbed as it should be in the DEA solution, there is no competitive absorption between the acid gases, which causes CO_2 to be almost completely removed from the NG feed.

The rich amine loading[6] was also compared: according to Abdulrahman et al. [5], the rich amine loading using 20 stages in the absorber is 0.45 mol acid gases/mol DEA, while gPROMS® calculated value is 0.18 mol acid gases/mol DEA (60% deviation). gPROMS® calculated rich amine loading stays

[6] Molar rate of acid gases absorbed/molar rate of rich amine (mol acid gases/mol DEA).

out of the usual range of this variable for DEA systems (0.43 to 0.73 mol acid gases/mol DEA [1]). However, it should be taken into account that the rich amine loading from Abdulrahman et al. [5] considers the absorption of H_2S and CO_2, and gPROMS® calculated value is only mainly for CO_2 absorption. Therefore, gPROMS® value for the loading was expected to be lower.

The rich amine temperature was also compared: according to Abdulrahman et al. [5], the temperature of the solvent leaving the absorber is 64.6 ºC, whereas gPROMS® calculated value is 53.2 ºC, which corresponds to a deviation of 17.6%.

The results for the flash tank (**A-7**) are presented in Table 17.

Table 17: Flash tank (**A-7**) simulation results

	Inlet	**Vapour outlet (A-8)**	**Liquid outlet**
Temperature (ºC)	53.9	53.9	53.9
Pressure (bar)	6.2	6.2	6.2
Mass flowrate (kg/s)	114.6	0.03	114.6
Mass composition (%)			
H_2S	0.1	31.5	0.1
CO_2	2.6	0.2	2.6
N_2	0	0.2	0
H_2O	62.9	1.5	62.9
CH_4	0	27.3	0
C_2H_6	0	21.3	0
C_3H_8	0	9.1	0
i-C_4H_{10}	0	2.2	0
n-C_4H_{10}	0	3.9	0
i-C_5H_{12}	0	1.2	0
n-C_5H_{12}	0	0.8	0
C_6H_{14}	0	0.8	0
DEA	34.4	0	34.4

In this unit, the hydrocarbons absorbed by the amine solution are removed due to a pressure reduction. Also, H_2S and some CO_2 are flashed off.

Finally, the results for the regeneration column (**A-10**) are given in Table 18.

Table 18: Main simulation results for the regenerator (**A-10**)

	Top (acid gases A-11)	**Bottom (lean solvent)**
Temperature (ºC)	83.7	122.3
Pressure (bar)	1.9	1.9
Mass flowrate (kg/s)	3.4	111.2
Condenser heat duty (kW)	6134	
Reboiler heat duty (kW)	21451	
Mass composition (%)		
H_2S	3.3	0
CO_2	82.3	0.2
H_2O	14.3	64.4
C_3H_8	0.1	0
DEA	0	35.4

At the top of the regenerator, the acid gases are removed, as well as some water. At the bottom, lean solvent is obtained with a DEA purity increased to 35.4 wt. % and with around 0.2 wt. % of CO_2.

It is important to notice that the temperature of the lean amine leaving the regenerator should not exceed 127 ºC, due to chemical degradation of the amine at this temperature [36].

5.1.2.2. Heat Transfer Models

In Table 19 the results for the amine-amine heat exchanger (**A-9**) are presented, as well as the results for the cooler **A-16**.

Table 19: Simulation results for the hot and cold stream of the amine-amine heat exchanger (**A-9**) and for the heat exchanger **A-16**

	A-9		**A-16**
	Cold stream	**Hot stream**	**Hot stream**
Inlet temperature (ºC)	53.9	122.3	81.7
Outlet temperature (ºC)	95.0	81.2	40
Temperature difference (ºC)	41.1	-41.1	-41.7
Inlet pressure (bar)	6.2	1.9	35.5
Pressure drop (bar)	0.7	0.7	0
Mass flowrate (kg/s)	114.6	111.2	111.7
Heat duty (kW)	14.8		14.1

5.1.2.3. Pump Model

The results for the pump **A-15** are presented in Table 20. A mechanical efficiency of 100% was considered, as well as an ideal one of 75%.

Table 20: Pump (**A-15**) simulation results

Inlet temperature (ºC)	81.0
Outlet temperature (ºC)	81.7
Inlet pressure (bar)	1.2
Outlet pressure (bar)	35.5
Pressure ratio	29.6
Mass flowrate (kg/s)	111.7
Power (W)	379

5.1.2.4. Water Make-up

Since there are some water losses throughout the simulation, a water make-up is needed to guarantee a supply of 400 m^3/h of DEA solution to the absorber and to avoid a build-up in DEA's concentration.

Table 21: Water losses throughout the simulation

H_2O in sweet gas[7] (kg/s)	0.026
H_2O in flash gas (kg/s)	4.31×10^{-4}
H_2O in acid gases (kg/s)	0.490
Total H_2O loss (kg/s)	0.516

As it can be seen in Table 21 the total water loss is around 0.516 kg/s, which corresponds to the water make-up (**A-12**) needed in the mixer.

5.1.3. Sensitivity Analyses

In this sub-chapter, the number of stages and pressure in the absorber, and the temperature of the NG feed and the lean solvent were changed to understand their impact in gPROMS® simulation results. In Appendix A-5.2, the actual results are presented, as well as the deviations from the base case.

5.1.3.1. Absorber's Number of Stages

First, the number of stages of the absorber was altered and the change in the rich amine loading is presented in Figure 40, as well as results from Abdulrahman et al. [5].

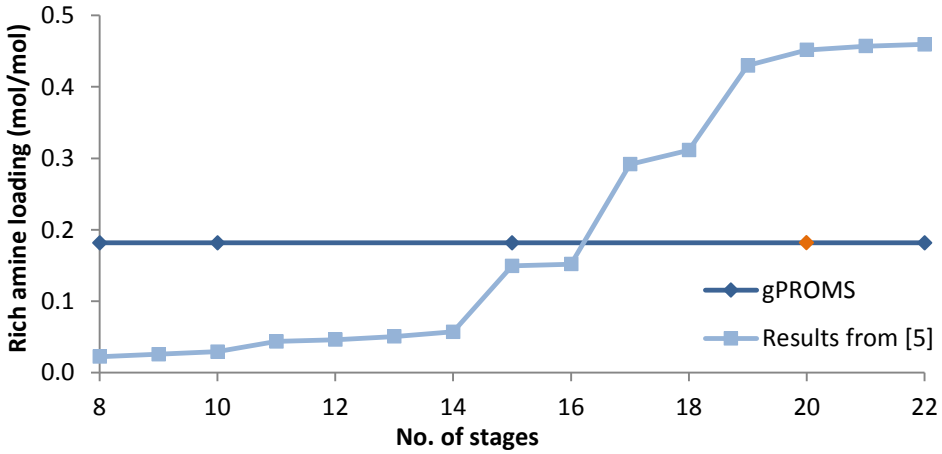

Figure 40: Influence of absorber's number of stages in the rich amine loading (the orange dot represents the base case)

The rich amine loading profile obtained with the models in gPROMS® is quite different compared to the one obtained by Abdulrahman et al. [5], since the profile obtained with gPROMS® is constant with the number of stages.

[7] Only the water from the lean solvent is taken into account.

According to Abdulrahman et al. [5] and analysing Figure 40, the rich amine loading increases with the increase in the absorber's number of stages until it reaches a certain value: after the 20th stage the loading stays constant, and therefore 20 stages in the absorber are considered ideal. However, according to gPROMS® results the loading remains unchanged from at least the 8th stage, whereby 8 stages in the absorber would be enough.

Since the rich amine loading remains constant and there is no loss of DEA in the sweet gas, regardless the number of stages in the absorber, the composition of the sweet gas also remains constant throughout the sensitivity analysis. However, if the loading profile was similar to the one from Abdulrahman et al. [5], a lower concentration of acid gases in the sweet gas would be expected with a higher number of stages since the contact between the solvent and the acid gases would be increased.

5.1.3.2. Natural Gas Feed's Temperature

The inlet NG temperature was changed and the variation in the sweet gas composition is presented in Figure 41.

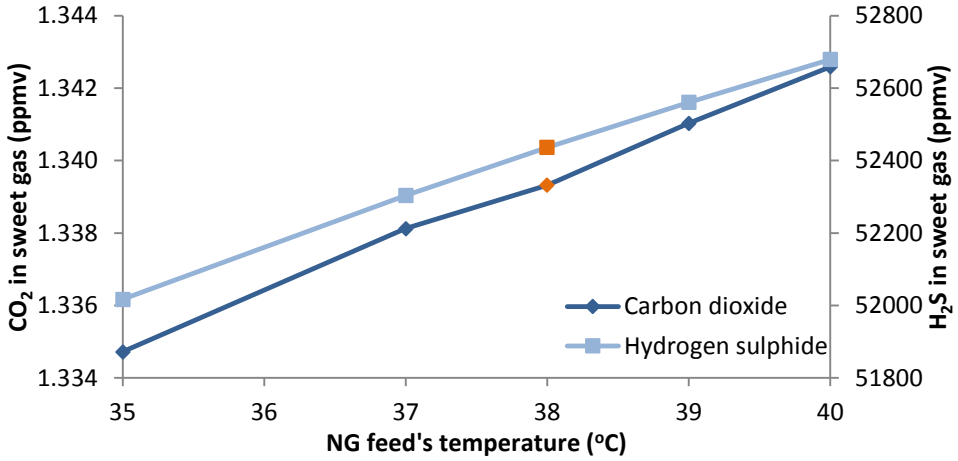

Figure 41: Influence of NG feed's temperature in the sweet gas composition (the orange dots represent the base case)

As stated before, the acid gases are physically absorbed into the solvent solution before undergoing reaction. Then, the chemical solvent can change the absorbed component either by ionizing it or transforming it into another component. This process continues until chemical and physical equilibrium is achieved.

Reactions are governed by equilibrium constants that are related with the concentration of the products: large equilibrium constants result in greater concentrations of products. According to Lunsford et al. [37], for the reactions involved in acid gases removal, the equilibrium constants increase with temperature, which suggests that the absorption of acid gases could be increased by higher temperatures if it was based entirely on equilibrium constants. However, physical absorption is another occurring process and the solubility of gases decreases with increasing temperature, which means that the absorption of acid gases into the solvent solution is decreased at higher temperatures.

Another important variable to be taken into account is the reaction rate, which is described by kinetics. If a chemical reaction is kinetically limited, the reaction may not approach equilibrium. For both

acid gases the chemical reaction with amines is so fast that equilibrium is approached for any time in a commercial absorber, according to Lunsford et al. [37].

According to Figure 41, by decreasing the NG feed's temperature the acid gases content in the sweet gas is decreased. This happens because a decrease in the NG temperature causes a decrease in the absorber's temperature profile (see Figure 69, Appendix A-5.2), which therefore increases the acid gases absorption into the solvent.

5.1.3.3. Lean Amine's Temperature

The lean solvent's temperature was also changed and the sensitivity analysis results are in Figure 42.

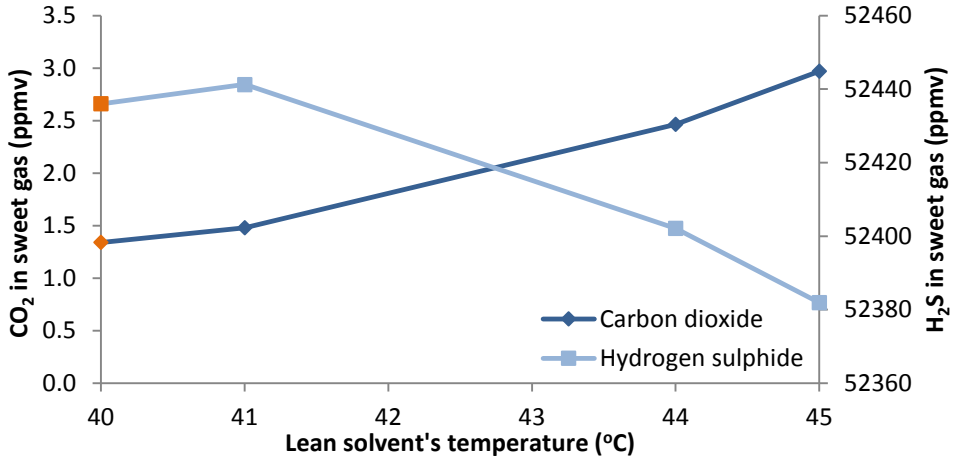

Figure 42: Influence of lean solvent's temperature in the sweet gas composition (the orange dots represent the base case)

Increasing the lean solvent's temperature causes the CO_2 content in the sweet gas to increase for the same reasons as the ones presented in the previous sensitivity analysis. Also, changing the lean amine's temperature has a greater impact in CO_2 content than changing NG feed's temperature, since it causes a greater variation in the absorber's temperature profile (see Figure 70, Appendix A-5.2), because the flowrate of solvent is higher than the one of the NG feed. Regarding H_2S, there is first an increase in H_2S concentration with an increase in 1 ºC in the lean amine's temperature, as it was expected. However, there is a decrease in its concentration in the sweet gas at 44 and 45 ºC, which was not expected since the solubility increases when increasing the temperature. Nonetheless, H_2S concentration only decreases 0.1% from 41 to 44 ºC, which is not significant.

5.1.3.4. Absorber's Pressure

Next, the pressure in the absorber was varied and the results are featured in Figure 43. It is clear that increasing the pressure in the absorber decreases the acid gases content in the sweet gas, since the solubility of gases increases while increasing the pressure [26].

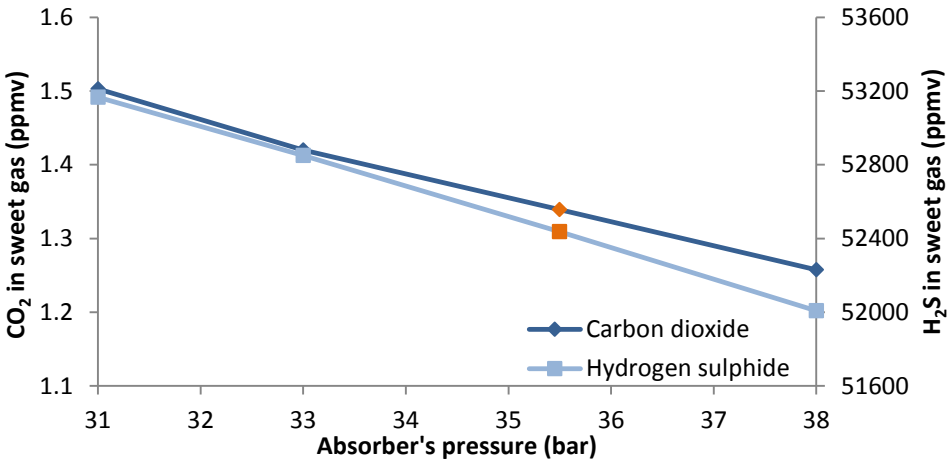

Figure 43: Influence of absorber's pressure in the sweet gas composition (the orange dots represent the base case)

5.2. Dehydration with Glycol

A flowsheet was assembled for the dehydration of NG using glycol, more precisely triethylene glycol (TEG), as a solvent. The flowsheet assembled was simulated in gPROMS® ModelBuilder and is based on data from Ghati [6]. First, the assembling of the flowsheet is explained and the specifications made in the models are presented. Next, the simulation results obtained are shown, as well as some sensitivity analyses performed.

5.2.1. Flowsheet Assembling

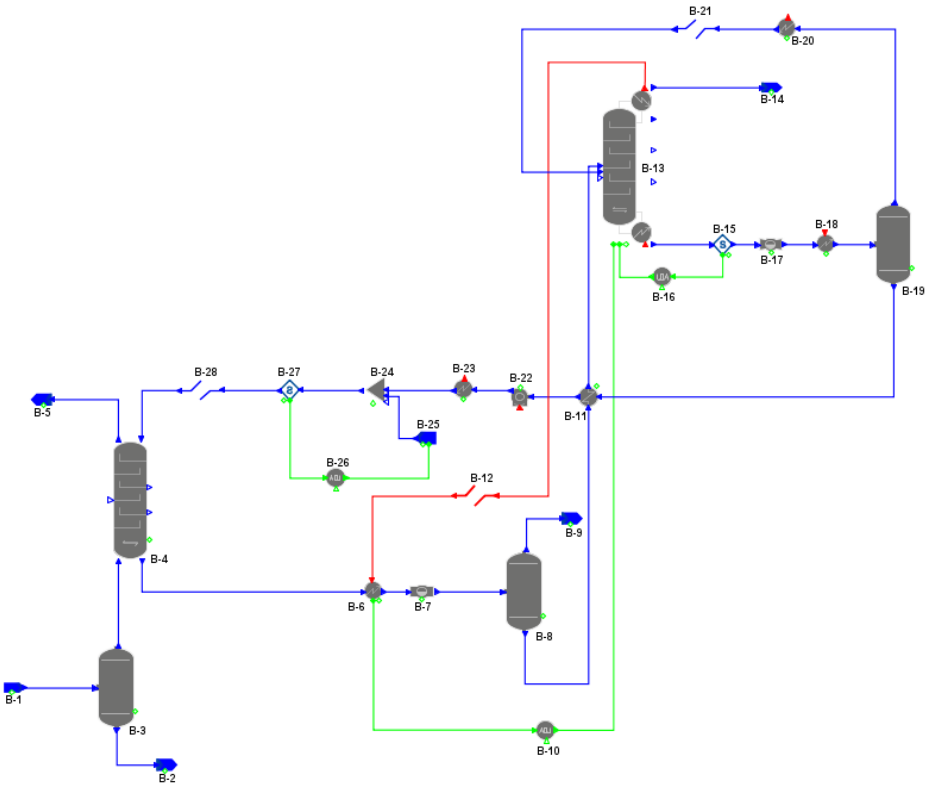

Figure 44: NG dehydration process flowsheet

The NG feed (**B-1**) enters in the dehydration unit (Figure 44) with a flow of 70 MMSCFD, at 30 ^{o}C and 81.7 bar. The composition of the NG feed is shown in Table 22.

Table 22: Composition of NG feed [6]

Component	Molar composition (%)
CH_4	97.00
C_2H_6	1.03
C_3H_8	0.31
i-C_4H_{10}	0.07
n- C_4H_{10}	0.09
i-C_5H_{12}	0.03
n-C_5H_{12}	0.03
C_6H_{14}	0.03
C_7H_{16}	0.11
C_8H_{18}	0.05
C_9^+	0.02
H_2O	0.13
CO_2	0.37
N_2	0.72

The NG feed enters an inlet scrubber (**B-3**) before entering the absorption column in order to remove liquids (**B-2**), which will decrease the amount of glycol needed and the size of the absorber. The absorber (**B-4**) has 3 equilibrium stages, operates at 81.7 bar, and works in counter current flow: the gas enters the bottom, while the liquid solvent enters at the top. The gas enters the column at 30 ^{o}C, while the solvent (TEG) is at 35 ^{o}C, with a glycol concentration of 99 wt. % (the remainder is water). The glycol circulation rate entering the top of the absorber column should be around 25 L of lean TEG/kg of absorbed water, according to Ghati [6]. This corresponds to a lean TEG mass flowrate of around 1250 kg/h.

The rich glycol then flows to the regenerator's (**B-13**) condenser as the cooling fluid. In gPROMS®, it is not possible to connect the solvent stream directly to the condenser, so an alternative was arranged. The rich solvent enters a heater (**B-6**) that has an external energy connection (represented by the red line **B-12**), which indicates that the heat duty of the heater **B-6** is the same as the regenerator's condenser. Since the outlet temperature of the heater is not specified, an adj_spec model (**B-10**) is used to assign it. This model is used to achieve a target outlet temperature in the heater by changing the reflux ratio of the regeneration column.

Table 23: Specification of the adj_spec (**B-10**) model [38]

Variable	Specification	Unit
Target variable	Outlet temperature	-
Target value	45	^{o}C
Adjust signal variables	Reflux molar ratio	-
Adjusted variable initial guess	1	mol/mol

After being heated, the rich solvent is flashed (**B-8**), due to a pressure reduction in a valve (**B-7**). The pressure is therefore reduced from 81.7 bar to 3.013 bar. After this, the rich solvent is heated again

in the glycol-glycol heat exchanger (**B-11**). In this heat exchanger, the hot stream is the rich solvent, while the lean solvent is the cold stream. So, the rich TEG is heated to 165 ºC before entering the regeneration column. Finally, the rich solvent is regenerated in a distillation column (**B-13**) with partial condenser and kettle reboiler. The specifications made in gPROMS® are presented in Table 24.

Table 24: Operating conditions specified for the regenerator [6]

Number of stages	5
Feed stage	3
Condenser set	Full reflux[8]
Average column pressure (bar)	1.2

The temperature of the reboiler is limited due to the possible decomposition of the solvent at high temperatures. Thus, the maximum allowable temperature in the reboiler is about 204 ºC. In order to achieve this temperature, another adj_spec model (**B-16**) is used, adjusting the boilup ratio of the distillation column.

Table 25: Specification of the adj_spec (**B-16**) model [6]

Variable	Specification	Unit
Target variable	Temperature	-
Target value	204	ºC
Adjust signal variables	Boilup molar ratio	-
Adjusted variable initial guess	1	mol/mol

There is another stream being fed to the regeneration column: the vapour at the top of the vacuum drum (**B-19**) that acts like a stripping gas in the regenerator. This stream enters at the bottom of the column.

The water vapour is recovered at the top of the regenerator, while the lean solvent leaves at the bottom at 204 ºC. The pressure of the lean solvent is reduced in a valve (**B-17**) to subatmospheric pressure (around 0.8 bar) and reheated to 204 ºC in a heater (**B-18**) before being fed to a vacuum drum (**B-19**). The vapour at the top is cooled to 165 ºC and recycled back to the regenerator.

The liquid at the bottom of **B-19**, which has the desired glycol concentration, is cooled in the glycol-glycol heat exchanger (**B-11**), the pressure is increased to 81.7 bar in the pump (**B-22**), and is cooled again to 30 ºC (**B-23**). Then, a solvent make-up (**B-25**) with the same composition as the lean solvent is added in a mixer (**B-24**) to adjust the flowrate of glycol needed in the absorber. This is achieved by adding an adj_spec model (**B-26**) that varies the mass flowrate of **B-25**.

Table 26: Specification of the adj_spec (**B-26**) model

Variable	Specification	Unit
Target variable	Mass flowrate	-
Target value	1250	kg/h
Adjust signal variables	Mass flowrate	-
Adjusted variable initial guess	1	kg/s

[8] Top product liquid flowrate set to 0 kg/h.

Finally, the lean solvent, with the required flowrate and purity, is recycled back to the absorber, closing the flowsheet.

5.2.2. Simulation Results

In this sub-chapter, gPROMS® simulation results are presented.

5.2.2.1. Separation Models

As stated before, the inlet scrubber (**B-3**) separates the NG feed into a vapour and liquid streams. The vapour stream exits at the top, while the liquid one leaves at the bottom. The results for the scrubber are shown in Table 27.

Table 27: Inlet and outlets of inlet scrubber (**B-3**)

	NG feed (B-1)	**Vapour outlet**	**Liquid outlet (B-2)**
Temperature (ºC)	30	30	30
Pressure (bar)	81.7	81.7	81.7
Mass flowrate (kg/h)	58610	58572	38
Mass composition (%)			
CH_4	92.9	93.0	0
C_2H_6	1.9	1.9	0
C_3H_8	0.8	0.8	0
$i\text{-}C_4H_{10}$	0.2	0.3	0
$n\text{-}C_4H_{10}$	0.3	0.3	0
$i\text{-}C_5H_{12}$	0.1	0.1	0
$n\text{-}C_5H_{12}$	0.1	0.1	0
C_6H_{14}	0.2	0.2	0
C_7H_{16}	0.7	0.7	0
C_8H_{18}	0.4	0.4	0
C_9^+	0.1	0.1	0
H_2O	0.1	0.07	100
CO_2	1.0	1.0	0
N_2	1.2	1.2	0

As expected, a small portion of water is removed in the inlet scrubber.

The results for the absorber column are shown in Table 28.

Table 28: Absorber (**A-4**) inlets and outlets results

	Lean solvent	**Wet gas**	**Rich solvent**	**Dry gas (B-5)**
Temperature (ºC)	35	30	30.5	30.7
Pressure (bar)	81.7	81.7	81.7	81.7
Mass flowrate (kg/h)	1250	58572	1292	58528
Mass composition (%)				
CH_4	0	93.0	0.07	93.0
C_2H_6	0	1.9	0	1.9
C_3H_8	0	0.8	0	0.8
$i\text{-}C_4H_{10}$	0	0.3	0	0.3

(continuation of previous table)				
n- C_4H_{10}	0	0.3	0	0.3
i-C_5H_{12}	0	0.1	0	0.1
n-C_5H_{12}	0	0.1	0	0.1
C_6H_{14}	0	0.2	0	0.2
C_7H_{16}	0	0.7	0	0.7
C_8H_{18}	0	0.4	0	0.4
C_9^+	0	0.1	0	0.1
H_2O	1.0	0.07	4.2	$4.4x10^{-5}$
CO_2	0	1.0	0.04	1.0
N_2	0	1.2	0	1.2
TEG	99.0	0	95.7	0

The water mass composition in the dry gas is around 44 ppm (41 ppmv), which corresponds to a removal of 94.2% of water in the absorber. The water content in the gas meets the specification for pipeline gas, but does not meet the required low water content for LNG plants (see Table 3). However, it is common practice in NG dehydration to use a glycol dehydration unit for bulk water removal followed by a unit with molecular sieves for further purification. This is done to reduce the size of the solid desiccant bed by reducing the mass of solid desiccant necessary for the final drying [8].

In Table 29 a comparison is made between the results from Ghati [6] and the ones from gPROMS® for the absorber.

Table 29: Comparison between the simulation results and the results from Ghati [6]

	Ghati [6]	**gPROMS®**	**Deviation (%)**
Dry gas temperature (ºC)	30.73	30.66	0.4
Dry gas mass flowrate (kg/h)	58500	58528	0.05
Rich glycol temperature (ºC)	30.55	30.50	0.2
Rich glycol mass flowrate (kg/h)	1299	1292	0.6
Absorption capacity (%)	98.2	94.2	4.1

The deviations are quite insignificant, except for the absorption capacity, which is higher in the simulation results from Ghati [6]. This is probably due to the physical properties package used by Ghati [6]: Aspen Hysys® includes a glycol package specially designed for TEG dehydration that uses Twu-Sim-Tassone equation of state [39] (Appendix A-4).

For the flash tank (**B-8**), the simulation results are in Table 30.

Table 30: Flash tank (**B-8**) simulation results

	Inlet	**Vapour outlet (B-9)**	**Liquid outlet**
Temperature (ºC)	42.7	42.7	42.7
Pressure (bar)	3.013	3.013	3.013
Mass flowrate (kg/h)	1292	1	1291
Mass composition (%)			
CH_4	0.07	80.2	0
C_2H_6	0	0.9	0
C_3H_8	0	0.1	0
H_2O	4.2	0.7	4.2

(continuation of previous table)			
CO_2	0.04	14.0	0
N_2	0	4.0	0
TEG	95.7	0	95.8

The major portion of hydrocarbons and CO_2 dissolved in the solvent are flashed at 3.013 bar, remaining a liquid stream with 95.8 wt. % of TEG that will be regenerated in the distillation column. For the regenerator (**B-13**), the main results are given in Table 31.

Table 31: Main simulation results for the regenerator (**B-13**)

	Top (B-14, water vapour)	**Bottom (lean solvent)**
Temperature (ºC)	105	204
Pressure (bar)	1.2	1.2
Mass flowrate (kg/h)	42	1266
Condenser heat duty (kW)	11.0	
Reboiler heat duty (kW)	62.6	
Reflux ratio (mol/mol)	0.41	
Boilup ratio (mol/mol)	0.24	
Mass composition (%)		
CH_4	0.2	0
H_2O	99.0	1.6
CO_2	0.8	0
TEG	0	98.4

The regenerator increases the purity of the solvent from 95.3 to 98.4 wt. % (within the expected range of 98-99 wt. % achieved in an atmospheric stripper [1]), which is not enough for the specifications required.

The results for the outlet streams of the vacuum drum (**B-19**) are presented in Table 32.

Table 32: Main simulation results for the vacuum drum (**B-19**)

	Vapour outlet	**Liquid outlet**
Temperature (ºC)	204	204
Pressure (bar)	0.8	0.8
Mass flowrate (kg/h)	16	1250
Mass composition (%)		
H_2O	52.8	1.0
TEG	47.2	99.0

With the vacuum drum, the desired glycol purity (99.0 wt. %) is achieved by reducing the pressure to around 0.78 bar.

5.2.2.2. Heat Transfer Models

The simulation results for all the heat exchangers are shown in Table 33.

Table 33: Simulation results for the heat exchangers

	B-11		B-18	B-20	B-23
	Cold stream	**Hot stream**	**Cold stream**	**Hot stream**	**Hot stream**
Inlet temperature (ºC)	48	204	199	204	86
Outlet temperature (ºC)	165	83	204	165	35
Temperature difference (ºC)	117	-121	5	-39	-51
Pressure (bar)	3.013	0.8	0.8	0.8	81.7
Mass flowrate (kg/h)	1292	1250	1266	16	1250
Heat duty (kW)	99.3		5.4	1.3	37.5

It is important to notice the outlet temperature of the hot stream in **B-11**, since the temperature before the pump (**B-22**) should be reduced to at least 90 ºC to protect the pump [8].

5.2.2.3. Pump Model

The results for the pump (**B-22**) are shown in Table 34. It is important to mention that a mechanical efficiency of 100% and an ideal one of 75% (default values of the model) were assumed.

Table 34: Pump (**B-22**) simulation results

Inlet temperature (ºC)	83
Outlet temperature (ºC)	86
Inlet pressure (bar)	0.8
Outlet pressure (bar)	81.7
Pressure ratio	105
Mass flowrate (kg/h)	1250
Power (kW)	2.6

5.2.2.4. Solvent Make-up

A solvent make-up is needed since there are some minor losses of glycol throughout the process. The losses of glycol are presented in Table 35.

Table 35: Solvent losses in the simulation

TEG in dry gas (kg/h)	2.3×10^{-2}
TEG in flash gas (kg/h)	9.7×10^{-6}
TEG in water vapour (kg/h)	2.1×10^{-6}
Total TEG loss (kg/h)	2.3×10^{-2}

99.9% of the solvent losses occur in the absorber, while minor losses take place in the flash tank and in the regenerator. The total glycol loss corresponds to 0.0018% of the flow of solvent entering the absorber. Hence, a make-up of 0.023 kg/h of glycol is needed.

5.2.3. Sensitivity Analyses

After getting results for the base case, the number of stages and pressure in the absorber, the temperature of the NG feed and the lean solvent, and the solvent purity were changed in order to understand their impact in the simulation results, specifically in the water content of the dry gas. All the simulation results, as well as the deviations from the base case, are presented in Appendix A-6.2.

5.2.3.1. Absorber's Number of Stages

First, the number of stages of the absorber was altered and the results are presented in Figure 45.

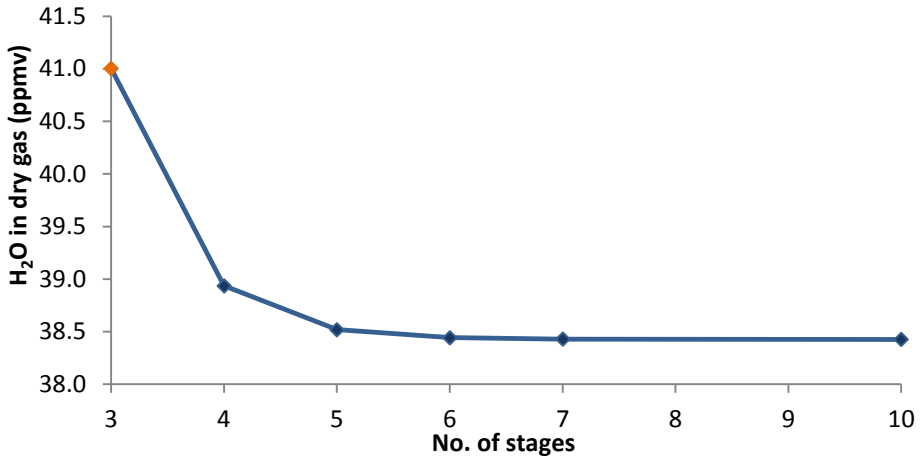

Figure 45: Influence of absorber's number of stages in the water content of the dry gas (the orange dot represents the base case)

The water content in the dry gas decreases slightly while increasing the number of stages of the absorber until it reaches a certain value: from 6 stages, the water content does not vary substantially. By increasing the number of stages, the contact between the solvent and the gas is also increased, therefore decreasing the water concentration in the dry gas. The behaviour of the curve in Figure 45 suggests that the contact between the two phases is the maximum with 6 stages in the absorber.

5.2.3.2. Natural Gas Feed's Temperature

Next, the temperature of the NG feed was changed and the results are shown in Figure 46.

The water content in the dry gas increases while increasing the NG feed's temperature. This happens because by increasing the temperature of the NG feed less water is condensed and removed in the inlet scrubber, which increases the water content in the gas stream fed to the absorber. Also, solubility of gases decreases while increasing the temperature. By increasing the inlet NG temperature, the temperature profile in the absorber also increases (see Figure 77, Appendix A-6.2). This increase in temperature decreases the solubility of the gaseous components in the solvent. However, the decrease in solubility is greater for water vapour, which therefore increases the water content in the dry gas [26], [37].

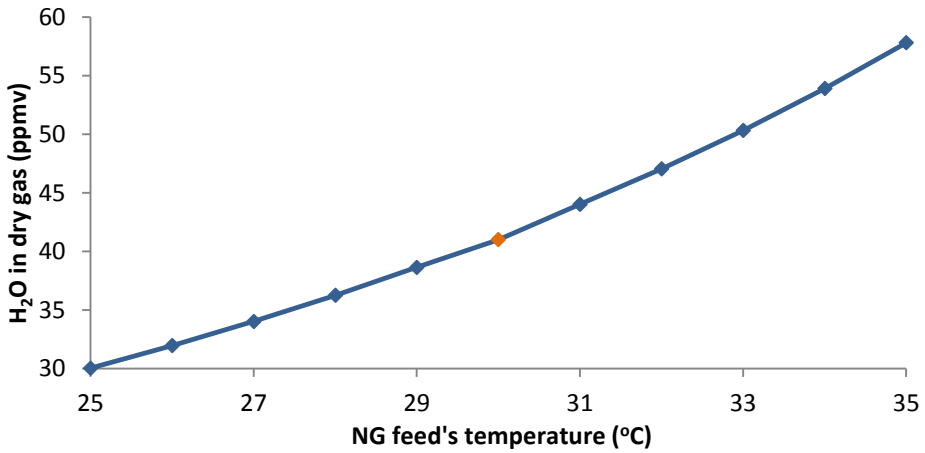

Figure 46: Influence of NG feed's temperature in the water content of the dry gas (the orange dot represents the base case)

5.2.3.3. Lean Solvent's Temperature

The temperature of the lean TEG was also changed and the simulation results are presented in Figure 47.

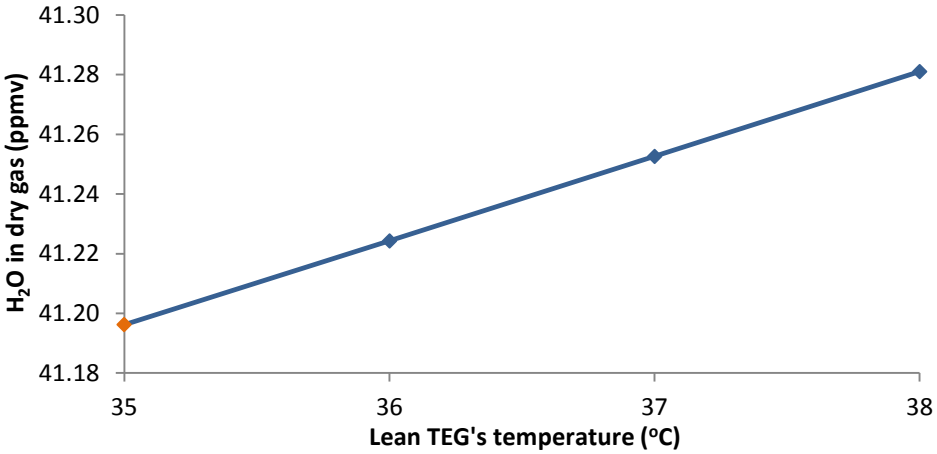

Figure 47: Influence of lean TEG's temperature in the water content of the dry gas (the orange dot represents the base case)

As stated before, an increase in temperature causes a decrease in the solubility of gases. Since increasing the lean solvent temperature causes a slight increase in the absorber's temperature profile (see Figure 70, Appendix A-6.2), the solubility of water decreases and therefore the water content in the dry gas is decreased. The effect of the temperature of lean solvent is lesser than the effect of NG feed's temperature, since the flowrate of TEG is quite smaller.

5.2.3.4. Absorber's Pressure

The absorber's pressure was changed and its impact in the water content in the dry gas is presented in Figure 48.

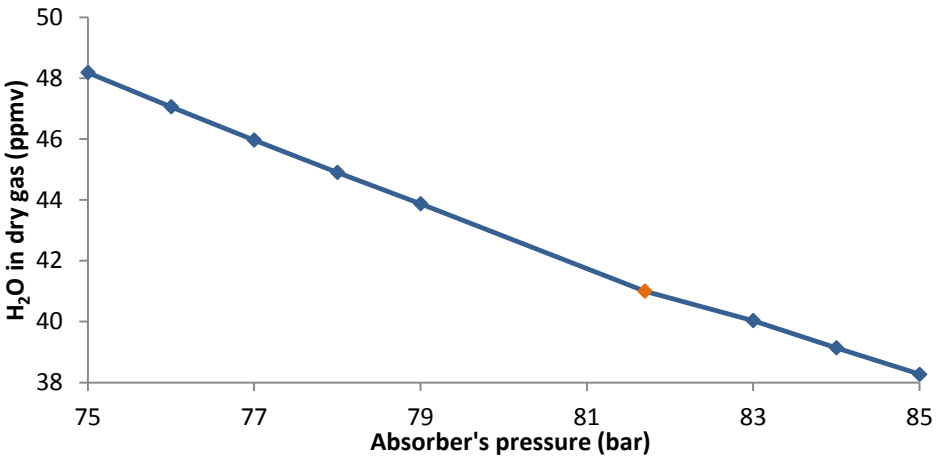

Figure 48: Influence of absorber's pressure in the water content of the dry gas (the orange dot represents the base case)

The water content in the dry gas decreases while increasing the absorber's pressure, for the same reasons as stated before: the solubility of gases increases while increasing the pressure. Therefore, the water content in the dry gas is lowered.

5.2.3.5. Lean Glycol Purity

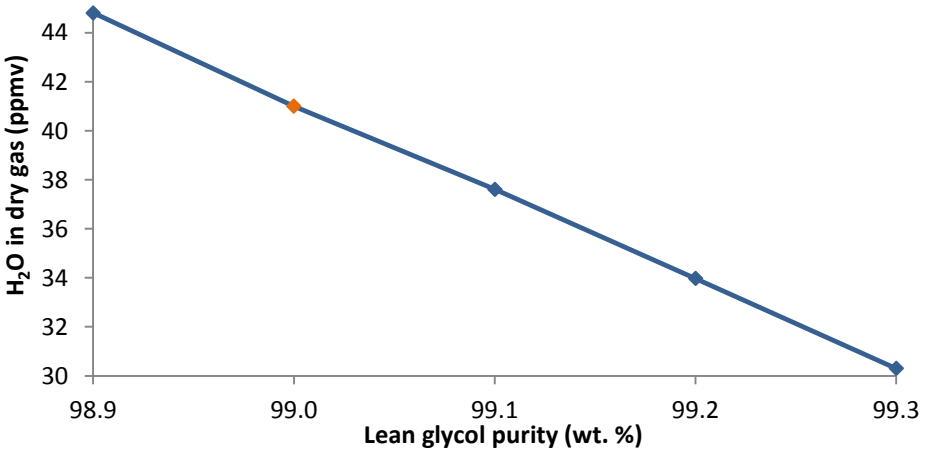

Figure 49: Influence of lean glycol purity in the water content of the dry gas (the absorber dot represents the base case)

Increasing the lean glycol purity decreases the water content in the dry gas, since the amount of glycol used to absorb water is higher, leading to a higher absorption of the solute.

5.2.4. Key Performance Indicators [6]

Key performance indicators (KPIs) are tools that allow the measurement of the level of performance of a process, showing how well the goals of the process are achieved. KPIs can be used to compare the performance of the same process, but with different operating conditions. The dehydration process was simulated with different operating conditions than the base case, and in order

to compare the results from the two cases, KPIs were calculated. The different conditions are presented in Table 36 and Table 37.

Table 36: NG feed compositions for base case (**1**) and new case (**2**) [6]

Component	Case 1	Case 2
	Mole composition (%)	
CH_4	97.00	53.90
C_2H_6	1.03	7.78
C_3H_8	0.31	12.96
i-C_4H_{10}	0.07	0.71
n- C_4H_{10}	0.09	1.55
i-C_5H_{12}	0.03	0.82
n-C_5H_{12}	0.03	1.45
C_6H_{14}	0.03	0.67
C_7H_{16}	0.11	0.37
C_8H_{18}	0.05	0.11
C_9^+	0.02	0.04
H_2O	0.13	0.79
CO_2	3.73	6.58
N_2	0.72	1.45
H_2S	0	10.8

Table 37: Operating conditions for base case (**1**) and new case (**2**) [6]

	Case 1	Case 2
NG feed		
Flowrate (kg/h)	58610	1018554
Temperature (ºC)	30	36
Pressure (bar)	81.7	65.6
Absorber liquid inlet (lean solvent)		
Flowrate (kg/h)	1250	151200
Temperature (ºC)	35	41
Pressure (bar)	81.7	65.6
Absorber column		
Pressure (bar)	81.7	65.6
No. of stages	3	5
Regenerator column		
Pressure (bar)	1.2	1.3
No. of stages	5	7
Valve (vacuum)		
Outlet pressure (bar)	0.78	0.84
Pump		
Outlet pressure (bar)	81.7	65.6
B-23		
Outlet temperature (ºC)	35	41

The KPIs used to do the comparison between the two cases were the following: energy supplied in heat transfer equipment (reboiler and heater **B-18**) per amount of water absorbed and per amount of

NG treated, energy removed in heat transfer equipment (coolers **B-20** and **B-23**) per amount of water absorbed and per amount of NG treated, and amount of solvent used per amount of water absorbed and per amount of NG treated. The KPIs mentioned are shown in Table 38.

Table 38: Results for the KPIs for both cases

	Case 1	**Case 2**
Energy input (kJ/kg NG treated)	4	18
Energy input (kJ/kg water absorbed)	5864	24687
Energy output (kJ/kg NG treated)	2	13
Energy output (kJ/kg water absorbed)	3283	17657
Solvent used (kJ/kg NG treated)	0.02	0.15
Solvent used (kg solvent/kg water absorbed)	30	199

It is clear that Case 2 needs more energy for the heat transfer equipment than Case 1, for the same amount of water absorbed, increasing the amount of utilities needed, and therefore increasing its costs. Also, the amount of solvent needed to absorb the same amount of water is higher in Case 2, also adding to the costs. This can be explained by taking a look at Table 37 and the sensitivity analyses (Chapter 5.2.3): although the number of stages of the absorber is higher in Case 2, its pressure is lower, and the NG feed's temperature is higher. Remembering Figure 46 and Figure 48, higher NG feed's temperatures and lower absorber's pressures increase the water content of the dried gas. Hence, this explains why the amount of solvent needed to absorb the same amount of water is higher in Case 2.

Other variables should also be considered, such as the size of the absorber and regenerator and therefore their costs. So, a more detailed economical evaluation should be performed.

Other variable that could be taken into account is the water content in the dry gas, shown in Table 39 for Cases 1 and 2.

Table 39: Water content in dry gas for both cases

	Case 1	**Case 2**
Water in dry gas (ppmv)	41	79

It is now clear that in a first and approximate analysis Case 1 offers more benefits than Case 2, since the water content in the dry gas is lower and taking into account the previous KPIs. This suggests that it could be advantageous to divide the flow of NG in two or more streams to be treated in smaller and more efficient dehydration units. However, as said before, a detailed economical evaluation should be made.

5.3. Dehydration with Molecular Sieves

At last, a flowsheet was assembled for the dehydration of NG using molecular sieves, more precisely zeolite 5A, for which some custom models were developed. This process was simulated in gPROMS® ProcessBuilder and unlike the previous ones, this is a dynamic simulation. It is important to notice that only the adsorption bed was assembled in gPROMS® and therefore is missing the bed regeneration unit.

In the first place, the custom models developed, which are based in the models developed by Gholami et al. [7], are explained. Next, the specifications made throughout the models used are presented. Finally, the simulation results obtained are shown, as well as some sensitivity analyses performed.

5.3.1. Custom Modelling

In order to simulate the dehydration of NG using molecular sieves, some custom models from Gholami et al. [7] were used: models to obtain the axial dispersion coefficient and the adsorption isotherm were developed. Also, the model of the mass transfer rate, more precisely the linear driving force (LDF) coefficient, was altered.

5.3.1.1. Axial Dispersion Coefficient

When a fluid flows through a packed bed, both axial and radial dispersion of mass can take place. However, it is common to neglect the effects of radial dispersion since the bed diameter is usually far greater than the adsorbent particle diameter [18].

For gaseous systems, there are two main mechanisms that contribute to axial dispersion: molecular diffusion (first term on the right hand side of equation 11) and turbulent mixing due to the splitting and recombination of flows around the adsorbent particles (second term on the right hand side of equation 11). So, the axial dispersion coefficient is given by the equation below:

$$D_{axi} = \gamma_1 D_{mi} + \gamma_2 d_p u \tag{11}$$

where γ_1 and γ_2 are constants usually equal to 0.7 and 0.5, respectively, D_{mi} is the molecular diffusivity of component i, d_p is the adsorbent particle diameter, and u is the interstitial gas velocity[9].

The constant γ_1 can be related to the bed voidage, according to Ruthven [19]:

$$\gamma_1 = 0.45 + 0.55\varepsilon_b \tag{12}$$

The molecular diffusivity of a single component in a mixture of n components is given by:

$$\frac{D_{m1}}{1 - Y_1} = \left(\sum_{i=2}^{n} \frac{Y_i}{D_{1i}} \right)^{-1} \tag{13}$$

where Y_i is the mole fraction of component i in the adsorbed phase, and D_{1i} is the diffusivity coefficient, obtained using Multiflash™.

5.3.1.2. Extended Dual Site Langmuir Isotherm

The equilibrium concentration of component i in the micropores (q_{ci}^*) is calculated using the extended dual site Langmuir isotherm for multi-component adsorption (refer to Ritter et al. [40] for more information):

$$q_{ci}^* = q_{si1} \frac{\beta_{i1} p_i}{1 + \sum_{j=1}^{n} \beta_{j1} p_j} + q_{si2} \frac{\beta_{i2} p_i}{1 + \sum_{j=1}^{n} \beta_{j2} p_j} \tag{14}$$

[9] Superficial gas velocity/Bed void.

where $p_{i,j}$ is the partial pressure of component i/j. The constants β_{ij} (affinity parameter for gas i in site j) and q_{sij} (specific saturation capacity of component i on site j) are temperature dependent constants, obtained by the following expressions:

$$\beta_{i1,2} = b_{01,2} exp\left(\frac{E_{i1,2}}{RT}\right) \quad (15)$$

$$q_{si1,2} = \frac{A_{i1,2}}{T} + A_{i1,2} \quad (16)$$

where b_{0j} is the pre-exponential factor on site j, E_{ij} is the adsorption energy of component i on site j, and A_{ij} are auxiliary adsorption equilibrium parameters. Also, the heat of adsorption of component i (ΔH_i^{ads}) was obtained by using an equation based on the Clausius-Clapeyron relation:

$$\Delta H_i^{ads} = \frac{E_{i1} q_{si1} \beta_{i1} (1 + \beta_{i2} p)^2 + E_{i2} q_{si2} \beta_{i2} (1 + \beta_{i1} p)^2}{q_{si1} \beta_{i1} (1 + \beta_{i2} p)^2 + q_{si2} \beta_{i2} (1 + \beta_{i1} p)^2} \quad (17)$$

5.3.1.3. Linear Driving Force Coefficient

The LDF model is used for the mass transfer rate through micropores volumes and it is given by the following equation:

$$\frac{\partial q_{ci}}{\partial t} = \frac{15 D_{ci}}{R_c^2} (q_{ci}^* - q_{ci}) \quad (18)$$

where q_{ci} is the mass of component i adsorbed into the micropore volume, D_{ci} is the crystalline diffusivity of component i and R_c is the sorbent crystal radius. The term $15 D_{ci}/R_c^2$ is referred to as the LDF coefficient.

The crystalline diffusivity is calculated using the following expression from Ruthven [19]:

$$D_{ci} = D_{0i} exp\left(-\frac{E_i}{RT}\right) \quad (19)$$

where D_{0i} is the diffusional pre-exponential factor of component i and E_i is the diffusional activation energy of component i.

5.3.2. Flowsheet Assembling [7]

The adsorption scheme assembled is represented in Figure 50.

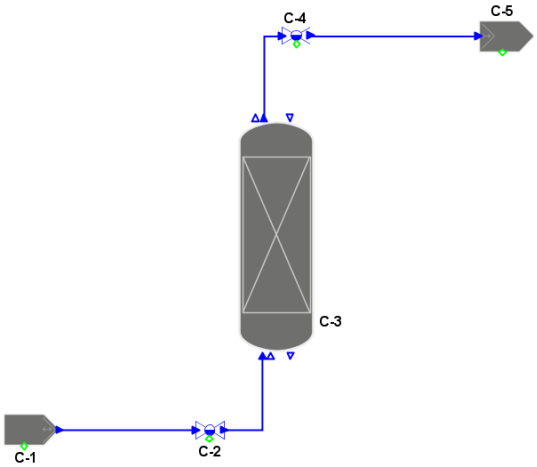

Figure 50: Adsorption scheme flowsheet

The NG feed (**C-1**) enters the dehydration unit (Figure 50) at 295.5 K and 64.8 bar, with a molar flowrate of 23929 kmol/h. The composition of the gas stream is presented in Table 40.

Table 40: Molar composition of NG feed [7]

Component	Molar composition (%)
H_2O	0.184
CO_2	0.998
CH_4	95.300
N_2	3.518

The adsorption bed (**C-3**) has one layer of zeolite 5A and the bed and adsorbent properties specified in gPROMS® are presented in Table 41.

Table 41: Bed and adsorbent properties specified [7]

Bed properties	
Layer length (m)	5.5
Bed internal diameter (m)	3.5
Bed void (m^3/m^3)	0.34
Adsorbent particle properties	
Particle density (kg/m^3)	1812.5
Particle void (m^3/m^3)	0.36
Particle diameter (m)	0.0026
Particle thermal conductivity (W/(m.K))	0.5
Particle heat capacity (J/(kg.K))	1000

Regarding the *Fluid (mass transfer)* tab of the adsorption bed model, a constant mass transfer coefficient was specified with a solid concentration mass transfer basis[10]. The parameters used in equations 18 and 19 for the calculation of the LDF coefficient are presented in Table 42.

Table 42: Auxiliary parameters for the calculation of LDF coefficient [7]

Component	D_o **(m^2/s)**	E **(J/mol)**	R_c **(m)**
H_2O	2.39×10^{-8}	17 288.47	0.5×10^{-6}
CO_2	5.90×10^{-11}	26 334	
CH_4	7.20×10^{-12}	12 551.94	
N_2	5.20×10^{-13}	6 275.97	

The axial dispersion coefficient was obtained using the custom model developed (dispersion_calculation model). The molecular diffusivities of the components were introduced in this tab (*Diffusivity constants*), shown in Figure 51 and were calculated according to equation 13.

[10] LDF model for mass transfer based on the difference in solid concentration between actual coverage and the coverage that is in equilibrium with the gas phase concentration predicted by the isotherm model.

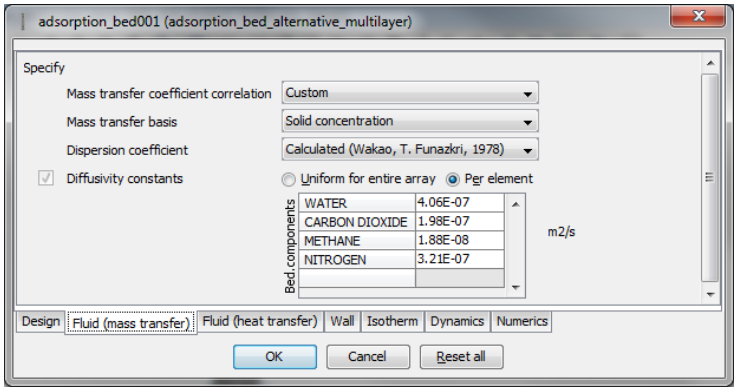

Figure 51: Specification dialog box of *Fluid (mass transfer)* tab

In what concerns heat transfer, an isothermal operation was considered for calculation simplification and reduction of the simulation time. In this manner, a bed temperature of 295.5 K was specified.

The isotherm custom model was used to obtain the equilibrium concentration of the components and the adsorption equilibrium and kinetic parameters of pure CH_4, CO_2, N_2, and water vapour are listed in Table 43.

Table 43: Adsorption equilibrium parameters in zeolite 5A [7]

Component	A_{11} **(mol.K/kg)**	A_{12} **(mol/kg)**	A_{21} **(mol.K/kg)**	A_{22} **(mol/kg)**
H_2O	-3799.940	18.711	3684.491	-4.450
CO_2	516.743	-0.794	-932.131	6.083
CH_4	348.971	0.542	348.971	0.542
N_2	605.423	-0.582	605.423	-0.582
Component	b_{01} **(kPa^{-1})**	b_{02} **(kPa^{-1})**	E_1 **(J/mol)**	E_2 **(J/mol)**
H_2O	3.58×10^{-7}	1.62×10^{-5}	44140.040	45199.990
CO_2	3.32×10^{-7}	6.43×10^{-7}	41077.100	29812.290
CH_4	6.77×10^{-6}	6.13×10^{-7}	13672.210	20307.220
N_2	3.73×10^{-5}	3.18×10^{-5}	7528.091	7941.248

The initial molar composition of the gas in the bed was assigned in the *Dynamic*s tab of the adsorption bed model.

Table 44: Initial gas composition in the bed [7]

Component	**Molar composition (%)**
H_2O	0
CO_2	0
CH_4	96.44
N_2	3.56

Finally, in the *Numerics* tab, a simplified momentum balance was chosen, as well as unidirectional flow mode and 80 discretisation points per layer as shown in Figure 52.

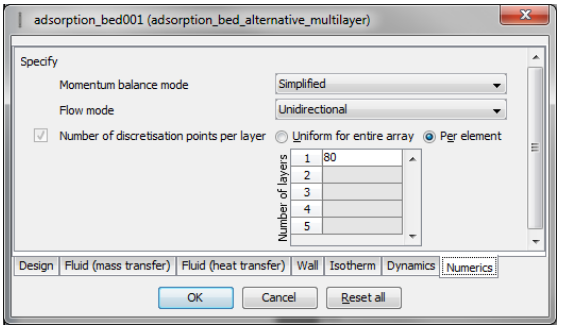

Figure 52: Specification dialog box of *Numerics* tab

Since the flow of gas is reversible, reversible valves were introduced in the flowsheet after the source model (**C-2**) and before the sink model (**C-4**). In both valves a performance design was selected and the specifications made are presented in Figure 53.

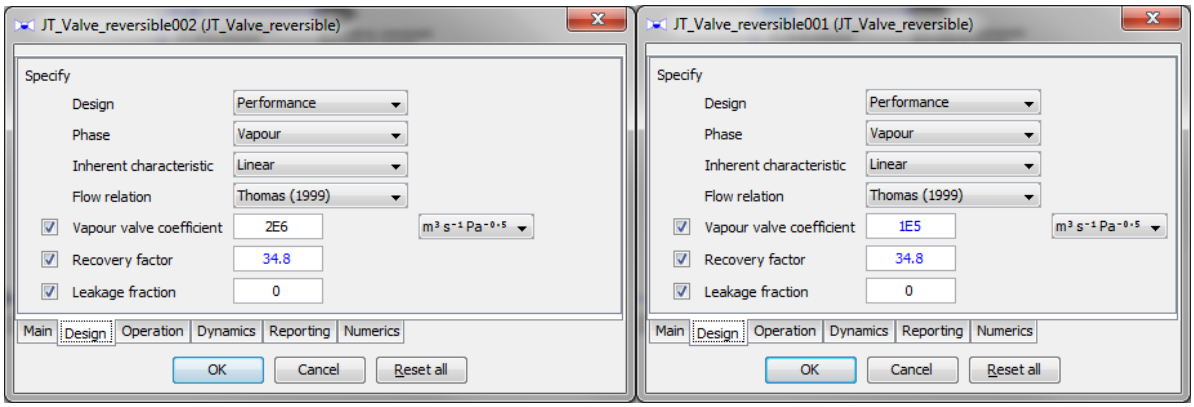

Figure 53: Specification dialog box of valves **C-2** (on the left) and **C-4** (on the right)

The stem position of valve **C-2** is perfectly controlled to maintain the outlet specifications assigned in the adsorption bed model (**C-3**), whereas the stem position of valve **C-4** was assigned a fixed value equal to 1.

The pressure and temperature of the dry gas were assigned in the sink model (**C-5**) (60.5 bar and 295.5 K, respectively), as well as the molar fraction, which is equal to the initial gas composition in the bed.

Unlike the other flowsheets assembled, the adsorption process flowsheet is a dynamic one, and therefore a SCHEDULE[11] was defined. The SCHEDULE was defined as the time it takes to achieve the adsorption bed saturation (breakthrough).

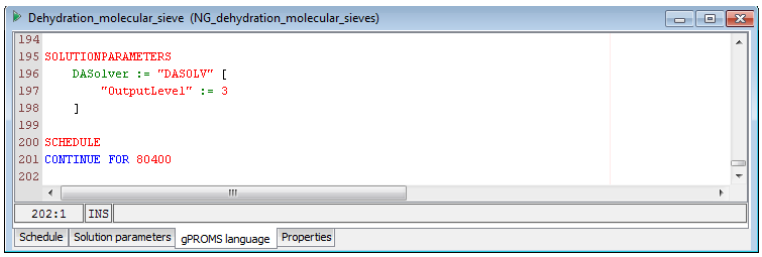

Figure 54: Example of *gPROMS language* tab of the adsorption bed Process

[11] Schedules are used in gPROMS® to define operating procedures, allowing the system to operate without any external disturbance over a specified period of time [21].

5.3.3. Simulation Results

The simulation results obtained for the dehydration process are presented in the following sub-chapters and compared with the results from Gholami et al. [7].

5.3.3.1. Adsorption Bed Model

In the first place, a comparison was made between gPROMS® results and from Gholami et al. [7] regarding the loading (or adsorption capacity) of the adsorbent. The loading is the amount of adsorbate taken up by the adsorbent per unit volume of the adsorbent [41] (mol adsorbate/m^3 adsorbent).

Figure 55 presents the loading in the adsorbent for both simulations after 10 minutes of adsorption.

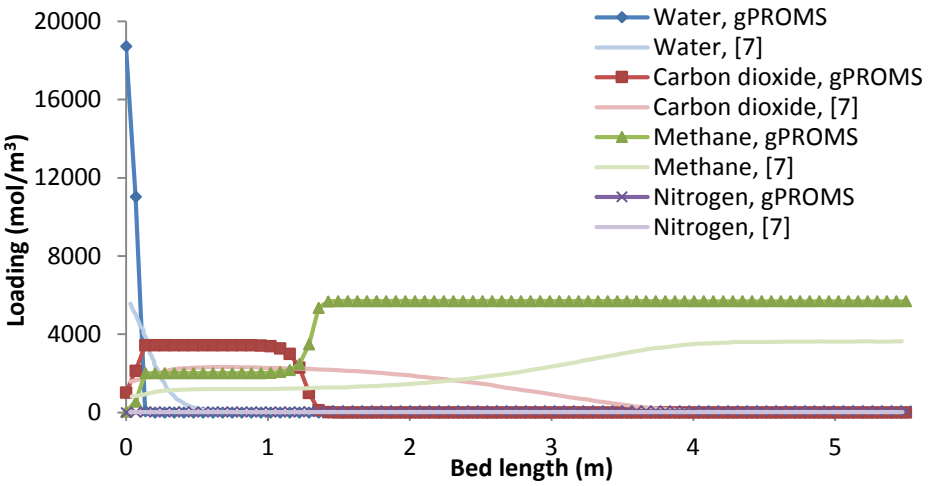

Figure 55: Loading along the bed from gPROMS® and Gholami et al. [7] after 10 minutes of adsorption

Analysing Figure 55 (see also Appendix A-7.3, page 100), it is clear that the results are quite different for both simulations and that the adsorption capacity is higher according to gPROMS®. However, the behaviour of both curves is similar.

For a more clear understanding of these results, Figure 56 presents the adsorption capacity after 10 minutes and 4 hours of adsorption.

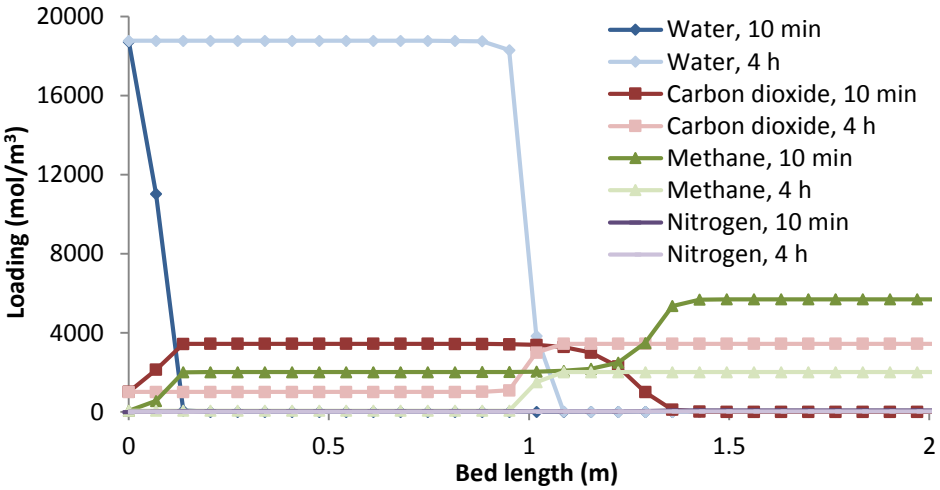

Figure 56: Loading along the bed after 10 minutes and 4 hours of adsorption

Examining Figure 56, it is possible to see that as more water is being adsorbed in the adsorbent particles (and the water loading curve is moving forward along the bed), less of the other components are being adsorbed. Therefore, it is possible to conclude that adsorption of water causes desorption of the other components, until the bed is entirely saturated with water vapour. When breakthrough occurs, the loading curve reaches the end of the bed and turns into a constant line, which means the entire adsorption bed is completely saturated with water vapour. If the bed is fully saturated, then the outlet gas has the same composition of the initial wet gas and the bed needs to be regenerated [8].

Also, one can see that in the beginning of the simulation CO_2 also causes desorption of methane and nitrogen.

Figure 57 represents the different zones formed during competitive adsorption.

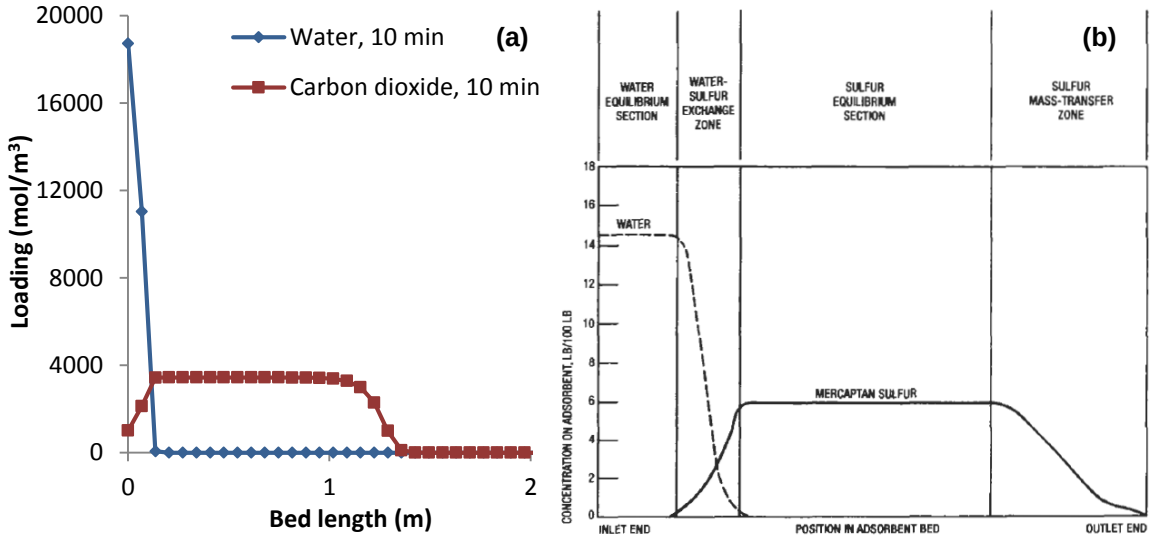

Figure 57: (a) Loading in the adsorbent for CO_2 and water after 10 minutes of adsorption; **(b)** Adsorption zones in a bed adsorbing both water vapour and mercaptans from NG [4]

Analysing Figure 56 again, one can see that the loading curves for water vapour and CO_2 after 10 minutes of adsorption are similar to the ones in Figure 57: since water is adsorbed more strongly than the other components, it concentrates at the inlet of the bed and it displaces the other impurities that had been previously adsorbed. The desorbed components are readsorbed farther down the column and these components' adsorption zones move along the bed in advance of the water adsorption zone [4].

Next, the results regarding water concentration in the gas phase along the bed and for different times are compared.

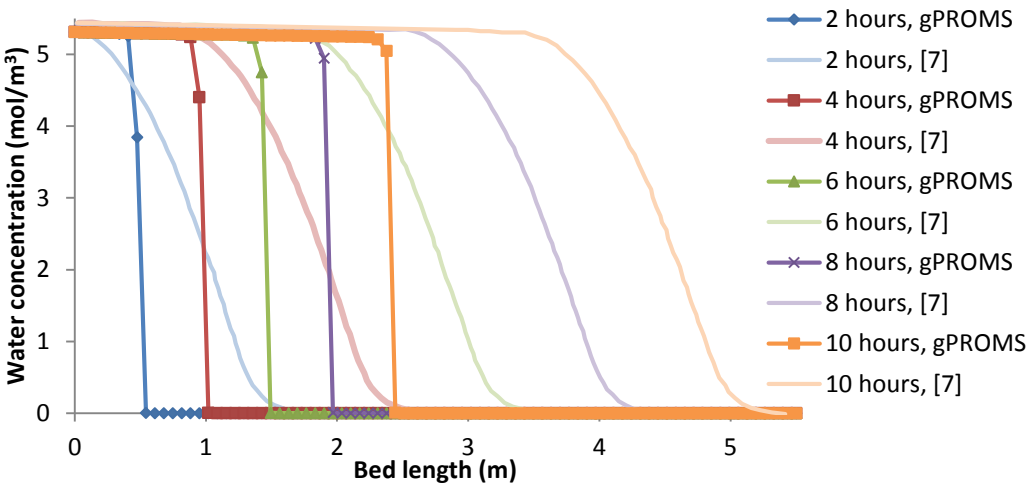

Figure 58: Water concentration along the bed at different times from gPROMS® and Gholami et al. [7]

One can see in Figure 58 that gPROMS® calculated values for the water concentration in the gas phase are similar to the ones from Gholami et al. [7]. However, gPROMS® obtained curves seem to be "delayed" in comparison with the curves obtained from Gholami et al. [7]: the length of the MTZ (see Figure 14 in Chapter 2.3.2.2) is smaller in gPROMS® results. The length of the MTZ is determined by the rate of mass transfer of adsorbate from the gas phase into the pores of the adsorbent. When the mass transfer rate is extremely high, the MTZ reduces to a plane [4]. Therefore, gPROMS® must predict a higher mass transfer rate. However, this is not expected since the LDF coefficient in gPROMS®, used to obtain the mass transfer rate, is based on data from Gholami et al. [7]. Smaller MTZ maximizes the bed capacity since this zone nominally holds only 50% of the adsorbate held by a comparable length of adsorbent at equilibrium. Therefore, a greater bed capacity is expected for gPROMS® simulation. In order to prove this, the breakthrough time was obtained and compared with the one from Gholami et al. [7]. Figure 59 shows water's breakthrough curve.

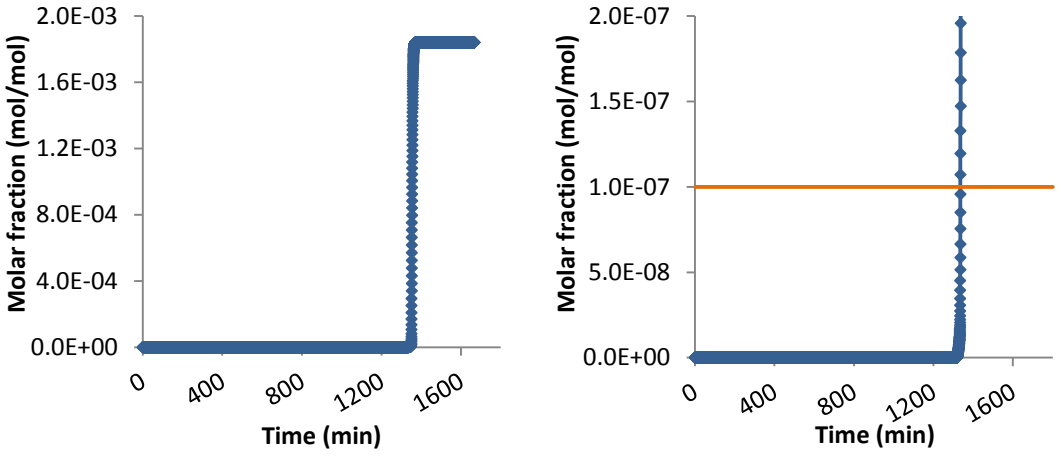

Figure 59: Molar fraction of water in the gas at the end of the bed along the simulation time (the orange line represents the concentration at breakthrough time)

Breakthrough was considered to take place when the water concentration at the end of bed reached the maximum allowable concentration in LNG plants (0.1 ppmv), represented by the orange line on the right of Figure 59. Table 45 presents the comparison between the breakthrough time obtained from gPROMS® and from Gholami et al. [7].

Table 45: Comparison between breakthrough time for gPROMS® and Gholami et al. [7]

	Breakthrough time (min)
gPROMS®	1336
Gholami et al. [7]	610
Deviation (%)	119

The results are very different: gPROMS® predicted breakthrough time is more than double than what it was expected. The breakthrough time depends on several factors, such as initial concentrations, flow rate, column length, temperature and adsorption capacities (and the shape of the isotherm itself) [42], [43]. All this data was provided by Gholami et al. [7] and used in gPROMS®, so such a difference in the breakthrough time was not expected. The factor that has the greater impact in the breakthrough time is probably the adsorption isotherm parameters, so a further investigation of these parameters was made.

In Table 46, a comparison is made for the specific saturations capacities obtained from gPROMS® and Ohlin [44]. Ohlin studied the removal of CO_2 and water from NG with zeolite ZSM-5 (pore size of around 5 Å) using the dual-site Langmuir isotherm.

Table 46: Comparison between specific saturation capacities from gPROMS® and Ohlin [44]

	gPROMS®	**Ohlin** [44]	**gPROMS®**	**Ohlin** [44]
Component	q_{si1} (mol/kg)		q_{si2} (mol/kg)	
H_2O	5.85	5.34	8.02	0.50
CO_2	0.95	2.78	2.93	0.04
CH_4	1.72	2	1.72	-

First of all, is important to mention that the values provided by Ohlin [44] are reported for a temperature equal to 35 ºC. However, it should be taken into account that the adsorption bed simulated in gPROMS® has a constant temperature of around 22 ºC, but the values of the parameters in the adsorption isotherm should not change largely with the temperature.

As one can see, the values of q_{si} are different, especially for the second adsorption site, where gPROMS® values are much higher. In the next table, the same comparison is made for the case of the affinity parameters.

Table 47: Comparison between affinity parameters in the adsorption sites from gPROMS® and Ohlin [44]

	gPROMS®	**Ohlin** [44]	**gPROMS®**	**Ohlin** [44]
Component	b_{i1} (kPa^{-1})		b_{i2} (kPa^{-1})	
H_2O	22.7	0.375	1583.7	79.0
CO_2	6.1	0.010	0.119	0.633
CH_4	0.002	0.001	0.002	-

Again, the results are quite different, especially for water.

This difference in the parameters of the adsorption isotherm is expected to have a great effect in the breakthrough time, as said before. Furthermore, an increase in the adsorption capacity (due to an increase in the parameters) of the more strongly removed component causes an increase in the breakthrough time, according to Marsh [42]. In fact, it seems that the parameters of the isotherm are

over-estimated for water, which is the most strongly adsorbed component, so this could explain the large deviation between breakthrough times.

The mean interstitial velocity was also compared for both simulations.

Table 48: Comparison of the results for mean interstitial velocity

	Mean interstitial velocity (m/s)
gPROMS®	0.71
Gholami et al. [7]	0.71
Deviation (%)	0.69

The mean interstitial velocity from gPROMS® fits very well the results from Gholami et al. [7] and the deviation is very small.

Also, the pressure drop in the adsorption bed was compared.

Table 49: Comparison of the results for mean pressure drop

	Mean pressure drop (bar)
gPROMS®	1.81
Gholami et al. [7]	1.78
Deviation (%)	1.7

Again, the mean pressure drop is very similar for both simulations, with a deviation of only 1.7 %.

5.3.4. Sensitivity Analyses

After getting results for the base case, some variables, more precisely the inlet gas pressure and temperature, the adsorption bed diameter, the adsorbent particle diameter, and the axial dispersion coefficient were changed in order to understand their impact in the simulation results. In all the tables presented in the following sub-chapter, the base case is highlighted in green.

5.3.4.1. Inlet Gas Pressure

In the first place, the inlet gas pressure, and therefore the pressure in the adsorption bed, was changed. The simulation results are presented in the next tables, regarding the breakthrough time, mean interstitial velocity, and mean pressure drop, and compared with the base case.

Table 50: Effect of inlet gas pressure in breakthrough time

Pressure (bar)	**Breakthrough time (min)**	**Δ Pressure (%)**	**Δ B. Time (%)**
45	1335	-29.7	-0.02
64	1336	-	-
80	1336	25.0	0.01

Table 51: Effect of inlet gas pressure in mean interstitial velocity

Pressure (bar)	**Mean interstitial velocity (m/s)**	**Δ Pressure (%)**	**Δ MIV (%)**
45	1.14	-29.7	59.4
64	0.71	-	-
80	0.61	25.0	-14

Table 52: Effect of inlet gas pressure in mean pressure drop

Pressure (bar)	Mean pressure drop (bar)	Δ Pressure (%)	Δ MPD (%)
45	2.88	-29.7	59.2
64	1.81	-	-
80	1.55	25.0	-14.3

The inlet gas pressure does not have an effect on the breakthrough time of the dehydration process, but it does have on the mean interstitial velocity: increasing the pressure causes a decrease in the interstitial velocity, which causes a decrease in the pressure drop.

5.3.4.2. Temperature

Next, the temperature was changed and the impact in the simulation results was studied.

Table 53: Effect of temperature in breakthrough time

Temperature (K)	Breakthrough time (min)	Δ Temperature (%)	Δ B. Time (%)
288	1368	-2.5	2.4
295.5	1336	-	-
308	1283	4.2	-4.0

Table 54: Effect of temperature in mean interstitial velocity

Temperature (K)	Mean interstitial velocity (m/s)	Δ Temperature (%)	Δ MIV (%)
288	0.69	-2.5	-3.7
295.5	0.71	-	-
308	0.76	4.2	6.1

Table 55: Effect of temperature in mean pressure drop

Temperature (K)	Mean pressure drop (bar)	Δ Temperature (%)	Δ MPD (%)
288	1.74	-2.5	-3.8
295.5	1.81	-	-
308	1.92	4.2	6.1

As it can be seen in Table 53, the breakthrough time decreases slightly while increase the temperature. This happens because by increasing the temperature, a smaller amount of water is adsorbed in the zeolite since this is an exothermic process. On the other hand, the mean interstitial velocity is increased by an increase in the temperature, which then causes an increase in the pressure drop.

5.3.4.3. Adsorption Bed Diameter

The bed diameter was also varied to study its impact in some variables. The consequent results are presented in the next set of tables.

Table 56: Effect of bed diameter in breakthrough time

Bed diameter (m)	Breakthrough time (min)	Δ Diameter (%)	Δ B. Time (%)
3	981	-14.3	-26.5
3.5	1336	-	-
4	1635	14.3	22.4

Table 57: Effect of bed diameter in mean interstitial velocity

Bed diameter (m)	Mean interstitial velocity (m/s)	Δ Diameter (%)	Δ MIV (%)
3	0.99	-14.3	37.8
3.5	0.71	-	-
4	0.55	14.3	-22.9

Table 58: Effect of bed diameter in mean pressure drop

Bed diameter (m)	Mean pressure drop (bar)	Δ Diameter (%)	Δ MPD (%)
3	3.37	-14.3	86.5
3.5	1.81	-	-
4	1.07	14.3	-40.6

One can see that increasing the bed diameter increases the breakthrough time since more water is adsorbed in the particles (the mass of solid desiccant is higher). Also, by increasing this diameter the mean interstitial velocity is decreased, as well as the pressure drop.

5.3.4.4. Adsorbent Particle Diameter

The zeolite particle diameter was changed and the next tables present the obtained results.

Table 59: Effect of particle diameter in breakthrough time

Particle diameter (mm)	Breakthrough time (min)	Δ Diameter (%)	Δ B. Time (%)
1	1336	-61.5	0
1.5	1336	-42.3	-0.01
2	1336	-23.1	-0.01
2.6	1336	-	-
3	1336	15.4	-0.01

Table 60: Effect of particle diameter in mean pressure drop

Particle diameter (mm)	Mean pressure drop (bar)	Δ Diameter (%)	Δ MPD (%)
1	5.7	-61.5	217.4
1.5	3.8	-42.3	111.8
2	2.9	-23.1	58.9
2.6	1.8	-	-
3	1.6	15.4	-12.9

Changing the adsorbent particle diameter does not have any visible effect in the breakthrough time. However, it has a great effect in the mean pressure drop across the bed: the pressure drop decreases while increasing the particle diameter.

5.3.4.5. Axial Dispersion

Finally, the axial dispersion coefficient was altered. This was done by choosing a *Specified* dispersion coefficient in gPROMS®, instead of the *Custom* option. The results are presented in the next table.

Table 61: Effect of axial dispersion coefficient in breakthrough time[12]

Axial dispersion (m^2/s)	Breakthrough time (min)	Δ Dispersion (%)	Δ B. Time (%)
$9.0x10^{-3}$	1333	868.2	-0.21
$9.3x10^{-4}$	1336	-	-
$9.0x10^{-5}$	1336	-90.3	0.01

As one can see, the axial dispersion does not have a great effect in the breakthrough time, only changing slightly the shape of the breakthrough curve, presented in Figure 60.

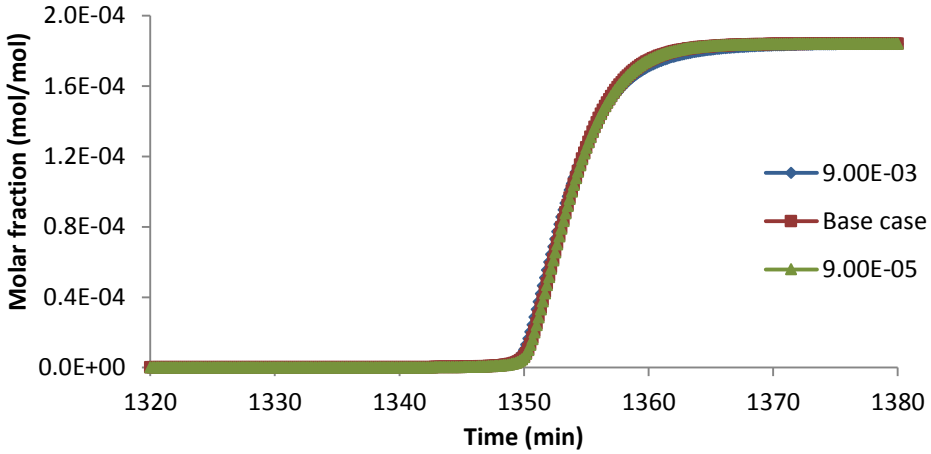

Figure 60: Effect of axial dispersion in breakthrough curve

On the other hand, changing the axial dispersion coefficient does not have any effect in the mean interstitial velocity and, therefore, in the mean pressure drop.

5.3.5. Non-isothermal Operation

Because adsorption is an exothermic process, heat is generated and conducted to the surface of the particles, which is then transferred to the gas phase by convection [7]. Therefore, in reality the adsorption process is not isothermal as considered in the base case. However, considering an isothermal operation diminishes the complexity of the problem, as said before. In order to confirm if this approximation is valid, at the end a simulation of the dehydration of NG using molecular sieves was performed by considering a non-isothermal bed. However, it was considered that the bed wall is fully insulated, so there is no heat exchanged between the wall and the bed.

[12] The axial dispersion coefficient for the base case is an average one, which is calculated in gPROMS® by summing the axial dispersion coefficients of all components and dividing it by the number of components.

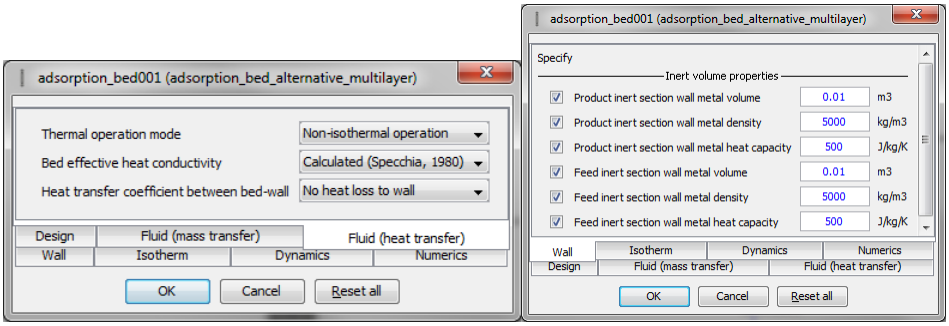

Figure 61: Dialog boxes of the adsorption bed model considering it is non-isothermal

The values considered in the *Wall* tab of the adsorption bed model, presented in Figure 61, are the default ones for the model, since there was no information available about these variables.

In Figure 62 a comparison of the breakthrough curves of water is presented for both isothermal and non-isothermal processes. A comparison is only made for the breakthrough time since this is the most important variable regarding an adsorption process.

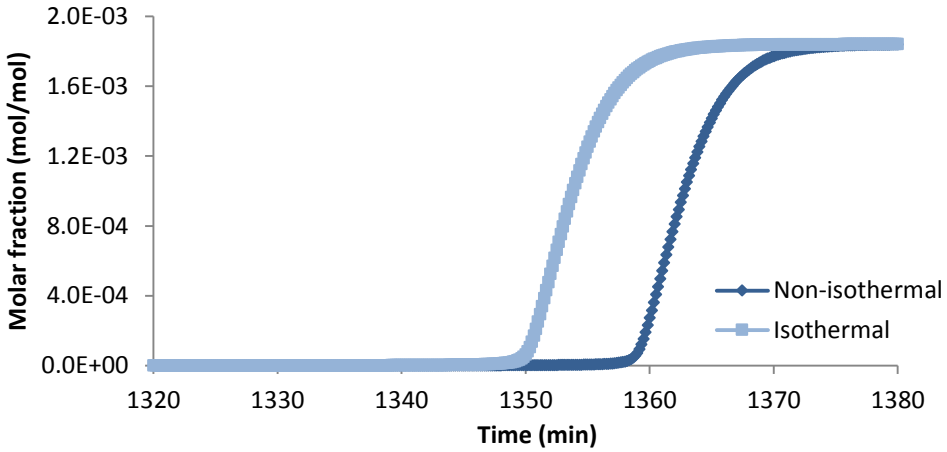

Figure 62: Water breakthrough curves for isothermal and non-isothermal operation

As one can see, the breakthrough curves are similar, only changing the actual breakthrough time: for a non-isothermal bed, the breakthrough time is around 1345 min, which corresponds to a deviation of 0.6% when considering an isothermal operation. Therefore, the simplification made is considered valid.

This page was intentionally left blank.

6. Conclusions and Future Work

6.1. Conclusions

The literature review done in the present dissertation showed that the global demand for natural gas (NG) is increasing rapidly. The costs of building a liquefied natural gas (LNG) plant have lowered since the mid-1980s, making LNG a major gas export method around the world instead of the less flexible pipelines. Since LNG plants require low temperatures, the improvement of the existing processes for NG treatment prior to liquefaction is therefore essential. This treatment is of great importance since NG contains several impurities that can cause several technical problems, such as corrosion, pollution, and plugging.

The composition of the NG extracted can vary largely depending on where it is extracted. In this manner, the adequate physical properties estimation is sometimes difficult to attain. On the other hand, this wide range in the composition causes the NG processing scheme to have a variety of different options, and their choice will depend on several factors.

There are some steps in NG treatment that are considered to be “industry standards” since they are reliable and well-known: it is the case of the acid gases removal from NG using amines. This process is well represented and explained in any book regarding gas purification and a great number of articles were found that replicated it. Even at Process Systems Enterprise Ltd. (PSE) the removal of CO_2 using different amines, and other solvents, is familiar in gCCS® (Carbon Capture and Storage). However, there was no available flowsheet for the simultaneous removal of CO_2 and H_2S from NG, especially using gPROMS® ProcessBuilder.

It is important to mention first that the assembling of flowsheets in gPROMS® is a user-friendly task since it is done by drag and dropping models and connecting them by hand. Therefore, most of the time spent with problem solving throughout the dissertation work had to do with initialization errors and loop closing problems.

In the construction of the flowsheet for NG sweetening, SAFT-VR SW equation of state was used in the form of a software recently developed (and still under development) at PSE, called gSAFT®. This software has the advantage to proper model strongly associating/reacting mixtures, such as CO_2 absorption in amine solutions. However, gSAFT® lacks validation for H_2S absorption in these solutions and the physical properties estimation is of extreme importance in modelling and simulating NG treatment. In this manner, the results obtained from gPROMS® simulation do not fit the results from the literature and the removal of H_2S is very low, especially compared to the almost complete removal of CO_2: the sweetened gas has 7.8 wt. % in H_2S (4.8 wt.% removal in the absorber) and only 1.3 ppmv in CO_2 (99.9 wt. % removal in the absorber), at the expense of around 21.5 MW of energy (7.3 GJ/ton acid gases absorbed). After making some sensitivity analyses, it was concluded that, without taking into account economic considerations, colder and high pressure absorbers decrease the acid gases content in the sweetened gas.

One of the most important steps in the treatment of NG is its dehydration, since the water specification for LNG plants is extremely tight. This dehydration may be accomplished in two different

ways: absorption or adsorption, which are by far the most common processes. These two methods were used in the present thesis since it is common in NG dehydration prior to liquefaction to first use the absorption method for bulk water removal, followed by adsorption for final purification.

First, a flowsheet for dehydration of NG using glycol was assembled and simulated. In the present work, an enhanced stripping process was used, since the use of a conventional atmospheric regenerator was not enough to achieve the desired glycol purity of 99 wt. % due to the temperature limitation in the reboiler. In the literature review it was not possible to find a complete assembled flowsheet with data available, only the description of enhanced stripping processes commonly used. For the conventional part of the flowsheet developed (without the enhanced process), typical data from the literature was used in the simulation. The dehydration flowsheet assembled in gPROMS®, which uses Peng-Robinson (PR) equation of state, fits well the simulation results from the literature, expect for a 4 % deviation in the absorption capacity that could be explained by the different physical properties package used. Therefore, a dried stream of NG is obtained with a water composition around 41 ppmv, with an energy consumption of 63 kW (5.4 GJ/ton water absorbed). Again, sensitivity analyses were performed and using colder and high pressure absorbers, as well as higher glycol purities, could achieve lower water contents in the dried gas.

Finally, the adsorption of water from NG using molecular sieves was modelled and simulated. The full process for dehydration with adsorption, with available data, was not found in the literature. However, there is information available concerning the water adsorption itself, such as typical data regarding the adsorption bed and adsorption isotherms. Therefore, custom models for the adsorption of water using zeolite 5A were developed. In the dynamic simulation, it was assumed an isothermal operation for the sake of simplicity and time. Because adsorption is an exothermic process, heat is generated and conducted to the surface of the particles, which is then transferred to the gas phase by convection. Therefore, in reality the adsorption process is not isothermal. However, according to the literature, the results for the breakthrough time (considered more relevant) did not change considerably when assuming a non-isothermal operation. In fact, a simulation of the dehydration of NG was made considering the adsorption as non-isothermal and the breakthrough time only increased in 0.6%. Thus, the simplification made is considered valid. The simulation results from gPROMS® do not fit well the results from the literature: the predicted breakthrough time (1336 min) is almost double. This happens since gPROMS® predicts significantly higher adsorption capacities. The adsorption isotherm parameters obtained in gPROMS® were compared with typical values. In fact, gPROMS® values are in most cases much higher, which could explain the difference observed between breakthrough times. After performing some sensitivity analyses, it was noted that an increase in the pressure and in the adsorbent particle diameter did not affect the breakthrough time, although it decreases the pressure drop on the bed. On the other hand, increasing the temperature caused a decrease in the breakthrough time and an increase in the mean pressure drop. Also, the breakthrough time was increased while increasing the adsorption bed diameter and the pressure drop was decreased. Finally, the axial dispersion coefficient does not have any visible effect in any of the adsorption variables considered above.

6.2. Future Work

Regarding the sweetening flowsheet, gSAFT® requires validation for the removal of H_2S with amines since its removal is of extreme importance in NG processing.

In what concerns the dehydration flowsheet with glycol, gSAFT® could be used as the physical properties package, after including all the necessary parameters regarding TEG, in order to compare gSAFT®'s results with Multiflash™'s.

For the flowsheet of water adsorption with molecular sieves, a more detailed investigation should be done in what concerns the adsorption isotherm model. In this way, other isotherm models should be found in literature and used in the flowsheet simulation, in order to investigate if the difference observed in the breakthrough times is actually due to the current model being used. Also, the regeneration of the zeolite could also be simulated in gPROMS®.

All the models used in the different flowsheets need validation with reliable experimental data, provided by customers, since in the present thesis gPROMS® simulation results were validated using simulation results from other modelling softwares.

The flowsheets for NG dehydration with TEG and acid gases removal are not robust, mainly due to the lack of robustness of the distillation_column model. Therefore, this model needs to be improved in what concerns its robustness in order to allow the usage of a wider range of operating conditions in the flowsheets.

Also, an optimization of all flowsheets should be performed in order to find the trade-off between the total costs and the impurities present in the treated gas.

After all the improvements are implemented, another thing that could be done is integrate all the flowsheets in an overall one: sweetening followed by dehydration with glycol and with molecular sieves in order to achieve the LNG specifications. However, to achieve pipeline specifications, it would be enough to integrate only the acid gases removal flowsheet with the glycol one.

At last, the remaining steps in NG processing (see Figure 2) need to be modelled, or their flowsheets assembled, and gather them all in a final flowsheet that would allow the simulation of a NG processing plant prior to liquefaction.

This page was intentionally left blank.

Bibliography

[1] A. J. Kidnay and W. R. Parrish, Fundamentals of Natural Gas Processing, Boca Raton: Taylor & Francis Group, 2006.

[2] Exxon Mobil, “The Outlook for Energy: A View to 2040,” Texas, 2013.

[3] World Energy Council, “World Energy Resources,” London, 2013.

[4] A. Kohl and R. Nielsen, Gas Purification, Texas: Gulf Publishing Company, 1997.

[5] R. K. Abdulrahman and I. M. Sebastine, “Natural gas sweetening process simulation and optimization: A case study of Khurmala field in Iraqi Kurdistan region,” *Journal of Natural Gas Science and Engineering,* no. 14, pp. 116-120, 2013.

[6] M. Ghati, “A Study on Selection and Design of Natural Gas Dehydration Technology,” Norwegian University of Science and Technology, Specialization Project, 2013.

[7] M. Gholami, M. R. Talaie and S. Roodpeyma, “Mathematical modelling of gas dehydration using adsorption process,” *Chemical Engineering Science,* no. 65, pp. 5942-5949, 2010.

[8] S. Mokhatab, W. A. Poe and J. G. Speight, Handbook of Natural Gas Transmission and Processing, Gulf Professional Publishing, 2006.

[9] [Online]. Available: http://www.plant-process.com/gas_processing/. [Accessed 8 April 2014].

[10] T. Eastwood, *Experience & Advances in Nitrogen Rejection from Natural Gas,* IChemE, 2011.

[11] [Online]. Available: refiningonline.com/abpg_kb/ABPG-5.pdf. [Accessed 18 August 2014].

[12] [Online]. Available: http://www.prosernat.com/en/processes/gas-sweetening/advamine/. [Accessed 9 October 2014].

[13] Gas Processors Suppliers Association, Engineering Data Book, Tulsa, Oklahoma: Gas Processors Suppliers Association, 2004.

[14] F. Lallemand, G. Perdu, L. Normand, C. Weiss, J. Magne-Drisch and S. Gonnard, *Extending the treatment of highly sour gases: part 1,* Prosernat, Total EP and IFP Energies Nouvelles, 2013.

[15] M. Stewart and K. E. Arnold, Gas Sweetening and Processing Field Manual, USA: Gulf Professional Publishing, 2011.

[16] M. L. Spears, K. M. Hagan, J. A. Bullin and C. J. Michalik, “Converting to DEA/MDEA mix ups sweetening capacity,” *Oil&Gas Journal,* 1996.

[17] R. H. Perry and D. W. Green, Perry's Chemical Engineers' Handbook, McGraw-Hill, 1997.

[18] W. J. Thomas and B. Crittenden, *Adsorption Technology & Design,* Elsevier Science & Technology Books, 1998.

[19] D. M. Ruthven, Principles of Adsorption and Adsorption Processes, John Wiley & Sons, Inc., 1984.

[20] [Online]. Available: http://www.psenterprise.com. [Accessed 1 May 2014].

[21] Process Systems Enterprise Limited, “Model Developer Guide,” London, 2013.

[22] Process Systems Enterprise Limited, “gPROMS ModelBuilder Guide,” London, 2013.

[23] Process Systems Enterprise Limited, “Physical Properties Guide,” London, 2013.

[24] Process Systems Enterprise Limited, *Process Model Library,* London, May 2013.

[25] Infochem Computer Services Limited, “User Guide for Models and Physical Properties,” London, 2013.

[26] [Online]. Available: http://www.elmhurst.edu/~chm/vchembook/174temppres.html. [Accessed 15 August 2014].

[27] M. Frost, E. Karakatsani, N. von Solms, D. Richon and G. Kontogeorgis, “Vapor-Liquid Equilibrium of Methane with Water and Methanol. Measurements and Modeling,” *J. Chem. Eng. Data,* no. 59, pp. 961-967, 2014.

[28] A. Bahadori, H. B. Vuthaluru and S. Mokhatab, “Analyzing solubility of acid gas and light alkanes in triethylene glycol,” *Journal of Natural Gas Chemistry,* no. 17, pp. 51-58, 2008.

[29] Y. Kayukawa, K. Fujii and Y. Higashi, “Vapor-Liquid Equilibrium (VLE) Properties for the Binary Systems Propane (1) + n-Butane (2) and Propane (1) + Isobutane (3),” *J. Chem. Eng. Data,* no. 50, pp. 579-582, 2005.

[30] T. Ishiguro, K. Matsumoto and Yakugaku-zasshi, *J. Chem. Eng. Data,* no. 75, pp. 1414-1417, 1955.

[31] A. K. Mostafazadeh, M. R. Rahimpour and A. Shariati, *J. Chem. Eng. Data,* no. 54, pp. 876-881, 2009.

[32] F. Gironi, M. Maschietti and V. Piemonte, “24th East European Symposium on Applied Thermodynamics Book of Abstracts,” Santiago de Compostela, June 27-July 1 2009.

[33] A. Gil-Villegas, A. Galindo, P. J. Whitehead, S. J. Mills, G. Jackson and A. N. Burgess, “Statistical associating fluid theory for chain molecules with attractive potentials of variable range (SAFT-VR),” *Journal of Chemical Physics,* no. 106, pp. 4168-4186, 1997.

[34] A. Galindo, L. A. Davies, A. Gil-Villegas and G. Jackson, “The thermodynamics of mixtures and the corresponding mixing rules in the SAFT-VR approach for potentials of variable range,” *Molecular Physics,* no. 93, pp. 241-252, 1998.

[35] A. Muhammad and Y. GadelHak, “Correlating the additional amine sweetening cost to acid gases load in natural gas using Aspen Hysys,” *Journal of Natural Gas Science and Engineering,* no. 17, pp. 119-130, 2014.

[36] R. N. Maddox and J. Morgan, Gas Conditioning and Processing: Gas Treating and Sulfur Recovery, vol. 4, Oklahoma: Campbell Petroleum Series, 2008.

[37] K. Lunsford and G. McIntyre, “Decreasing Contactor Temperature Could Increase Performance,” in *Proceedings of the Seventy-Eight GPA Annual Convention*, Nashville, 1999.

[38] D. L. Christensen, “Gas Dehydration - Thermodynamic simulation of the water/glycol mixture,” Aalborg University Esbjerg, Master Thesis, 2009.

[39] Aspen Technology, Inc., “Hysys 2004.2 Simulation Basis,” Cambridge, 2005.

[40] J. A. Ritter, S. J. Bhadra and A. D. Ebner, “On the Use of the Dual-Process Langmuir Model for Correlating Unary Equilibria and Predicting Mixed-Gas Adsorption Equilibria,” *Langmuir,* no. 27, pp. 4700-4712, 2011.

[41] K. S. Knaebel, *Adsorbent Selection,* Dublin: Adsorption Research, Inc..

[42] H. Marsh, Activated Carbon Compendium, United Kingdom: Elsevier Science, 2001.

[43] F. Zeinali, A. A. Ghoreyshi and G. D. Najafpour, “Adsorption of Dicloromethane from Aqueous Phase Using Granular Activated Carbon: Isotherm and Breakthrough Curve Measurements,” *Middle-East Journal of Scientific Research,* no. 5, pp. 191-198, 2010.

[44] L. Ohlin, “Adsorption of Water, Carbon Dioxide and Methane in Zeolite ZSM-5 Studied Using in-situ ATR-FTIR Spectroscopy,” Lulea University of Technology, Lulea, April 2013.

[45] eni saipem, Oil and Gas Production and Processing: Engineering and Construction Project References, Milan: Saipem S.p.A., 2011.

[46] C. H. Twu, V. Tassone, W. D. Sim and S. Watanasiri, “Advanced equation of state method for modeling TEG-water for glycol gas dehydration,” *Fluid Phase Equilibria,* no. 228-229, pp. 213-221, 2005.

[47] Process Systems Enterprise, *gML Libraries for Pressure Swing Adsorption (PSA),* London.

Appendices

A-1. Industrial Applications [45]

In this appendix, projects for the opening/revamping/change of NG processing plants, more precisely for sweetening and dehydration, are presented.

A-1.1. Sweetening

Table 62: NG sweetening plants' projects

Country, Location	Company	Capacity (MMSCFD)	Scope of work[13]	On stream
United Arab Emirates, Shah Field	Abu Dhabi Gas Development Company Ltd.	4x250	EPC	Under execution
Algeria, Arzew	Sonatrach	918	EPC	Under execution
Saudi Arabia, Hawiyah	Aramco Overseas CO. BV / Saudi Aramco	816	EPC	2008
Libya, Mellitah	Agip Gas BV – Libyan Branch	3x255	EPC	2007
Qatar, Mesaieed	Qatar Petroleum (QP)	15, 55, 110	EPC	2005
Iran, Assaluyeh	Hyundai Engineering & Construction Co.	2 000, 70	ES	2004
Iran, Assaluyeh	Agip Iran B.V.	2 000, 70	ES	2001
Malaysia, Tok Arun	Petronas Gas Berhad	2x44, 2x640	EPC	1998
Italy, Val d'Agri	Agip S.p.A.	90	ES	1996
United Arab Emirates, Jarn Yaphour	Abu Dhabi National Oil Company (ADNOC)	60	ES	1993
Italy, Ferrandina	Agip S.p.A.	12 (expansion)	L	1986
Italy, Ferrandina	Agip S.p.A.	35	ES	1983
Italy, Cupello	Agip S.p.A.	46	ES	1980
Russia, Grozny	V/O Machinoimport	261	EP	1973
United Arab Emirates	Government – Public Works Department	50	EPC	1969
Russia, Perm	V/O Machinoimport	63	EP	1969
Argentina, Pico Truncado	Gas Del Estado	224	ES	1965
Italy, Ferrandina	Agip S.p.A.	35	ES	1965

A-1.2. Dehydration

Table 63: NG dehydration plants' projects

Country, Location	Company	Capacity (MMSCFD)	Scope of work	On stream
United Arab Emirates, Shah Field	Abu Dhabi Gas Development Company Ltd.	2x340	EPC	Under Execution
Kuwait, West Kuwait	Kuwait Oil Company	234	EPC	Under execution

[13] EPC: Engineering, procurement and construction; EP: Engineering and procurement, ES: Extended settlement

(continuation of previous table)				
Turkmenistan	Dragon Oil (Turkmenistan) Ltd.	202	ES	Under execution
Algeria, Arzew	Sonatrach	875	EPC	Under execution
Kuwait, South East Kuwait	Kuwait Oil Company	250	EPC	Under execution
Algeria, Hassi Messaoud	Sonatrach	3x283	EPC	Under execution
Libya, Mellitah	Agip Gas BV – Libyan branch	3x255	EPC	2007
Qatar, Al Khaleej	Exxomobil Middle East	750	EPC	2006
Kuwait, North Kuwait	Kuwait Oil Company	250	EPC	2005
Iran, Darquain Field	Agip Iran BV	83	EPS	2004
Iran, Assaluyeh	Hyundai Engineering & Construction Co.	4x500	ES	2004
Saudi Arabia, Qatif	Aramco Overseas Co. BV/Saudi Aramco	364	EPC	2004
Egypt, Port Said	BP Global Investment Ltd.	1 000	ES	2004
Qatar, Ras Laffan	Ras Laffan LNG Co. Ltd.	730	EPC	2003
Qatar, Dukhan	Qatar Petroleum (QP)	250	EPC	2002
Iran, Assaluyeh	Agip Gas BV	4x500	ES	2001
Nigeria, Obiafu, Obrikom, Irri, Kwale	Nigerian Agip Oil Co. Ltd. (NAOC)	347	ES	2001
United Arab Emirates, Asab	Abu Dhabi National Oil Company (ADNOC)	2x375	EPC	2001
Oman, Saih Rawl	Petroleum Development Oman (PDO)	2x520	EPC	1999
Oman, Barik	Petroleum Development Oman (PDO)	777	EPC	1999
United Arab Emirates, Sahil	ADCO	36	EPC	1998
Malaysia, Tok Arun	Petronas Gas Berhad	2x640	EPC	1998
Algeria, Bir Rebaa Nord	Agip (Africa) Ltd. Sonatrach	141	EP	1996
Argentina, Loma La Lata	YPF S.A.	2x740	ES	1995
Algeria, Hamra	Sonatrach	530	EP	1995
Libya, Bu Attifel	Agip (N.A.M.E.) Ltd.	388	EPC	1995
United Arab Emirates, Jarn Yaphour	ADNOC	60	ES	1993
Italy, Gela	Agip S.p.A.	2	ES	1992
Egypt, El Qara	Agip S.p.A.	300	ES	1992
Algeria, Rhourde Nouss	Sonatrach	4x375	EPC	1988
Oman, Birba	PDO	32	ES	1988
Italy, Falconara	Agip S.p.A.	343 (expansion)	ES	1988
Tanzania, Songo-Songo Island	Tanzania Petroleum Development Corporation	100	ES	1987
Egypt, Abu Madi	Egyptian General Petroleum Corporation (EGPC)	251	EPC	1987
Egypt, Abu Madi	Belayim Petroleum Company (PETROBEL)	120 (expansion)	EPC	1985

China, Zhong Yuan Whenlin	China National Technical Import & Export Corp.	45	ES	1985
Italy, Minerbio	Agip S.p.A.	1 590 (expansion)	ES	1984
Iraq, Buzurgan	Agip S.p.A.	110	ES	1982
Iraq, Misan	Agip S.p.A.	298	ES	1982
Iraq, North Rumaila	State Organization for Oil Projects (SCOP)	1 046	ES	1981
Oman, Yibal	Ministry of Petroleum	124	EPC	1978
Italy, Malossa	Agip S.p.A.	424	ES	1976
Iraq, North Rumaila	Iraq National Oil Company (INOC)	53	EPC	1976
Italy, Sergnano	Agip S.p.A.	1 271 (expansion)	ES	1975
Russia, Grozny	V/O Machinoimport	261	EP	1973
Russia, Perm	V/O Machinoimport	63	EP	1969
Argentina, Pico Truncado	Gas del Estado	373	ES	1965
Iraq, Rumaila	Ministry of Industry and Minerals	53	EPC	1962

This page was intentionally left blank.

A-2. Peng-Robinson Equation of State [25]

The total pressure using the Peng-Robinson (PR) equation of state is given by:

$$P = \frac{nRT}{V-b} + \frac{a}{V^2 + 2bV - b^2} \tag{20}$$

The standard (Van der Waals 1-fluid) mixing rules are:

$$n = \sum_i n_i \tag{21}$$

$$a = \sum_{ij} \sqrt{a_i a_j}\left(1 - k_{ij}\right) n_i n_j \tag{22}$$

$$b = \sum_i b_i n_i \tag{23}$$

where a and b are function of pure component critical temperature, pressure, and acentric factor.

$$a_i = a_{ci}\left(1 + \kappa_i\left(1 - \sqrt{T/T_{ci}}\right)\right)^2 \tag{24}$$

$$a_{ci} = 0.45724\frac{R^2 T_{ci}^2}{P_{ci}} \tag{25}$$

$$\kappa_i = 0.37464 + 1.54226\omega_i - 0.26992\omega_i^2 \tag{26}$$

$$b_i = 0.07780\frac{RT_{ci}}{P_{ci}} \tag{27}$$

This page was intentionally left blank.

A-3. Binary Interaction Parameters

The *k* constants introduced in Multiflash™, which predict the relation between binary interaction parameters and temperature, are presented in Table 64.

Table 64: k constants introduced in Multiflash™ and coefficients of determination of all the regressions

Binary system	k_0	k_1 (K^{-1})	k_2 (K^{-2})	R^2
CO_2-CH_4	0.67	-5.19×10^{-3}	1.17×10^{-5}	0.339
CO_2-C_2H_6	0.51	-2.96×10^{-3}	5.86×10^{-6}	0.620
CO_2-i-C_4H_{10}	0.57	-3.32×10^{-3}	6.02×10^{-6}	0.939
CO_2-n-C_4H_{10}	0.60	-3.28×10^{-3}	5.65×10^{-6}	0.900
CO_2-C_3H_8	-0.31	2.25×10^{-3}	-2.44×10^{-6}	0.694
CO_2-i-C_5H_{12}	8.92	-0.05	5.74×10^{-5}	0.956
CO_2-n-C_5H_{12}	1.43	8.10×10^{-3}	1.24×10^{-5}	0.871
CO_2-H_2S	0.11	-5.46×10^{-4}	5.60×10^{-6}	0.789
CO_2-N_2	5.22	-0.04	8.52×10^{-5}	0.678
CO_2-TEG	-0.02	3.65×10^{-4}	0	0.992
H_2S-i-C_4H_{10}	0.76	-4.61×10^{-3}	7.35×10^{-6}	0.845
H_2S-i-C_5H_{12}	2.01	-0.01	1.81×10^{-5}	0.998
H_2S-n-C_5H_{12}	0.97	5.82×10^{-3}	9.18×10^{-6}	0.993
H_2S-C_6H_{14}	0.12	-1.20×10^{-4}	0	0.996
H_2S-CH_4	-0.06	4.61×10^{-4}	0	0.948
H_2S-H_2O	-0.27	7.87×10^{-4}	0	1
H_2S-TEG	0.06	1.32×10^{-4}	0	0.838
CH_4-C_3H_8	0.09	-7.62×10^{-4}	1.66×10^{-6}	0.313
CH_4-n-C_4H_{10}	0.14	-1.27×10^{-3}	3.02×10^{-6}	0.897
CH_4-H_2O	-1.40	3.44×10^{-3}	0	0.985
CH_4-N_2	0.30	-4.21×10^{-3}	1.59×10^{-5}	0.930
CH_4-C_6H_{14}	0.18	1.13×10^{-3}	1.86×10^{-6}	0.482
CH_4-TEG	0.04	6.12×10^{-4}	0	0.999
C_2H_6-CH_4	0.13	-1.40×10^{-3}	3.68×10^{-6}	0.808
C_2H_6-C_3H_8	0.41	-3.33×10^{-3}	6.46×10^{-6}	0.498
C_2H_6-i-C_4H_{10}	0.93	-6.11×10^{-3}	9.88×10^{-6}	0.941
C_2H_6-n-C_4H_{10}	1.46	-8.62×10^{-3}	1.29×10^{-5}	0.504
C_2H_6-n-C_5H_{12}	0.73	-4.51×10^{-3}	7.00×10^{-6}	0.931
C_2H_6-C_6H_{14}	2.27	-0.01	1.71×10^{-5}	1
C_2H_6-N_2	-0.50	3.83×10^{-3}	-6.55×10^{-6}	0.937
C_2H_6-TEG	0.07	3.83×10^{-4}	0	0.991
C_3H_8-i-C_4H_{10}	0.02	1.00×10^{-4}	0	0.235
C_3H_8-H_2O	-0.65	1.49×10^{-5}	0	0.999
C_3H_8-TEG	0.05	3.74×10^{-4}	0	0.976
n-C_4H_{10}-N_2	1.72	-0.01	1.66×10^{-5}	0.573
n-C_4H_{10}-H_2O	-0.71	1.55×10^{-3}	0	0.998
C_6H_{14}-H_2O	1.16	-6.15×10^{-3}	9.06×10^{-6}	0.490
C_6H_{14}-N_2	-1.03	7.32×10^{-3}	-1.13×10^{-5}	0.925
C_6H_{14}-n-C_5H_{10}	26.82	-0.18	2.94×10^{-4}	1
TEG-H_2O	-2.92	7.67×10^{-3}	0	0.998

This page was intentionally left blank.

A-4. Twu-Sim-Tassone Equation of State [46]

Twu, Sim and Tassone developed CEoS/A^E mixing rules that allow a smooth transition of the mixing rules to the conventional van der Waal's one-fluid mixing rule. Also, they proposed a new cubic equation of state to better predict properties of polar and heavy components and a G^E model, which when combined with the mixing rules allows the description of van der Waal's fluids and highly non-ideal mixtures over a wide range of temperatures and pressures.

The Twu-Sim-Tassone (TST) cubic equation of state is represented by the following equation:

$$P = \frac{R}{v-b} - \frac{a}{v^2 + 2.5bv - 1.5b^2} \tag{28}$$

The values of a and b at the critical temperatures are given by:

$$a_c = 0.470507 \frac{R^2 T_c^2}{P_c} \tag{29}$$

$$b_c = 0.0740740 \frac{RT_c}{P_c} \tag{30}$$

$$Z_c = 0.296296 \tag{31}$$

The values of Z_c from the Redlich Kwong Soave (RSK) and PR equations of state are both larger than 0.3, but the value for TST is slightly below 0.3, which is closer to the typical value for most components.

The parameter a is a function of temperature, as it is shown in equation 32:

$$a = T_r^{N(M-1)} e^{L\left(1-T_r^{NM}\right)} a_c \tag{32}$$

The parameters L, N and M are unique to each component and are obtained from the regression of pure component vapour pressure data.

The parameters a and b for zero-pressure are given by the following equations:

$$a^* = b^* \left[\frac{a^*_{vdw}}{b^*_{vdw}} + \frac{1}{C_r} \left(\frac{A_0^E}{RT} - \frac{A_{0vdw}^E}{RT} \right) \right] \tag{33}$$

$$b = b_{vdw} \tag{34}$$

$$a^* = \frac{Pa}{R^2 T^2} \tag{35}$$

$$b^* = \frac{Pb}{RT} \tag{36}$$

Expressions for calculation of A^E_{0vdw}, C_r, a_{vdw} and b_{vdw} are presented in [46].

Also, a multi-component equation for a liquid activity model was proposed to be used in the TST excess energy mixing rules:

$$\frac{G^E}{RT} = \sum_i^n x_i \frac{\sum_j^n x_j \tau_{ji} G_{ji}}{\sum_k^n x_k G_{ki}} \tag{37}$$

$$\tau_{ji} = \frac{A_{ji}}{T} \tag{38}$$

$$G_{ji} = exp\left(-\alpha_{ji}\tau_{ji}\right) \tag{39}$$

This page was intentionally left blank.

A-5. Sweetening

A-5.1. Simulation Results

In the following figures, the composition profiles of CO_2 and diethanol amine (DEA), in the liquid and vapour phases, in the absorber and regenerator are presented, as well as the temperature profile in these columns.

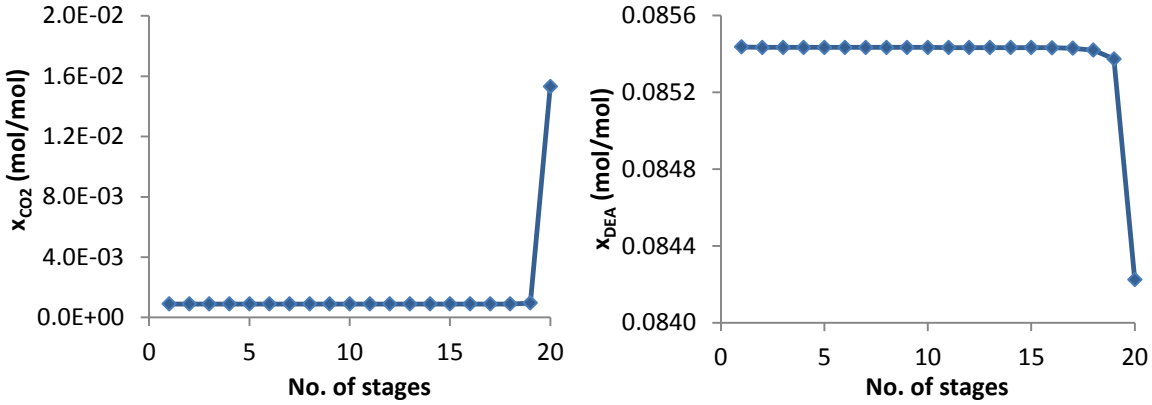

Figure 63: Composition profiles in the liquid phase of CO_2 and DEA, in the absorber

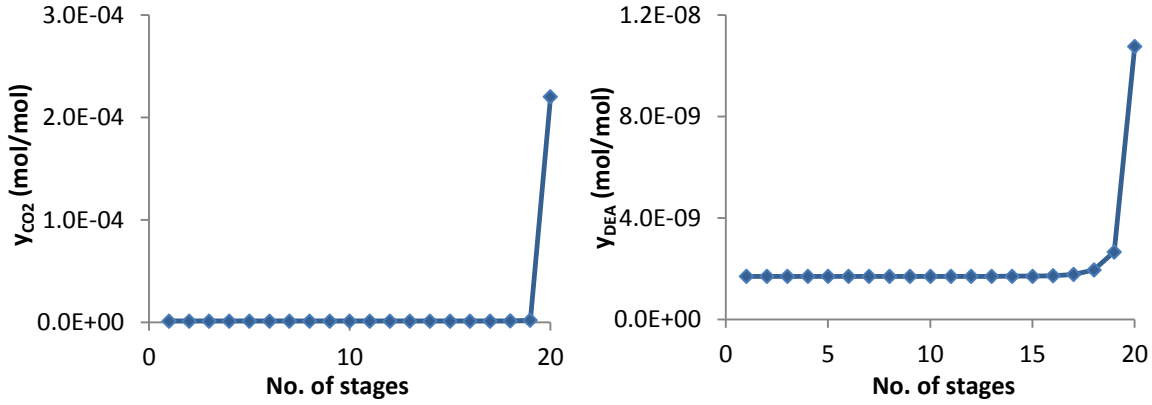

Figure 64: Composition profiles in the vapour phase of CO_2 and DEA, in the absorber

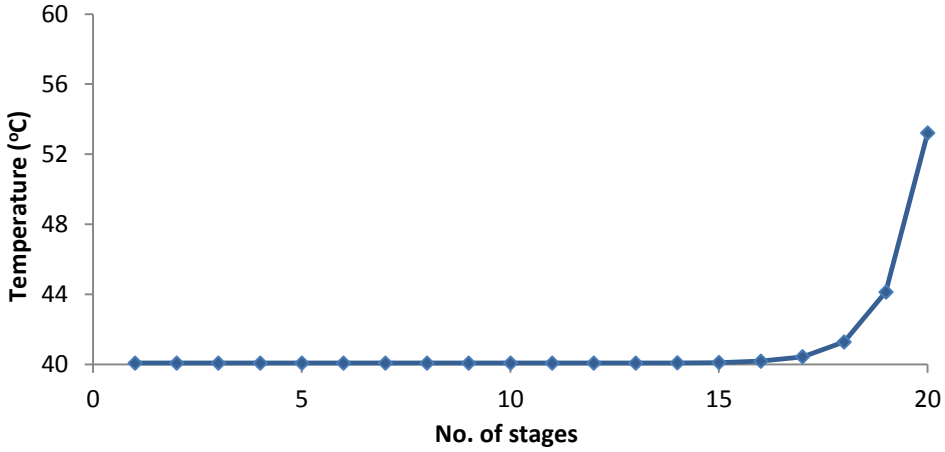

Figure 65: Temperature profile of the absorber

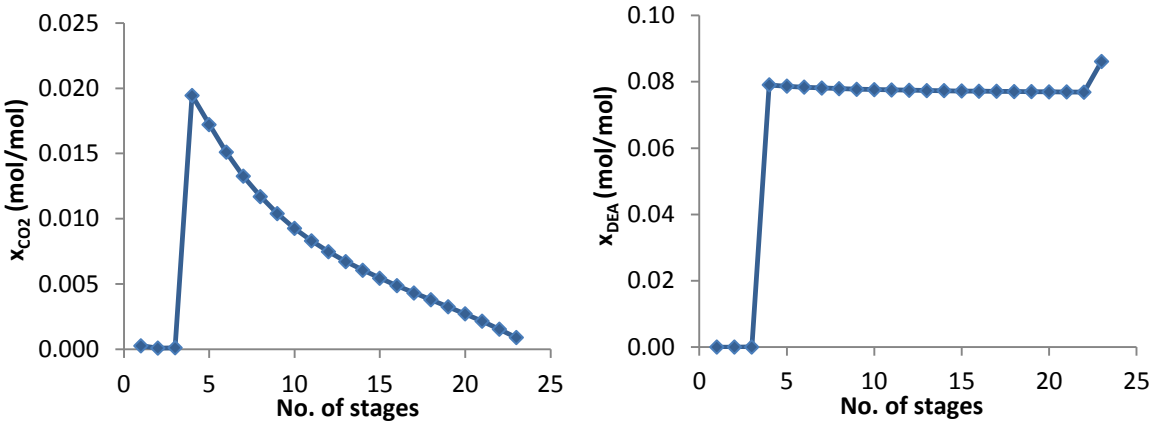

Figure 66: Composition profiles in the liquid phase of CO_2 and DEA, in the regeneration column

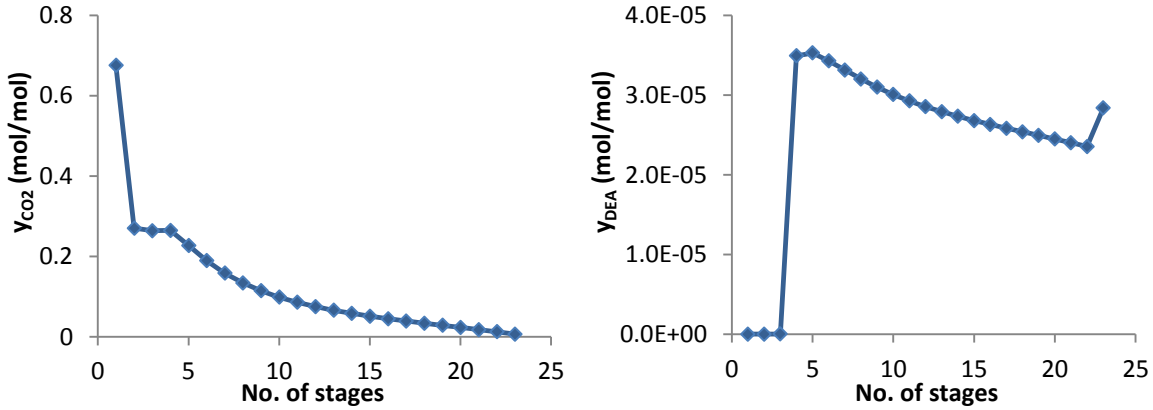

Figure 67: Composition profiles in the vapour phase of CO_2 and DEA, in the regeneration column

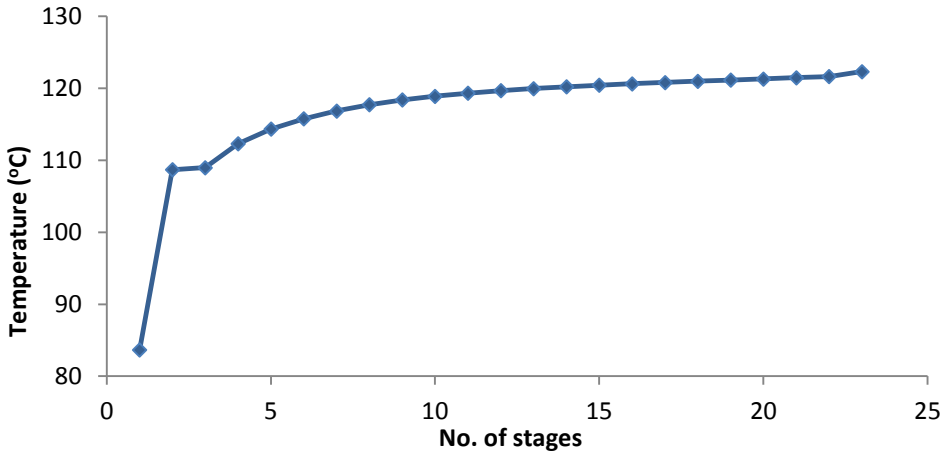

Figure 68: Temperature profile of the regeneration column

A-5.2. Sensitivity Analyses Results

In this appendix, the results of the sensitivity analyses performed for the acid gases removal are available. So, in the following tables the values of the variables changed are presented, as well as their impact in other variables. Also, the deviation between the sensitivity analyses' results and the base case are presented. In all the tables presented, the base case is highlighted in green.

Table 65: Results and deviations from changing the number of stages in the absorber

N	CO_2 (ppmv)	H_2S (ppmv)	Rich loading	Δ N (%)	Δ CO_2 (%)	Δ H_2S (%)	Δ Loading (%)
8	1.3390	52436.10	0.181769	-60	$-2.7x10^{-2}$	$1.5x10^{-4}$	$7.3x10^{-3}$
10	1.3389	52436.11	0.181766	-50	$-3.3x10^{-2}$	$1.7x10^{-4}$	$5.8x10^{-3}$
15	1.3387	52436.14	0.181770	-25	$-4.6x10^{-2}$	$2.3x10^{-4}$	$7.8x10^{-3}$
20	1.3393	52436.02	0.181755	-	-	-	-
22	1.3391	52436.05	0.181759	10	$-1.3x10^{-2}$	$5.7x10^{-5}$	$2.1x10^{-3}$

Table 66: Results and deviations from changing the inlet temperature of NG

NG feed's temperature (°C)	CO_2 (ppmv)	H_2S (ppmv)	Δ T (%)	Δ CO_2 (%)	Δ H_2S (%)
35	1.335	52017	-7.9	-0.3	-0.8
37	1.338	52304	-2.6	-0.1	-0.3
38	1.339	52436	-	-	-
39	1.341	52561	2.6	0.1	0.2
40	1.343	52679	5.3	0.2	0.5

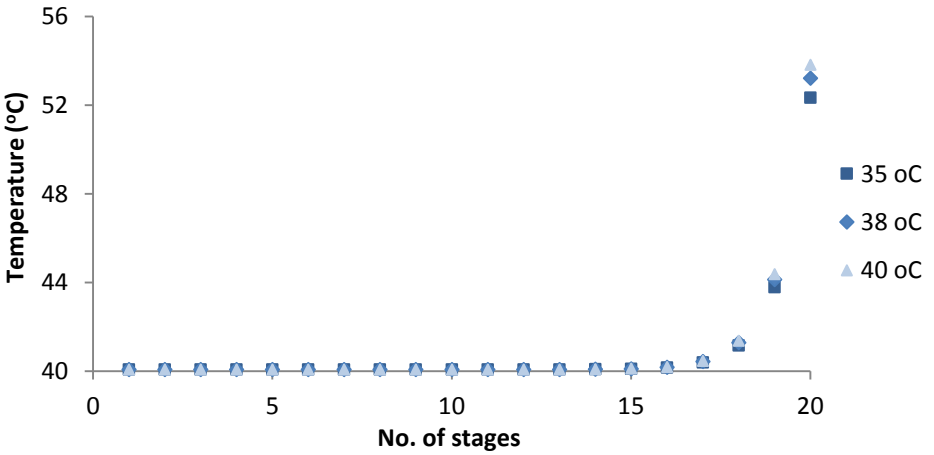

Figure 69: Absorber's temperature profile caused by the variation of NG feed's temperature

Table 67: Results and deviations from changing the lean solvent's temperature

Lean amine's temperature (°C)	CO_2 (ppmv)	H_2S (ppmv)	Δ T (%)	Δ CO_2 (%)	Δ H_2S (%)
40	1.34	52436	-	-	-
41	1.48	52441	2.5	10.5	0.01
44	2.46	52402	10.0	84.0	-0.06
45	2.97	52382	12.5	121.9	-0.10

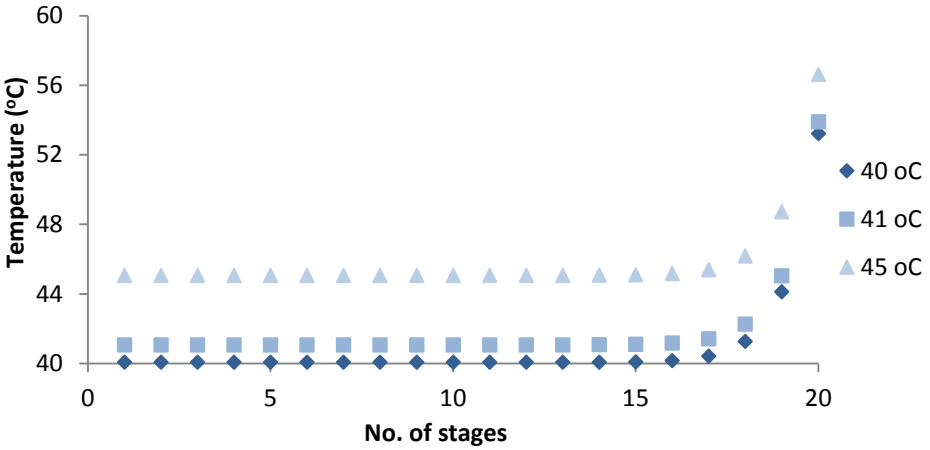

Figure 70: Absorber's temperature profile caused by the variation of lean solvent's temperature

Table 68: Results and deviations from changing the pressure in the absorber

Absorber's pressure (bar)	CO_2 (ppmv)	H_2S (ppmv)	Δ P (%)	Δ CO_2 (%)	Δ H_2S (%)
31.0	1.50	53167	-12.7	12.2	1.4
33.0	1.42	52851	-7.0	6.0	0.8
35.5	1.34	52436	-	-	-
38.0	1.26	52008	7.0	-6.1	-0.8

A-6. Dehydration with Glycol

A-6.1. Simulation Results

In the following figures, the composition profiles of water and triethylene glycol (TEG), in the liquid and vapour phases, in the absorber and regenerator are presented, as well as the temperature profile in these columns.

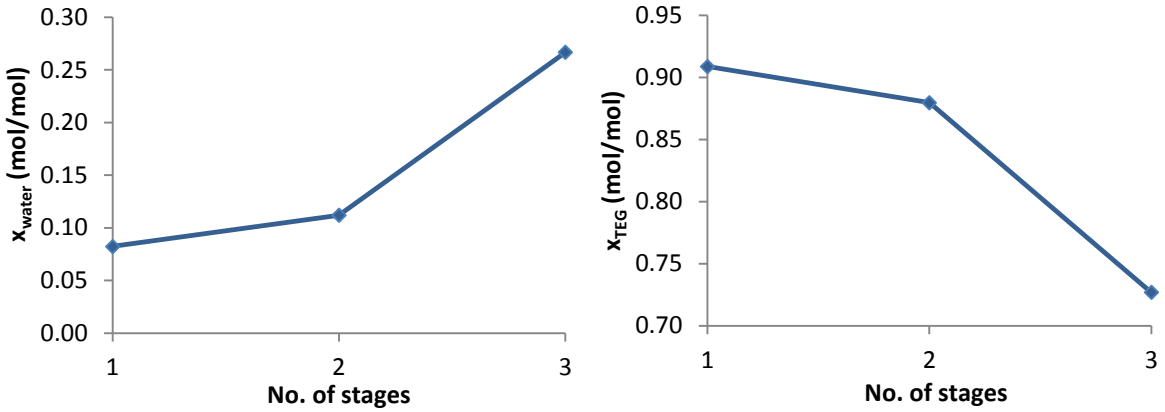

Figure 71: Composition profiles in the liquid phase of water and TEG, in the absorber

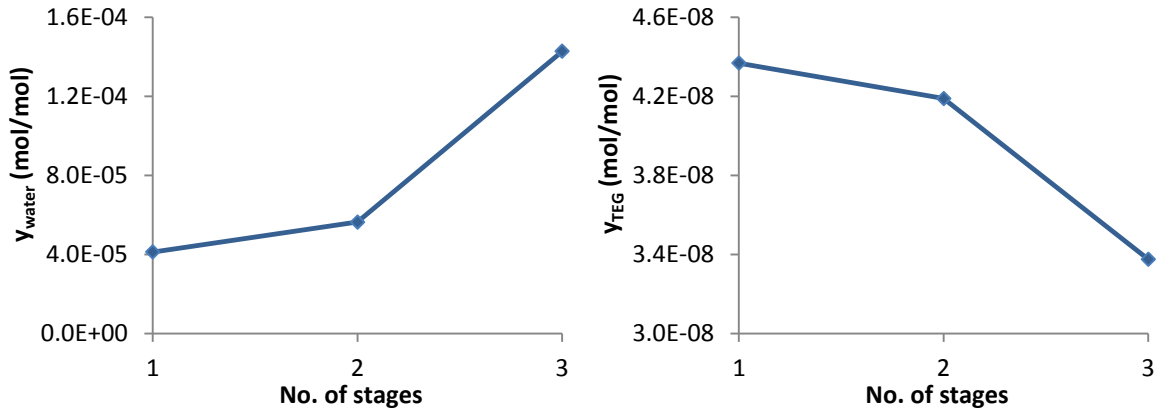

Figure 72: Composition profiles in the vapour phase of water and TEG, in the absorber

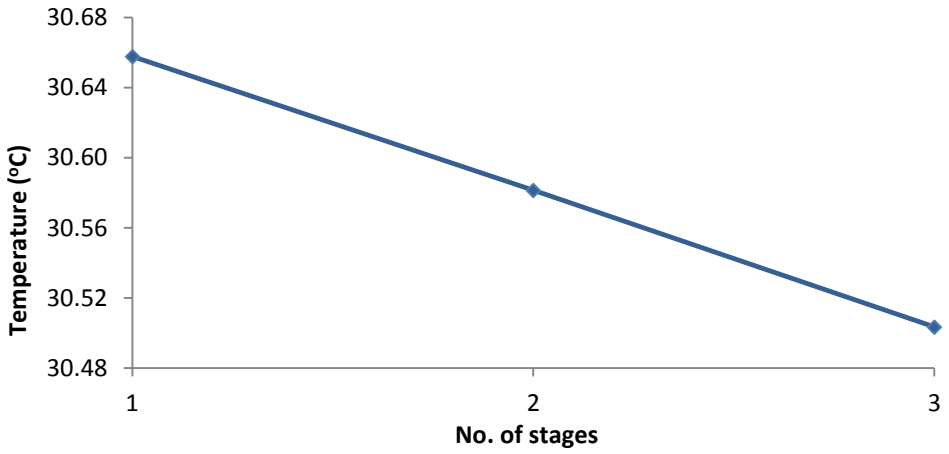

Figure 73: Temperature profile of the absorber

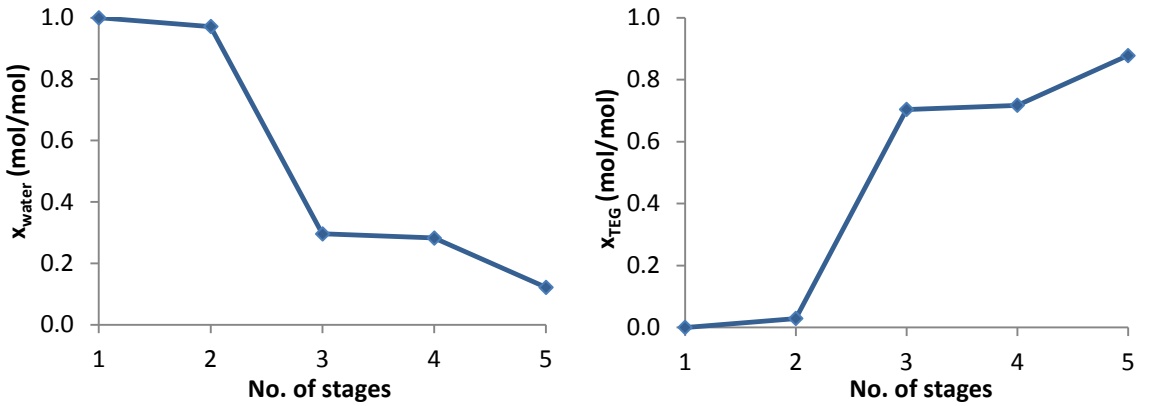

Figure 74: Composition profiles in the liquid phase of water and TEG, in the regeneration column

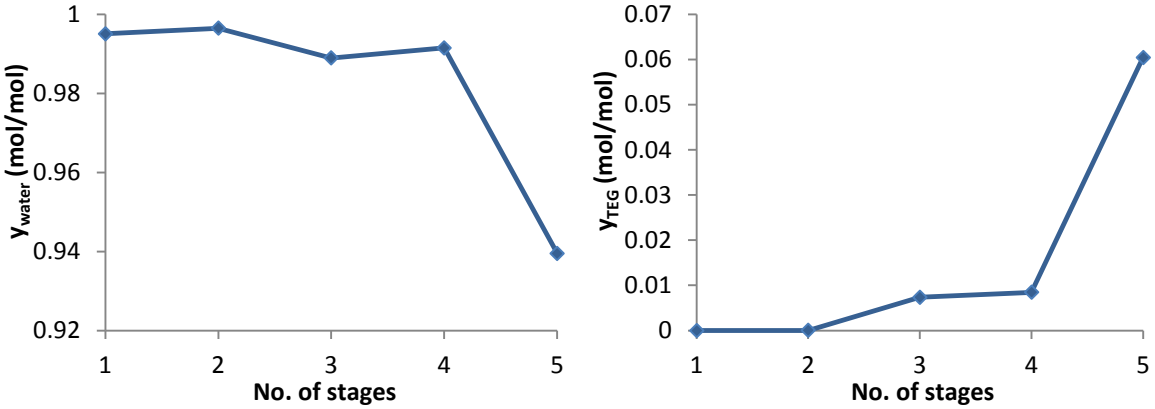

Figure 75: Composition profiles in the vapour phase of water and TEG, in the regeneration column

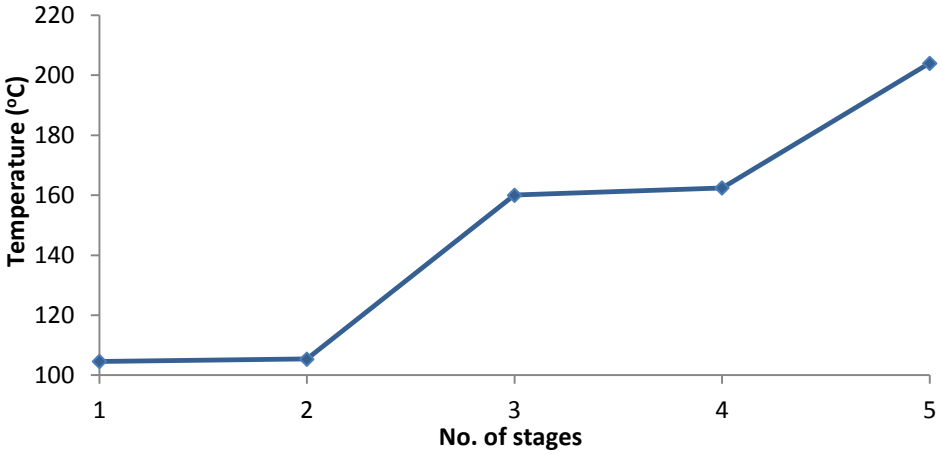

Figure 76: Temperature profile of the regeneration column

A-6.2. Sensitivity Analyses Results

Again, the sensitivity analyses results are presented in the following tables. In all the tables presented, the base case is highlighted in green.

Table 69: Results and deviations from changing the number of stages in the absorber

N	H_2O content (ppmv)	Δ N (%)	Δ H_2O (%)
3	41.00	-	-
4	38.94	33.3	-5.0
5	38.52	66.7	-6.1
6	38.44	100.0	-6.2
7	38.43	133.3	-6.3
10	38.43	233.3	-6.3

Table 70: Results and deviations from changing the temperature of the NG feed

NG feed's temperature (°C)	H_2O content (ppmv)	Δ T (%)	Δ H_2O (%)
25	30.0	-16.7	-26.8
26	32.0	-13.3	-22.1
27	34.0	-10.0	-17.0
28	36.3	-6.7	-11.6
29	38.6	-3.3	-5.7
30	41.0	-	-
31	44.0	3.3	7.4
32	47.0	6.7	14.8
33	50.3	10.0	22.8
34	53.9	13.3	31.5
35	57.8	16.7	41.0

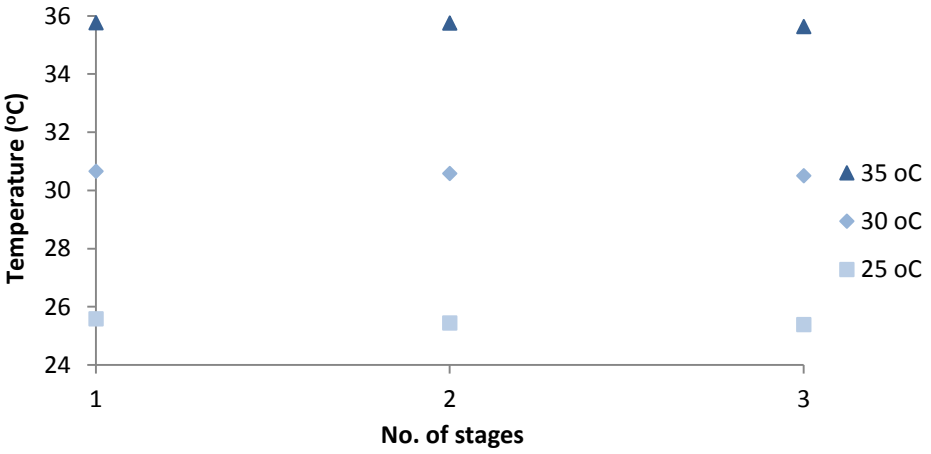

Figure 77: Absorber's temperature profile caused by the variation of NG feed's temperature

Table 71: Results and deviations from changing the lean solvent's temperature

Lean TEG temperature (°C)	H_2O content (ppmv)	Δ T (%)	Δ H_2O (%)
35	41.20	-	-
36	41.22	2.9	0.07
37	41.25	5.7	0.14
38	41.28	8.6	0.21

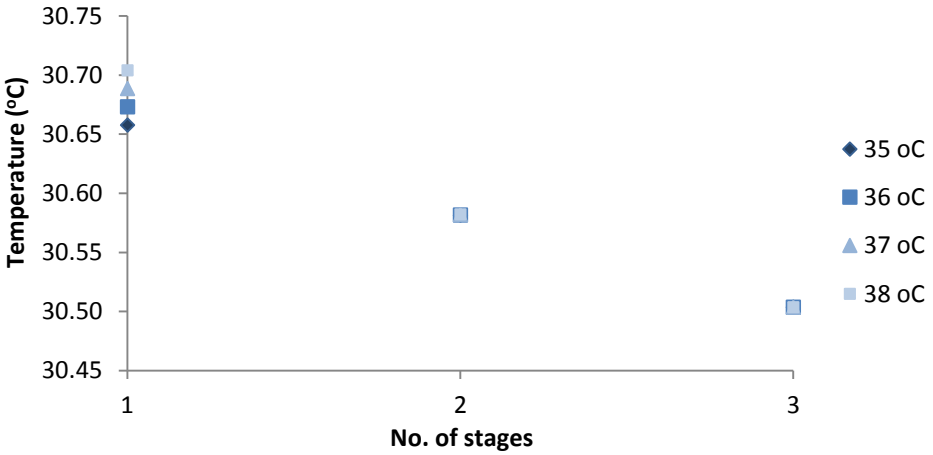

Figure 78: Absorber's temperature profile caused by the variation of lean solvent's temperature

Table 72: Results and deviations from changing the pressure in the absorber

Absorber's pressure (bar)	H_2O content (ppmv)	Δ P (%)	Δ H_2O (%)
75.0	48.2	-8.2	17.5
76.0	47.1	-7.0	14.8
77.0	46.0	-5.8	12.1
78.0	44.9	-4.5	9.5
79.0	43.9	-3.3	7.0
81.7	41.0	-	-
83.0	40.0	1.6	-2.4
84.0	39.1	2.8	-4.5
85.0	38.3	4.0	-6.7

Table 73: Results and deviations from changing the purity of the solvent

Glycol purity (wt. %)	H_2O content (ppmv)	Δ Purity (%)	Δ H_2O (%)
98.9	44.8	-0.1	9.3
99.0	41.0	-	-
99.1	37.6	0.1	-8.3
99.2	34.0	0.2	-17.1
99.3	30.3	0.3	-26.1

A-7. Dehydration with Molecular Sieves

A-7.1. Adsorption Bed Models [47]

In this sub-chapter, the models in the General Process Engineering (GPE) adsorption libraries, which were not changed, are presented.

A.7.1.1. Bed Loading

The total bed void is obtained through the following equation:

$$\varepsilon_{tot} = \varepsilon_b + (1 - \varepsilon_b)\varepsilon_p \tag{40}$$

Additionally, the density of the adsorbent particle is calculated as:

$$\rho_p = \frac{\rho_b}{(1 - \varepsilon_b)\left(1 - \varepsilon_p\right)} \tag{41}$$

$$\rho_{p,bulk} = \frac{\rho_b}{1 - \varepsilon_b} \tag{42}$$

A.7.1.2. Mass Transport

The continuity equation for each component in the fluid phase, assuming that the mass transfer driving force is on a solid coverage basis, is given by:

$$\varepsilon_{tot}\frac{\partial(\rho x_i)}{\partial t} + \frac{\partial(\rho u x_i)}{\partial z} = \varepsilon_b \frac{\partial}{\partial z}\left(\rho D_{axi}\frac{\partial x_i}{\partial z}\right) - \rho_b MW_i k_i (q_{ci}^* - q_{ci}) \tag{43}$$

The boundary conditions for this equation are:

$$(inlet)\ \ \frac{F_{in}x_{in}}{A} = \frac{F_{in}x_i}{A} - \varepsilon_b \rho D_{axi}\frac{\partial x_i}{\partial z}, \quad for\ i = 1, \dots, n-1 \tag{44}$$

$$(outlet)\ \ \varepsilon_b \rho D_{axi}\frac{\partial x_i}{\partial z} = 0, \ \ for\ i = 1, \dots n-1 \tag{45}$$

On the other hand, the mass balance for the adsorbed phase is given by the following equation, which is, again, in a solid coverage basis:

$$\frac{\partial q_{ci}}{\partial z} = k_i (q_{ci}^* - q_{ci}) \tag{46}$$

A.7.1.3. Energy Transport

The energy balance is described by the following equation:

$$\frac{\partial U_b}{\partial t} = \varepsilon_b D_{axi}\frac{\partial}{\partial z}\left(\rho\frac{\partial h}{\partial x}\right) - \frac{\partial u\rho h}{\partial z} + \frac{\partial}{\partial z}\left(\lambda_z\frac{\partial T}{\partial z}\right) - k_{T,bw}\frac{4}{d_b}(T - T_w) \tag{47}$$

The effective bed heat conductivity presented in the previous equation is obtained by using the Specchia correlation:

$$\lambda_z = \left(\varepsilon_b\lambda + \frac{1 - \varepsilon_b}{\frac{0.22{\varepsilon_b}^2}{\lambda} + \frac{2}{3\lambda_{ad}}}\right) \tag{48}$$

The boundary conditions for equation 48 are:

$$(inlet)\ \ \frac{F_{in}h_{in}}{A} = u\rho h - \varepsilon_b \rho D_{axi}\frac{\partial h}{\partial z} - \lambda_z \frac{\partial T}{\partial z}, \quad z = 0 \tag{49}$$

$$(outlet)\ \ \frac{\partial T}{\partial z} = 0, \quad z = L \tag{50}$$

The internal energy of the bed includes contributions from the fluid and solid phases:

$$U_b = \varepsilon_{tot}(\rho h - P) + \rho_b \left(\sum_i q_i h_{ad,i} + C_{p,ads}\left(T - T_{ref}\right) \right) \tag{51}$$

$$h_{ad,i} = h_i^{\emptyset}(T.P) + \Delta H_{ad,i} + \Delta C_{p,ad,i}\left(T - T_{ref}\right) \tag{52}$$

A.7.1.4. Momentum Balance

The pressure drop in the bed is determined from the Ergun equation:

$$-\frac{\partial P}{\partial z} - 150\upsilon \frac{(1-\varepsilon_b)^2 u}{{\varepsilon_b}^3 {d_p}^2} - \frac{1.75(1-\varepsilon_b)\rho u^2}{{\varepsilon_b}^3 d_p} = 0 \tag{53}$$

A-7.2. Adsorption Bed Custom Models

In this chapter, the variables and parameters defined in the custom models developed for the dehydration of NG using molecular sieves are presented.

A.7.2.1. Axial Dispersion Coefficient

Table 74: Parameters defined in the dispersion_calculation model

Symbol	gPROMS® name	Definition	Unit	Distribution
-	components	Components of the process	-	-
γ_1	gamma_1	Auxiliary parameter for axial dispersion coefficient	-	-
γ_2	gamma_2	Auxiliary parameter for axial dispersion coefficient	-	-
D_m	molecular_diffusivity	Molecular diffusivity of the component	m²/s	Components

Table 75: Variables defined in the dispersion_calculation model

Symbol	gPROMS® name	Definition	Unit	Distribution
u	u	Superficial velocity in the bed	m²/s	Axial
ε_b	Bed_Void	Porosity of the bed	m³/m³	Axial
d_p	Dp	Adsorbent particle diameter	m	Axial
T	T	Gas temperature	K	Axial
P	P	Bed pressure	bar	Axial
D_{ax}	dispersion	Axial dispersion coefficient	m²/s	Axial

A.7.2.2. Extended Dual Site Langmuir Isotherm

Table 76: Parameters defined in the isotherm_custom_section model

Symbol	gPROMS® name	Definition	Unit	Distribution
-	components	Components of the process	-	-
-	no_layers	Number of adsorbent layers	-	-
E_1	E1	Adsorption energy on site 1	J/mol	Components
E_2	E2	Adsorption energy on site 2	J/mol	Components
A_{11}	A11	Auxiliary adsorption equilibrium parameter	mol.K/kg	Components
A_{12}	A12	Auxiliary adsorption equilibrium parameter	mol/kg	Components
A_{21}	A21	Auxiliary adsorption equilibrium parameter	mol.K/kg	Components
A_{22}	A22	Auxiliary adsorption equilibrium parameter	mol/kg	Components
b_{01}	b01	Pre-exponential factor of site 1	kPa^{-1}	Components
b_{02}	b02	Pre-exponential factor of site 2	kPa^{-1}	Components

Table 77: Variables defined in the isotherm_custom_section model

Symbol	gPROMS® name	Definition	Unit	Distribution
T	T	Gas temperature	K	Axial
p	p	Partial pressure	bar	Components, axial
ΔH_i^{ads}	heat_of_adsorption	Heat of adsorption of the component	kJ/mol	Components, axial
q_{ci}^*	qeq	Equilibrium concentration of the component in the particle	mol/kg	Components, axial
q_{si1}	qsi_1	Specific saturation capacity of the component in adsorption site 1	mol/kg	Components, axial
q_{si2}	qsi_2	Specific saturation capacity of the component in adsorption site 2	mol/kg	Components, axial
β_{i1}	bi_1	Affinity parameter of the component in site 1	kPa^{-1}	Components, axial
β_{i2}	bi_2	Affinity parameter of the component in site 2	kPa^{-1}	Components, axial
q_{ci}	q	Concentration of the component in the particle	mol/kg	Components, axial
-	C	Molar concentration of the component	mol/m^3	Components, axial

A.7.2.3. Linear Driving Force Coefficient

Table 78: Parameters defined in the mass_transfer_adsorption_multilayer model

Symbol	gPROMS® name	Definition	Units	Distribution
-	components	Components of the process	-	-

Table 79: Variables defined in the mass_transfer_adsorption_multilayer model

Symbol	gPROMS® name	Definition	Units	Distribution
T	T	Gas temperature	K	Axial
-	mass_transfer_coefficient	Linear driving force coefficient	s^{-1}	Components, axial
D_{ci}	Dc	Crystalline diffusivity of the component	m^2/s	Components, axial
R_c	Rc	Mean crystal diameter	m	-
D_{0i}	D0c	diffusional pre-exponential factor of the component	m^2/s	Components
E_i	Ec	Diffusional activation energy of the component	J/mol	Components

A-7.3. Simulation Results

In this sub-chapter, the loading profiles in the adsorbent are shown for each component after 10 minutes of adsorption.

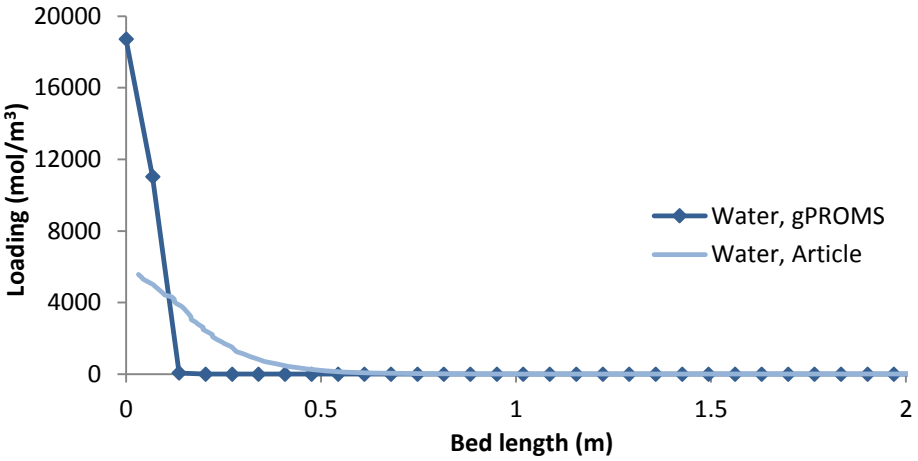

Figure 79: Water loading along the bed after 10 minutes of simulation

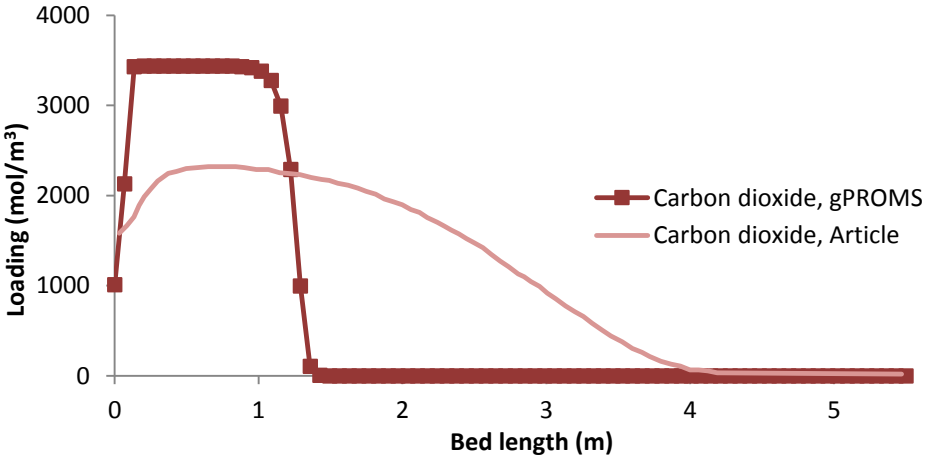

Figure 80: Carbon dioxide loading along the bed after 10 minutes of adsorption

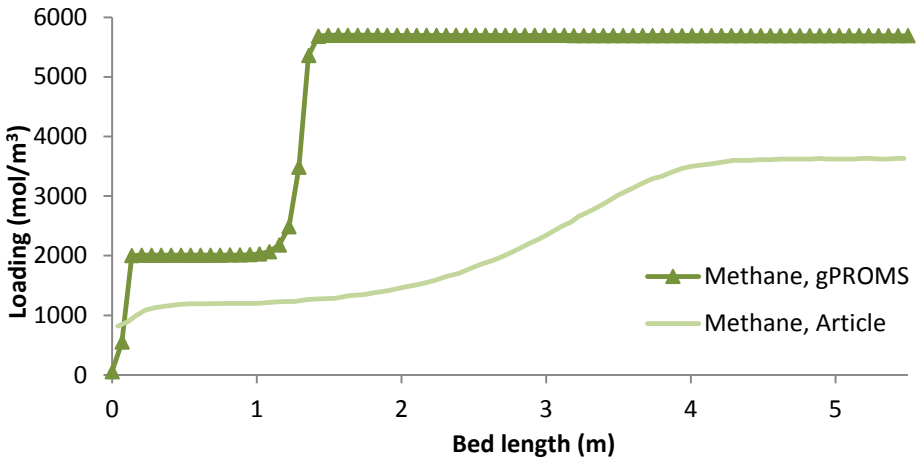

Figure 81: Methane loading along the bed after 10 minutes of adsorption

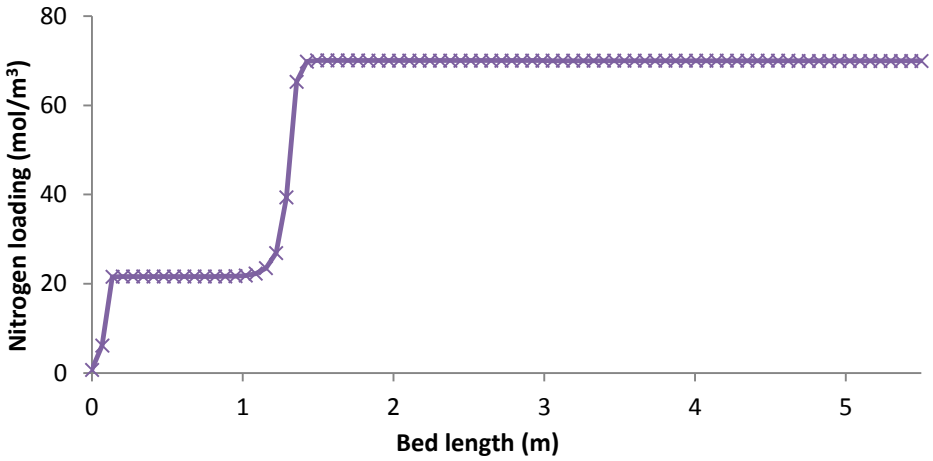

Figure 82: Nitrogen loading according to gPROMS® along the bed after 10 minutes of adsorption